U.S. DEPARTMENT OF ENERGY

PNNL-18374

Prepared for the U.S. Department of Energy
under Contract DE-AC05-76RL01830

Effect of Melter-Feed-Makeup on Vitrification Process

PR Hrma
MJ Schweiger
BM Arrigoni
CJ Humrickhouse
VV Mantay
J Marcial
JA Moody
TT Rainsdon
CP Rodriguez
RM Tate
NE TeGrotenhuis
BH Tincher

April 2009

Pacific Northwest
NATIONAL LABORATORY

DISCLAIMER

PACIFIC NORTHWEST NATIONAL LABORATORY
operated by
BATTELLE
for the
UNITED STATES DEPARTMENT OF ENERGY
under Contract DE-ACO5-76RL01830

Printed in the United States of America

Available to DOE and DOE contractors from the
Office of Scientific and Technical Information,
P.O. Box 62, Oak Ridge, TN 37831-0062;
ph: (865) 576-8401
fax: (865) 576 5728
email: reports@adonis.osti.gov

Available to the public from the National Technical Information Service,
U.S. Department of Commerce, 5285 Port Royal Rd., Springfield, VA 22161
ph: (800) 553-6847
fax: (703) 605-6900
email: orders@nits.fedworld.gov
online ordering: http://www.ntis.gov/ordering.htm

PNNL-18374

Effect of Melter-Feed-Makeup on Vitrification Process

PR Hrma
MJ Schweiger
BM Arrigoni
CJ Humrickhouse
VV Mantay
J Marcial
JA Moody
TT Rainsdon
CP Rodriguez
RM Tate
NE TeGrotenhuis
BH Tincher

April 2009

Prepared for
the U.S. Department of Energy
under Contract DE-AC05-76RL01830

Pacific Northwest National Laboratory
Richland, Washington 99352

Abstract

Increasing the rate of glass processing in the Hanford Tank Waste Treatment and Immobilization Plant (WTP) will allow shortening the life cycle of waste cleanup at the Hanford Site. While the WTP melters have approached the limit of increasing the rate of melting by enhancing the heat transfer rate from molten glass to the cold cap, a substantial improvement can still be achieved by accelerating the feed-to-glass conversion kinetics. This study investigates in detail how the feed-to-glass conversion process responds to changes in the feed makeup, including the chemicals used for glass-forming and modifying additives, silica grain-size, and heat-generating reactants. By identifying the means of control of primary foam formation and silica grain dissolution, it provides quantitative data needed for a meaningful and economical design of large-scale experiments aimed at achieving faster melting in WTP melters.

Summary

S.1 Effect of Melter-Feed-Makeup on Vitrification Process

S.1.1 Feed-to-Glass Conversion and the Rate of Melting

Understanding the relationship between melter-feed makeup and the feed-to-glass conversion process will help accelerate the rate of glass processing in the Hanford Tank Waste Treatment and Immobilization Plant (WTP). The mission of the WTP is to vitrify the Hanford nuclear waste. This will be done in continuous all-electric melters that contain a pool of molten glass in which the temperature is kept constant by passing electrical current through it. Feed is introduced into the melter from above in the form of water slurry. As water evaporates, a crust of dry feed, called the cold cap, floats on the melt pool and turns into melt at its bottom surface.

In the continuous glass melter, the rate of processing is jointly controlled by the rate of heat-transfer from molten glass to the cold cap and by the kinetics of various chemical reactions and phase transitions within the cold cap. Advanced melters that have been developed for the WTP have reached a level of heat transfer at which the rate of melting is controlled mainly by the conversion kinetics within the cold cap. Therefore, the feed-to-glass conversion process is the main focus of this study.

Melter feed is a mixture of many diverse components that respond to heating in a complex manner. Because of this complexity of the cold-cap process, it is impossible to determine the rate of melting in a large continuous melter with laboratory crucible experiments alone. Nevertheless, laboratory studies provide insight into the feed conversion process that can guide melter experiments to obtain the relationship between the feed-makeup parameters and the rate of melting in a well focused, timely, and economic manner.

The aim of this laboratory study can be simply put as follows:

1. *This study investigates in detail how the melter-feed conversion process responds to changes in the feed makeup.*
2. *The intended outcome of this study is to provide as detailed and useful information as possible to prepare feeds designed for accelerating the rate of melting in continuous melters.*

S.1.2 Experimental Approach

The reactions within the cold cap proceed as the feed moves from the top, where slurry is fed onto its surface, to the bottom, where the feed becomes molten glass. To simulate these conditions in the laboratory as closely as possible, feeds were heated at a rate of 5°C/min rather than using isothermal heat treatments. Feed conversion reactions advance while the temperature is increasing in a similar manner in a crucible as when the feed moves through a steep temperature gradient that exists in the cold cap.

One of the main conversion-rate controlling parameters is the heat conductivity of the cold cap. The others are the feed density, the effective conversion-rate coefficient, and the conversion heat. Additionally, to make a valid assessment of feed reactivity, great care was made to simulate not only the chemical composition of the waste in terms of oxides, but also its physical form and its chemical form in terms of compounds (e.g., oxides versus hydroxides or nitrates).

Feed density can vary extensively within the cold cap but to a great extent depends upon the extent of gas entrapment in the form of bubbles and cavities, known as primary foam, found in the lower layer of the cold cap. The primary foam develops when there is an overlap between the evolution of gases and the formation of connected glass-forming melt.

The conversion-rate coefficient represents the ease of melting and depends on the reactivity of feed additives.

Finally, the conversion heat determines how much feed is converted to glass per heat delivered to the cold cap from the melt below. The presence of an internal heat source within the cold cap can substantially decrease the conversion heat.

These parameters, i.e., the density, heat conductivity, conversion-rate coefficient, and conversion heat, are affected by the feed makeup. The relationship between feed makeup and these parameters must be examined to understand the interplay of various processes that take place within a cold cap and ultimately determine its rate of melting.

The main factors that control the feed reactivity and the extent of gas entrapment in the feed are the nature of inorganic salts (nitrates and carbonates) and the size of silica particles. A powerful source of internal heat within the cold cap can be provided through exothermic reactions of carbohydrates, such as sucrose or cellulose, with oxyanionic salts, especially nitrates and nitrites. These parameters are examined in laboratory tests described below.

S.1.3 Experimental Methods

This study tests and demonstrates the effects of feed-makeup parameters, both individually and in combination. It uses carefully chosen feed chemicals, varies the size and shape of silica particles, and introduces an internal heat source. Also, it identifies the mechanisms at which these variables operate.

Various methods of testing and analysis were used. Flux migration testing was conducted to verify that molten salts are not likely to migrate out of the cold cap. Differential thermal analysis-thermal gravimetric analysis (DTA-TGA), X-ray diffraction (XRD), and scanning electron microscopy-energy-dispersive spectroscopy (SEM-EDS) identified the main feed reactions. Visual examination and optical microscopy of crucible melts and photographic recording of feed pellets and loose batches in quartz-glass crucibles were employed for detailed characterization of volume changes associated with the conversion process. Finally, temperature-field-evolution monitoring introduced a temperature gradient, thus allowing us to measure the thermal conductivity of feed and providing a step towards understanding heat transfer in an actual cold-cap situation.

S.1.4 Scope

The study began with testing the high-level waste (HLW) feeds previously used in melter experiments conducted at the Vitreous State Laboratory (VSL): the baseline feed with the processing rate of 42 $kg/m^2/h$ and a slow-melting (23 $kg/m^2/h$) Al-Na-limited feed (referred to as VSL feeds). The slurry feeds were dried before testing. After these preliminary studies, the main study was conducted with Al-limited feeds containing the high-alumina-waste simulant. All feeds were prepared in the form of slurry that was subsequently dried for testing. The base Al-limited feed, denoted as A0 feed, was formulated to produce a glass designed at VSL but with chemicals selected to simulate the waste as truly as possible and with easy-reacting additives.

The following three series of experiments were completed in FY 2008:

- In the A-Series, glass-forming and modifying additives were varied. Five variations of A0 feed were prepared and tested. Fractions of B_2O_3, CaO, Li_2O, Na_2O, and MgO were varied by changing additive precursors while keeping the waste composition and loading constant.
- In the A0-X series, silica-grain size was varied from small to large; A0 feed was prepared with fine silica (≤ 5 μm), silica flour (≤ 75 μm), and large-grain sand (350 to 850 μm, 550 μm on average).
- In the C- and S-Series, cellulose or sucrose was added to feeds acidified with HNO_3. The acid was added to A0 slurry feed to reach pH 1, and then cellulose ($C_6H_{10}O_5$) or sucrose ($C_{12}H_{22}O_{11}$) was added to various C/N atomic ratios (from C/N = 0.75 to C/N = 1.5).

In FY 2009, examination of the feed conversion process is continuing in the following areas:

- The impact of silica grain size on feed expansion and the extent of conversion are being examined more systematically. Two types of silica are used: glass-maker's sand and crushed quartz, both of various size fractions.
- Feeds containing sucrose are being systematically studied. The HNO_3 addition is being reduced to determine its impact on primary foam. Feeds with additives in the form of alkali and alkaline earth nitrates are also being tested.
- The effect of combined variations of silica-grain sizes and sucrose-nitrate addition is being examined.

S.1.5 Experimental Testing

S.1.5.1 Feed Migration Test

The feed migration test was performed for the VSL feeds. The mass fraction of feed that migrated into the porous wall of a silica crucible at 500°C was 0.011±0.005; after heating to 1000°C, it decreased to 0.003±0.001 (above 500°C, the salts reacted with the crucible material releasing gases). This small fraction was within experimental error; no migrated salt was visible when the crucibles were cross-sectioned for examination. This low mobility of molten salt within the HLW feed can be attributed to the large specific surface area of the feed solids that immobilizes the molten salt via wetting the particles. Hence, molten salt is unlikely to migrate in the HLW melter feeds.

Visual Examination of Quenched Samples
A sample of the baseline feed heated in ceramic crucibles became sintered at 600°C; a sample of the Al-Na-limited feed sintered at 700°C. Both feeds swelled with the primary foam whose bubbles gradually coalesced to larger cavities that later burst. Bubbles were no longer seen in the baseline sample at 1000°C, but still prevailed at this temperature in the Al-Na-limited glass sample, obviously as a result of higher viscosity of the Al-Na-limited glass melt.

Temperature Field Evolution
The temperature-field-evolution was measured in large silica crucibles (200 mm tall and 135 mm in diameter) equipped with a battery of thermocouples. The furnace temperature increased at 5°C/min. At feed temperatures between 300 and 600°C, the horizontal temperature distribution in the feed was close to parabolic. The heat flux was calculated using the measured temperature difference across the crucible wall (the heat conductivity of the crucible material was 1.3 $W/m^2/K$). Based on the temperature distribution within the feed, the heat conductivity of the feed could be estimated for the temperature

interval from 300 to 600°C. Its value was 1.28±0.17 W/m^2/K for the VSL baseline and 1.99±0.82 W/m^2/K for the Al-Na-limited feed. Thus, no significant difference was found between the feeds, and the heat conductivity was virtually independent of temperature. Above 700°C, large cavities formed under the cold portion of the feed.

The temperature field in sucrose-containing feeds, both with C/N = 1.5, experienced a jump from ~100°C to ~300°C, caused by an exothermic reaction between nitrate and carbohydrate. This jump propagated throughout the feed from the crucible wall to the axis. The likely reaction between nitric acid and sucrose is

$$12HNO_3 + C_{12}H_{22}O_{11} = 12CO_2 + 17H_2O(g) + 6NO + 3N_2 - 3.28 \text{ MJ/mol}$$

The corresponding heat generated per glass was 3.15 MJ/kg for the feed with 0.72 g HNO_3 per g glass at C/N = 1.0. Various schemes suggested for reaction of cellulose with $NaNO_3$ resulted in 1.7 to 3.2 MJ/kg of glass, a similar value to that estimated for the reaction of HNO_3 with sucrose. The heat needed to convert dry feed to glass can be estimated as 2.5 MJ/kg; for slurry feed containing 55% of water, the conversion heat is 4.6 MJ/kg of glass. The heat to increase dry feed temperature by 200°C is ~0.8 MJ/kg. This value is much lower than the heat released by the sucrose reaction with nitrates. This reaction probably partially occurred during drying, i.e., before adding the feed into the test crucible.

Feed Expansion

To observe volume changes of feeds, pellets and loose batches in silica-glass crucibles were heated at 5°C/min. Photographs were taken as the temperature of each sample increased, and the photos were evaluated with Photoshop software. The minimum volume of VSL feeds at the start of expansion was close to the initial (room temperature) volume. The major difference between the fast-melting baseline feed and the slow-melting Al-Na-limited feed was that the latter expanded at a higher temperature, starting at ~700°C and culminating at ~900°C, as compared to the range of ~600°C to ~800°C of the former. Thus, as also was seen in the small crucible melts mentioned above, the VSL-baseline feed became a bubble-free glass at a temperature lower by more than 100°C than the Al-Na-limited feed.

The density of loose feed was ~1 g/cm^3. This value changed little from room temperature up to the beginning of expansion (foaming). During expansion, feed turned to primary foam whose density decreased to a value as low as ~0.2 g/cm^3 (the specific volume of ~5 to 6 cm^3/g), containing less than 8 vol% of melt with solid residues.

A-series feeds reached the minimum volume around 800°C both in pellets and in crucibles. The expansion was most rapid around 850°C in pellets and around 900°C in crucibles. Maximum expansion was reached around 910°C in pellets and around 980°C in crucibles. The earlier responses seen in pellets were possibly caused by the smaller volume of the pellets. The average minimum relative expansion (maximum initial shrinkage) was 0.69, and the maximum relative expansion was 0.92. The relative expansion extent was higher in crucibles (average minimum 0.87 and average maximum 1.56). No correlation between feed expansion behavior and the estimated viscosity was found. The specific volumes reached the maximum of 0.9 to 2.4 cm^3/g when the melt viscosity was 30 to 100 Pa·s. At this low viscosity, the feed is already converted to a bubbly melt and thus is no longer in the cold cap. Hence, the maximum expansion of A-series feeds was caused by fining gases (gases from redox reactions) rather than batch-reaction gases.

The silica grain size (AO-X Series) strongly affected the melting behavior. The temperature interval of expansion increased as the silica grain size increased, starting with the minimum expansion temperature of ~700°C for feed with 5-μm silica grains, and reaching nearly 900°C for feed with 550-μm silica grains. The maximum expansion in all samples occurred at a temperature ~200°C higher than the minimum. As the silica grain size increased, all three temperatures—minimum, inflection, and maximum—grew with a nearly identical slope of 1.02 K^{-1}; the intercepts were at 689, 768, and 900°C, respectively. The expansion extent decreased exponentially with silica grain size in nearly the same manner for feed in pellets and in crucibles. The feed with 550-μm silica grains barely expanded at all before heating was terminated at 1000°C.

The purpose of adding HNO_3 and sucrose (S Series) was to provide an internal heat supply rather than to affect expansion. However, the effect on feed expansion was both profound and complex. For both pellets and crucibles, the expansion of feeds with sucrose and C/N < 1 was about twice as high as that of A0 feed. At C/N = 1, the expansion sharply dropped, reaching the A0 level.

The expansion also increased when A0 feed was acidified without adding sucrose. Acidification with HNO_3 converts carbonates, hydroxides, and some oxides to nitrates and keeps within the feed a high partial pressure of oxygen. These conditions lead to an increased volume of foam, probably caused by gases evolved through a redox reaction, unless enough carbon is available to destroy nitrates at a low temperature (100 to 300°C).

The temperatures for the expansion interval (i.e., the minimum, inflexion, and maximum) in pellets of S Series feeds nearly linearly increased with the carbon/nitrogen (C/N) ratio (for C/N from 0.75 to 1.5) with identical slopes (the common slope of the lines was 59 K). No such relationship could be established for silica-glass crucible data; it seems that feeds in crucibles were more subjected to random events, such as growth and collapse of large bubbles, than feeds in pellets. The feeds with cellulose reacted rather violently at ~200°C, precluding the pellet expansion test to be performed.

XRD

According to XRD results, silica began to react with feed fluxes at temperatures below 400°C; only a small silica residue was found at 900°C and none at 1000°C in both VSL feeds. Also in A-series feeds, the solid silica was gone only when the temperature approached 1000°C regardless of feed formulation. More silica reacted early (below 500°C) in feeds with carbohydrate addition, but the temperature at which the undissolved silica disappeared was the same in these feeds as in A0 feed without additions. It appears that early conversion of silica into silicate melt increases the viscosity of this melt and, hence, slows down the dissolution of silica in the later stages.

Several crystalline phases other than silica were detected in feeds using XRD. Hematite formed from amorphous iron oxyhydrate. Spinel formed from hematite starting at 500°C and peaked just above 600°C. Hematite completely dissolved below 800°C. Dissolving spinel remained in the glass even at 1000°C. In the Al-Na-limited feed, nepheline and sodium salts-containing aluminosilicates appeared at temperatures above 400°C and were gone by 900°C.

SEM-EDS
In the baseline feed at 600°C, SEM-EDS confirmed the presence of the glass phase, hematite [or possibly aegirine ($NaFeSi_2O_6$)], and spinel (probably hausmannite, Mn_3O_4, or hetaerolite $ZnMnO_4$), as well as dissolving particles of silica. At 700°C, apart from glass phase and dissolving silica particles, the patterns of spinel suggested hausmannite (Mn_3O_4) and franklinite $(Fe,Mn,Zn)(Fe,Mn)_2O_4$. Corundum was also detected. At 800°C, various forms of spinel were indicated by EDS: from hausmanite-franklinite solid solution; magnetite-jacobsite-trevorite ($MnFe_2O_4$-$NiFe_2O_4$) was also likely to form. At 900°C, the feed turned mostly to glass containing submicron crystals of spinel and silica residues. Silica was gone at 1000°C while spinel $(Ni,Fe,Mg,Mn)(Fe,Cr)_2O_4$ was surviving.

In the Al-Na-limited feed, inclusions of phosphate glass were suspected at 700°C. Particles of corundum, nepheline, and eskolaite (Cr_2O_3) or chromate (Na_2CrO_4) were clearly detected. Nepheline, needles of calcium phosphate, and spherolites of eskolaite were seen at 800°C. At 900°C, most of the sample was a connected amorphous phase containing rounded silica particles, spinel, and nepheline. At 1000°C, tiny crystals of chromite ($FeCr_2O_4$) were detected on the surfaces of bubbles.

Samples from the A and S Series may be tested further on an as-needed basis.

DTA-TGA
These tests, conducted on VSL and most Pacific Northwest National Laboratory (PNNL) feeds, showed that the major mass loss begins in feeds at ~150°C and continues to 600°C, above 600°C, it proceeds at a rather slow rate.

S.2 Discussion: Feed-Melt Interface Position and the Rate of Melting

The temperature of the cold-cap bottom is an important parameter because it affects, together with the melt viscosity, the heat-transfer rate from melt to cold cap. The temperature difference between the melt (usually fixed at 1150°C) and the cold-cap bottom is the driving force for the convective heat transfer. Where is the cold-cap bottom located in the melter? This question cannot be answered from experiments thus far conducted. One possibility is that the melt-feed interface is positioned where the melt viscosity is low enough to be dragged by the convection currents away from the cold cap. However, one can argue that the bubbly melt under the cold cap is stabilized by its low density and thus can resist convective currents. If this is the case, the cold-cap bottom would effectively be around the temperature of maximum expansion (i.e., 800°C in the VSL baseline).

If the cold-cap bottom is at the temperature of maximum expansion, would A0 feed melt faster or slower than VSL Al-Na limited feed? Both reach maximum expansion at ~900°C. However, there is a substantial difference in the expansion extent: VSL Al-Na-limited feed expands three times as much as A0 feed. The maximum expansion of VSL Al-Na-limited feed corresponds to primary foam that collapses at the ~92% void fraction, whereas the maximum expansion of A0 feed at the 82% void fraction is a bubbly melt (secondary foam). Would, then, the cold-cap bottom be located at a viscosity of 100 Pa·s for A0 feed, but at T > 900°C for Al-Na limited feed? A melter experiment can determine which feed melts faster.

S.2.1 Cold-Cap Model

From the point of view of an external observer, the temperature, velocity, and conversion extent of feed within the cold cap are distributed along the vertical coordinate. Ideally, when a steady state is established, this distribution is time-independent. The spatial distribution in the cold cap can be translated to the temporal history of the feed. In this work, the temperature history imposed in the laboratory crucible (the 5°C/min temperature-increase rate) roughly simulated a typical temperature history that a feed particle experiences within the cold cap.

Somewhat simplifying, the cold cap consists of two layers: the upper layer of granular solids soaked with low-viscosity molten salts and the lower layer of primary foam of glass-forming melt and dispersed solid residues, mainly silica and spinel. Most of the conversion reactions occur in the upper layer. It is there where the chemically bonded water is released, where oxyionic salts melt and react with organics and with solids, and where the first borates and silicates form.

In the lower layer, the borosilicate glass-forming melt becomes connected. Gases generated in this layer are trapped as primary foam. This foam collapses when enough gas is evolved to cause the melt films separating the bubbles to break. A distinction needs to be made between primary and secondary foam. Secondary foam is produced by redox reactions (known as fining reactions in commercial technology) at temperatures >900°C. This foam affects the rate of melting, but is not a part of the cold cap.

S.2.1.1 Conversion Process Control

Most of the heat for feed-to-glass conversion is consumed in the upper layer of the cold cap. Enough heat must be conducted to evaporate water, to heat up the feed components, to provide energy for feed reactions, and to heat up feed gases, including steam. This heat is transferred from molten glass through the primary-foam layer. The thickness and the effective heat conductivity of the primary-foam layer in the melter are unknown. Both depend on the interaction between the internal gas-phase source and the glass-forming melt.

As has been demonstrated in this study, the gas-phase source within the glass-forming melt can be decreased, and perhaps entirely eliminated, by an appropriate selection of feed additives, especially the size of silica grains. However, the ultimate impact of the absence of primary foam on the rate of melting is difficult to assess. We also need to consider that the formation and collapse of primary-foam bubbles help dissolve the solid residues and homogenize the melt.

The evolution of gases produced by redox reactions at higher temperatures can also be controlled, but this is tricky because carbon from the pyrolysis of carbohydrates can survive to higher temperatures and produce CO_x by reacting with polyvalent oxides.

Whereas the relationship between the feed-expansion extent and the rate of melting is unknown at present, it is obvious, based on energy balance, that the melting process can substantially be accelerated through exothermic reactions within the upper layer of the cold cap. As has been demonstrated in this study, carbohydrates, such as sucrose and cellulose, produce ample heat provided that an oxygen source is present in the feed. The best source of oxygen is from nitrates and nitrites that are either already present in nuclear waste or are deliberately introduced with feed additives. Nitrates and nitrites react with hydrocarbons at sufficiently low temperatures of 100 to 300°C and thus deliver heat where it is most

needed in the cold cap. More powerful reductants may be undesirable because they may reduce some feed oxides to metals.

S.3 Conclusion

Although it is not fully understood at this stage to what extent the decrease or avoidance of primary foam will affect the rate of melting, the present study identifies the means of control of primary foam formation. This study also clarifies the effect of exothermic reactions on the feed-to-glass conversion process. The approach developed in this study can provide quantitative data needed for a meaningful and economic design of large-scale experiments aimed at achieving faster melting in WTP melters. Moreover, mathematical models can now be developed that include the cold cap as a body with temperature and velocity fields rather than a mere mass source and heat sink with no vertical dimension.

Acronyms

BL	baseline
C/N	carbon/nitrogen (ratio)
DIW	deionized water
DSC	differential scanning calorimetry
DTA	differential thermal analysis
EDS	energy-dispersive spectroscopy
HLW	high-level waste
IOPS	Integrated Operations System
LAW	low-activity waste
NQARD	Nuclear Quality Assurance Requirements Description
PNNL	Pacific Northwest National Laboratory
SEM	scanning electron microscopy
TC	thermocouple
TGA	thermal gravimetric analysis
VSL	Vitreous State Laboratory
WTP	Hanford Tank Waste Treatment and Immobilization Plant
XRD	X-ray diffraction

Acknowledgments

The authors are grateful to Albert Kruger, the glass scientist from the U.S. Department of Energy Office of River Protection, for establishing this project, for inspired guidance, for continuous interest in the progress of the study, including periodic visits to the laboratory, and for his presence at our weekly seminars. We also thank Dong Kim for a thorough review and Wayne Cosby for expert editing.

Contents

Figures

Tables

1.0 Introduction

The majority of nuclear waste in the world originated from the nuclear fuel cycle and nuclear weapons reprocessing. At least 108 sites containing radioactive waste exist in the United States. The most prominent among them is the Hanford Site in the State of Washington, where 177 underground radioactive waste tanks contain roughly 200,000 m^3 of radioactive liquid and sludge from plutonium production during the 1944-to-1987 period.

Radioactive tank waste presents an environmental danger and must be immobilized for safe storage. Hanford waste will be processed in the Hanford Tank Waste Treatment and Immobilization Plant (WTP). First, it will be pretreated and separated into high-level waste (HLW) and low-activity waste (LAW) fractions and then vitrified in continuous all-electric melters. Melter feeds will be made by mixing HLW slurries and LAW solutions with glass-forming and modifying additives in proportions designed to guarantee good processing behavior and a good quality product.

Waste-glass melters contain a pool of molten glass kept at a constant temperature by electric current passing through it. To prevent electrode damage, the melt temperature cannot increase above 1150 to 1200°C. Melter-feed slurry is introduced into the melter from above. Slurry water evaporates, and a crust of dry feed, called the cold cap, floats on the melt pool, turning into melt at its bottom surface.

It is desirable that the processing rate, usually expressed as the mass of glass produced per square meter of the melt–cold-cap interface per hour, is as high as possible. In this report, the processing rate is also called the rate of melting, the rate of feed-to-glass conversion, or simply conversion rate.

In a continuous glass melter, the rate of processing is jointly controlled by the rate of heat-transfer from molten glass to the cold cap and by the kinetics of various chemical reactions and phase transitions within the cold cap. The heat is transferred to the cold cap by convection: the hot glass is carried to the cold cap both by buoyancy (natural convection) and by forced convection driven by bubbling gas through the melt.

The heat transfer by natural convection increases as the difference increases between the temperature of the bulk melt and the temperature of melt at the melt–cold-cap interface. Because of the necessity to keep a constant melter-processing temperature, the rate of melting cannot be increased by increasing heat flux through the melt temperature. With advanced WTP melters equipped with bubblers that release air from the bottom of the melter, which percolates through the melt, the heat is delivered to the cold cap predominantly by forced convection. The temperature difference is still important, but the heat flux is decreased by compressing the thermal boundary layer under the cold cap.

An important property that influences the thermal-boundary-layer thickness is melt viscosity. As the viscosity becomes lower, the boundary layer becomes thinner, and the heat transfer from the melt to the cold cap is more efficient.

Provided that enough heat is delivered to the cold cap that its bottom temperature becomes close to that of the bulk melt, the rate of processing will become fully controlled by the conversion kinetics within the cold cap. Because of bubbling, it is likely that the WTP melters are close to this situation, and thus the feed-to-glass conversion is of utmost importance for the rate of melting.

Feed-to-glass conversion is the main focus of this report. Its subject is an exploratory study that investigates the vitrification process at the conditions close to those that exist in the cold cap.

Valuable experience has been accumulated in feed-to-glass conversion studies over the years (Hrma 1982, 1988, 1990a, 1990b, 1991, 2002, Schill 1982, Bickford et al. 1990, Kim and Hrma 1990, Lucktong and Hrma 1988, Elliott et al. 1989, pp. 5.17 and 6.12; Cable 1984, Russell and Ott 1980, Cable and Siddiqui 1983, Taylor and Rowan 1983, Thomason and Wilbum 1960, Bader 1979, Bunting and Bieler 1969, Vierneusel et al. 1981, Anderson et al. 1994, Kim and Hrma 1994, Smith et al. 1995, and Izak et al. 2001). However, the cold cap still remains the least understood element in glass-processing technology. We are facing complexity at various levels: the material itself (a mixture of granular and dissolved solids), its response to heating (generation of molten salts, evolution of copious gases, precipitation of various intermediate crystalline phases, and formation of molten glass), and the conditions that exist in the melter.

Because of the complexity of the cold-cap process, it is impossible to determine the rate of melting established in a large continuous melter by laboratory crucible experiments alone. Nevertheless, laboratory studies provide valuable insight into the feed conversion process. The detailed knowledge of this process achieved in the laboratory can guide expensive and time-consuming melter experiments. This way, we can eventually obtain the desired relationships between the feed makeup parameters and the rate of melting that will allow us to increase the rate of melting far above the current level.

1.1 A Simplified Cold-Cap Model

The rate of melting is jointly controlled by the heat-transfer rate and the rate of feed-to-glass conversion consisting of various chemical reactions and phase transitions (Hrma 1990b). In a simplified model of a solid cold cap floating on a pool of liquid, the melting rate can be expressed as a function of these two rates as follows (Hrma 1990b):

$$N = \frac{N_C^2}{2N_H}\left[\left(1+\frac{4N_H^2}{N_C^2}\right)^{1/2} - 1\right] \tag{1.1}$$

where N is the rate of melting (mass per time and area), N_C is the conversion-controlled rate of melting, and N_H is the heat-transfer-controlled rate of melting. These rates are related to material parameters as

$$N_C = \left[\frac{k\rho\lambda_C\left(T_M - T_C\right)}{Q}\right]^{1/2} \tag{1.2}$$

and

$$N_H = \frac{\lambda_H\left(T_M - T_C\right)}{\delta Q} \tag{1.3}$$

where λ_C and λ_H = effective heat conductivities of the cold cap and molten glass
T_C = temperature at which feed-to-glass conversion begins
T_M = temperature of the bulk melt
δ = thermal boundary layer thickness
k = conversion-rate coefficient
ρ = feed density
Q conversion heat (the energy needed to turn slurry feed under ambient conditions to 1 kg of molten glass).

The thickness of the thermal boundary layer is defined as $\delta = (T_M - T_I)/(\delta T/\delta y)_{y=0}$, where y is the vertical distance from the cold-cap–melt interface, and T_I is the temperature of the cold-cap–melt interface.

1.2 Feed-to-Glass Conversion Rate

In a Vitreous States Laboratory (VSL) study (Matlack et al. 2007), feeds with 0.5-kg glass solids per liter were processed in DM100 melters operating at 1150°C with bubblers operating at 9 L/min. Glasses of various compositions (with high levels of Bi, Cr, Al, and Al+Na) were formulated with comparable melt viscosity (6 to 10 Pa·s at 1150°C), as confirmed by measurement. Figure 1.1 displays the processing rate in terms of waste oxides. Thus, for Al-limited waste glass, the waste-oxide processing rate was 10 kg/m^2/h. With the waste loading at 0.45, the glass processing rate was 23 kg/m^2/h. The glass processing rates of the feeds tested varied in a wide range from 17 to 48 kg of glass per /m^2 and hour (8 to 19 kg of waste oxides per m^2 and hour) with two of them—Al and Al+Na—below the nominal rate of 33 kg/m^2/h (15 kg/m^2/h in terms of waste oxides).

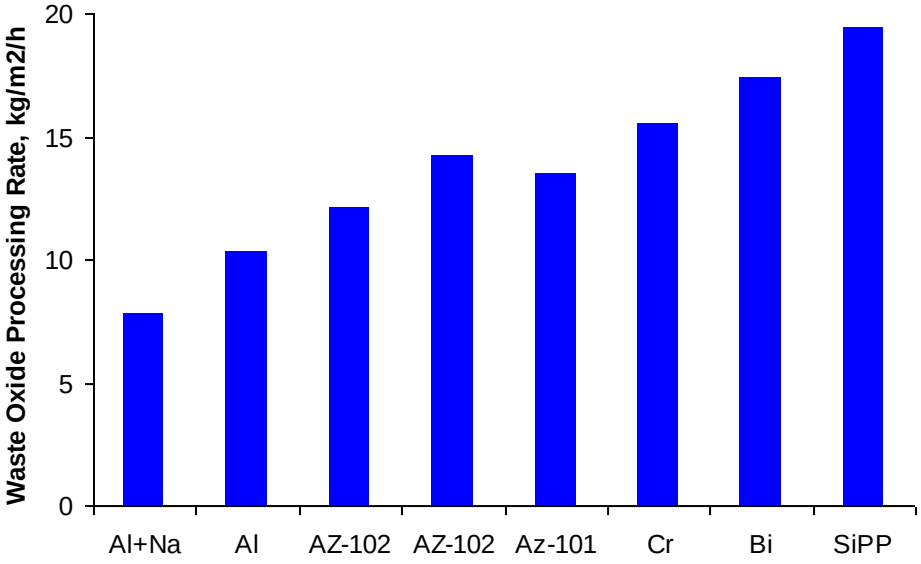

Figure 1.1. Processing Rates for Various Feeds Used at VSL

Heat can be transferred from the hot melt to the cold cap faster by increasing the melt temperature and by bubbling (Matlack et al. 2007). For example, based on the data reported by Lutze et al. (Lutze et al. 2007) for AZ-101 glass, the production rate increased 2.6 times when bubbling was used. Bubbling

enhances melt circulation, removes foam accumulated under the cold cap, and even breaks through the cold cap, exposing a larger interface area to melting. The Duratek melter, equipped with bubbling, has probably achieved vigorous enough melt circulation (see Matlack et al. 2007, Chapman 2004) to approach the limit at which melting is controlled mainly by the rate of conversion. At such a limit, the temperature of the bottom of the cold cap (the interface of the cold cap and the melt) would be close to the bulk-melt temperature, and a more vigorous bubbling would no longer increase the rate of melting. Because the bulk-melt temperature is limited by the electrode material to 1150 to 1200°C, the heat transfer from melt to the cold cap can no longer be intensified. Hence, the rat of melting would be fully controlled by the rate of feed-to-glass conversion reactions.

Increased melt circulation (by increased temperature, by decreased viscosity, and by bubbling) suppresses the thermal boundary layer under the cold cap, thus increasing the heat flux to the boundary of the melt with the cold cap. Based on the proved efficiency of melter bubbling, we can assume that the substantial differences in processing rates of VSL feeds were associated predominantly with the differences in rates of conversion within the cold cap, i.e., the differences in simulant compositions and makeup, waste loadings and compositions, mineral forms, and particle sizes of the glass-forming and modifying additives.

When the conversion rate is the rate-controlling factor, i.e., if $N_C/N_H << 1$, the right-hand side of Equation (1.1) can be developed into a Taylor series, obtaining[(a)]

$$N = N_C - \frac{N_C^2}{2N_H} + \frac{N_C^3}{8N_H^2} + \ldots \tag{1.4}$$

By Equations (1.2) and (1.3), the second right-hand-side term in Equation (1.4) is $\frac{1}{2}(\lambda_C/\lambda_H)k\rho\delta$. This term becomes small when the thermal boundary layer is suppressed by strong convection (bubbling) and low viscosity in the case of forced convection, $\delta \sim \nu^{1/6} v^{-1/2}$, where ν is the kinematic viscosity, and v is the velocity). Consequently, the main rate-controlling process is feed-to-glass conversion described by Equation (1.2).

Note that Equation (1.2) oversimplifies the conversion process by reducing a rather complex set of parallel and sequential reactions and transitions with one rate coefficient, k. In reality, the conversion process proceeds in several stages. As the feed temperature increases, low-viscosity molten ionic salts begin to melt (Hrma et al. 2007), forming the primary melt. However, both the heat transfer and the conversion process are upset if the ionic salts migrate out of the cold cap. This leads to cold-cap freezing and an inability to reach a steady state in the melter.

Next, the reactive components of the primary melt, such as carbonates and nitrates, react with silica, creating the glass-forming melt while leaving behind less reactive sodium sulfate that only gradually dissolves in the glass-forming melt. Once the glass-forming melt connects into a continuous body, the residues of molten salts and oxidation-reduction reactions generate gases that are trapped inside the melt in the form of bubbles. The resulting primary foam increases the melt volume several times (Izak et al. 2001, Hrma et al. 2002, Kim and Hrma 1990, 1991) and collapses as soon as the melt viscosity decreases below a certain level.

(a) For $N_H << N_C$, Equation (1) can be developed into the series $N = N_H - N_H^3/N_C^2 + 2N_H^5/N_C^4 - \ldots$

1.3 Effect of Viscosity

An important factor affecting the heat-transfer rate is the melt viscosity that influences the velocity of natural convection in the melter and the extent of foam accumulation under the cold cap (Kim and Hrma 1990, 1991). Because viscosity depends on glass composition, glass formulation is of a crucial importance for melter operation. For fast melting, the viscosity near the cold-cap bottom surface should be as low as possible.

The effect of composition and temperature on the melt viscosity can be expressed as

$$\eta = \exp\left(A + \frac{\sum_{i=1}^{N} B_i x_i}{T} \right) \tag{1.5}$$

where, η is the viscosity, T is the temperature, x_i is the i-th component mass fraction, and A and B_i are constant coefficients (Hrma 2008). The validity of Equation (1.5) is limited to glasses with $\eta < 10^3$ Pa·s. Tables in Appendix A show that the most potent glass component with respect to the decrease in viscosity is Li_2O, followed by Na_2O. Also note that CaO and B_2O_3 closely follow Na_2O in their impact on glass viscosity.

The viscosity calculation based on Equation (1.5) is subjected to uncertainty caused by the presence of many minor components in the waste glass whose coefficients have not been evaluated separately (the effects of these components are jointly expressed through a coefficient ascribed to "Others"). Other sources of uncertainty are component interactions, especially for glasses that are far away from the centroid (baseline [BL]) composition in the composition space, even within the model validity region. Therefore, it is advisable to measure the viscosity of glasses after they have been formulated with the property-composition models.

Figure 1.2 depicts the relationship between the rate of melting and the viscosity of glasses measured at 1150°C, compiled from VSL reports (Matlack et al. 2007, Matlack et al. 2008, Kot and Pegg 2007).

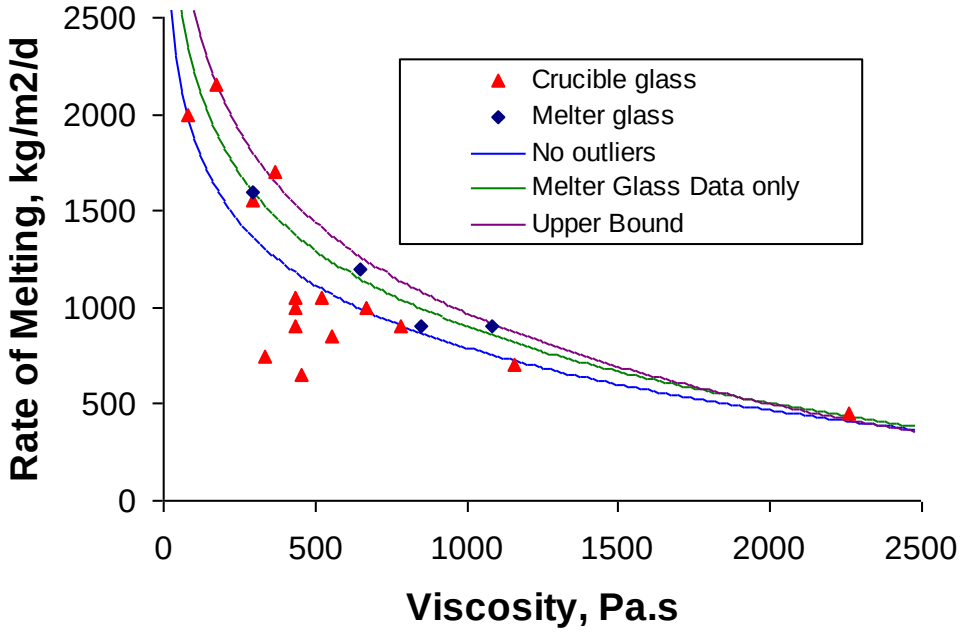

Figure 1.2. Rate of melting as a Function of Melt Viscosity at 1150°C. Data points represent measured viscosities of glass samples taken from the melter (diamonds) and melts prepared in the laboratory (triangles). The lines were fitted to selected data.

In Figure 1.2, trendlines of $N = -N_1\ln(\eta/\eta_0)$ were fitted to data; here N is the rate of melting, η_0 the viscosity at which $N = 0$, and N_1 the rate of melting at which $\eta/\eta_0 = 0.368$. The values of the coefficients are listed in Table 1.1.

Table 1.1. Coefficients Relating the Rate of Melting to Melt Viscosity at 1150°C by Equation $N = -N_1\ln(\eta/\eta_0)$

		Sin 4 Outliers	Melter Only	Upper Bound
N_1	kg/m^2/d	467	570	676
η_0	Pa·s	5463	4863	4205

The inequality $N \le -N_1\ln(\eta/\eta_0)$ with the coefficients listed in the last column of Table 1.1 represents the upper bound for the rate of melting; the < sign indicates that the rate of melting is hindered by the slowness of the feed conversion reactions. This upper boundary is not necessarily caused by the impact of viscosity on the heat transfer from the melt to the cold cap. As will be argued in this report, viscosity stabilizes primary foam that forms the lower portion of the cold cap.

1.4 Cold-Cap Parameters

Whereas the value of $T_M - T_C$ does not significantly vary from feed to feed, ρ, λ_C, k, and Q (see terms in Equations 1.2 and 1.3) can be substantially influenced by the feed makeup. The feed makeup affects the extent to which gases accumulate in the cold cap, forming primary foam (secondary foam is produced from fining gases in commercial melts and by gases from redox reactions in waste glass melts). The feed

makeup also determines the rate of individual feed reactions. And finally, it is possible to deliberately produce exothermic reactions within the cold cap. The ρ, λ_C, k, and Q parameters are related to feed makeup as follows:

- The values of ρ and λ_C are sensitive to the accumulation of gases in the conversion layer of the cold cap.
- The value of k characterizes the ease of melting, i.e., the reactivity of feed additives.
- Since $N \sim q/Q$, where q is the heat flux delivered to the cold cap from the melt, a smaller Q results in faster melting.

From this, we can suggest that the rate of melting can be increased by those changes in feed makeup that promote

- a decrease in gas entrapment in the cold cap (primary foam)
- an increase in the ease of melting
- a decrease of the conversion heat described in the three subsections below.

1.4.1 Feed Expansion (Primary Foam)

Little doubt exists about the impact of the ease of melting and the conversion heat on the rate of melting. However, the role of primary foam is uncertain. Its impact on the rate of melting is not well understood. Though primary foam insulates the cold cap by deceasing its density and heat conductivity, the growing bubbles help to homogenize the melt, thus helping dissolve the solid particles (Kim and Hrma 1994). However, if melter experiments will show that the absence of primary foam increases the rate of melting, its homogenizing effect is less important because the melt has a plentiful opportunity for homogenization within the melt pool.

1.4.2 Ease of Melting

It is well known that pre-reacted raw materials allow faster melting. Therefore, the feed additives should be chosen carefully. Fusing feed additives into a frit to facilitate the incorporation of the waste components into the vitrified form has been used previously. However, frit may actually be less reactive than a carefully designed mix of additive precursors because the silica content of the frit and thus its viscosity is higher than that of the final waste glass.

In melter tests with simulated waste components, it is important to simulate not only the chemical composition of the waste in terms of oxides, but also its physical form and its chemical form in terms of compounds. For example, it makes a difference in the rate of melting whether an alumina in a high-alumina waste is introduced as aluminum oxide, aluminum hydroxide, or aluminum oxy-hydrate. Many other components will also affect the ease of melting.

1.4.3 Conversion Heat

The conversion heat can be substantially decreased by an internal heat source through exothermic reactions that internally supply heat to the cold cap independent of heat transfer from the melt pool or plenum heaters. A powerful source of internal heat is a reaction of reductants, such as sugar or cellulose, with oxyanionic salts, especially nitrates and nitrites, and with high-valence oxides, such as Fe_2O_3 and Mn_2O_3. These reactions occur at low temperatures, reducing the content of oxyanionic salts in the cold cap, which decreases the potential for flux separation that leads to cold-cap freezing.

Minimizing the water content in melter feed and evaporating water by plenum heaters that supply radiant or microwave heat are additional ways of enhancing the rate of melting. However, these methods are outside the scope of this study, in which mainly dried feeds were tested.

2.0 Materials Used

The initial phase of testing involved a series of techniques, listed below, that were applied to two melter feeds: the VSL BL feed (processing rate 42 kg/m^2/h) and the Al-Na-limited glass feed (a slow-melting feed, 23 kg/m^2/h). These feeds were formulated and tested at VSL (Matlack et al. 2007a, 2007b). The compositions of the BL, Al-limited, and Al-Na-limited glasses and feeds are listed in Appendix B. Figure 1.1 illustrates the differences between the processing rates of various feeds described in VSL reports (Matlack et al. 2007a, 2007b). In the second phase of this research, the Al-limited waste simulant was used to formulate glasses and vary feed makeup with the aim to indentify the impact of glass formulation and feed-makeup variables on feed behavior (see Section 4).

3.0 Experimental Methods

The fast heat transfer in Duratek melters (Matlack et al. 2007a) was achieved by minimizing the water content of the slurry feed, by formulating glasses with low viscosity, and by bubbling the melt. As argued above, the melting-rate differences among various feeds are to a high degree associated with differences in the rates of the feed-to-glass conversion. If this reasoning is correct, we may be able, at least in principle, to assess the rate of feed-to-glass conversion by testing the feeds in the laboratory. If features of feed behavior are identified that are predictive of the rate of melting, simple laboratory techniques may became available for fast and economic selection of feeds to be tested in continuous melters that require a considerable expense of time and resources. However, in this report, we set for ourselves a more modest goal of characterizing feeds with respect to controlling their volume expansion (the extent of primary foam), the rate of dissolution of silica particles, and the internal heat supply through exothermic reaction. A direct connection between these characteristics and the rate of melting will be established once the rates of melting of various feeds are determined in actual melters.

Various experimental approaches to examining feed melting were suggested in reference (Kim and Hrma 1994) that documents additional useful references. A larger spectrum of techniques was employed in our later work (Hrma et al. 2002). Useful techniques were developed in connection with bulk vitrification of LAWs (Hrma et al. 2007). Also, a series of tests were conducted at Savannah River National Laboratory (Lorier 2001, Stone and Josephs 2001, Josephs and Stone 2001, Lambert et al. 2001, Smith et al. 2004a, 2004b, 2007, including crucible tests (Lorier 2001) in which dry feeds were heated for 2 hours at temperatures from 700°C to 900°C at 50°C intervals and Bickford's melt-rate-furnace test (Stone and Josephs 2001) in which a metallic beaker with feed was heated from below, and the temperature evolution in the feed was recorded by an array of thermocouples. This test inspired a method of monitoring the evolution of the temperature field within the feed placed in a large ceramic crucible used in this study and described below.

Various methods of feed-to-glass conversion analysis are reviewed below: gradient-temperature furnace treatment (Anderson et al. 1994), X-ray diffraction (XRD), optical and scanning electron microscopy (SEM) (Kim and Hrma 1994), evolved gas analysis (Hrma et al. 2002), flux migration testing (Hrma et al. 2007), visual observation in quartz-glass crucible (Kim and Hrma 1990), and a melt-rate ranking method designed at Savannah River (Bickford 2004). Not all these methods were used in this study. Some were deemed unnecessary (gradient temperature furnace), and some were not used because of budget and schedule constraints (evolved gas analyses, differential-scanning calorimetry).

3.1 Gradient-Temperature Furnace Treatment

Glass batches and feeds have been investigated by exposing them to a temperature gradient Anderson et al. 1994). The batch or dry feed is added into a long Pt or ceramic boat and placed into a preheated gradient-temperature furnace to cover the temperature interval from the beginning of the melting reactions (around 300°C) to bubble-free molten glass. Longitudinal thin sections are made from the melts (Anderson et al. 1994).

The gradient-temperature furnace treatment allows us to identify various stages of the progress of conversion, such as:

- sintering with solid-state reactions
- molten salt generation
- vigorous gas-evolving reactions of molten salts with solid grains
- formation of intermediate crystalline forms and the glass-forming melt that becomes connected and bubbly
- dissolution of residual solids
- release of bubbles to the atmosphere.

These stages and their temperature intervals are discerned using optical observations assisted with SEM-energy dispersive spectroscopy (EDS) and XRD analysis.

The disadvantage of this method is that it does not simulate the actual melting process. Melter processing does not occur isothermally, but during a gradual increase of temperature. In the gradient-temperature furnace, the batch is heated up as fast as possible and then kept for a certain time before the sample is removed from the furnace. Thus, the slow low-temperature reactions receive the same time exposure as the fast high-temperature processes. A slow insertion of the boat into the furnace brought an improvement, but required more sophisticated equipment. The gradient-temperature method was not applied in this study.

3.2 Crucible Melts

The traditional time and labor consuming method of crucible melts is still used because of a flexibility of controlling the temperature history of the samples (Lorier 2001). Batches are heated at a controlled rate to a set temperature and then quenched and analyzed. The rate of heating can be an experimental variable. The melts are sectioned, observed visually with optical microscopy, studied with SEM-EDS, and then subjected to XRD analysis.

The outcome of these tests is similar to that achieved by the gradient-temperature furnace treatment, except that the results can be more closely related to the actual furnace conditions because of the flexibility in setting the temperature history. In particular, the dynamics of primary foam formation and breakdown can be observed and photographed. This method was used in this study.

3.3 Differential Thermal Analysis-Thermal Gravimetric Analysis (DTA-TGA) and Differential Scanning Calorimetry (DSC)

These classical analyses have been widely used for batch reaction analyses. Reactions of batch components were studied separately and in various combinations (see the classical works by Wilburn and Thomasson (Thomason and Wilburn 1960, Wilburn and Thomasson 1958). The problem with this method is the smallness of the samples. The reactions are thus influenced by crucible walls and the external atmosphere, and thus they proceed differently from reactions that occur in a large volume of batch in a melter or furnace. Nevertheless, these methods provide valuable information that complements results obtained with other techniques. DTA-TGA was used for this study.

3.4 Evolved Gas Analysis

Evolved gas analysis (Hrma et al. 2002) brought a new insight into the feed conversion process because it determines the time-evolution of individual gaseous species released from batches heated at a constant rate. Gas chromatography and mass spectrometry were used in combination. Evolved gas analysis was not used in the present work.

3.5 Monitoring Feed Volume Changes

The volume changes during heating can be monitored either in loose feeds placed in silica-glass crucibles or in compressed feeds in the form of pellets. A silica-glass crucible was first used by Nemec (Nemec 1974) in his classical study of glass fining. It was later applied by Kim (Kim and Hrma 1990) in his studies of foaming. The silica-glass crucible method allows the feed volume to be precisely measured as the feed first contracts and later expands after the glass-forming melt becomes connected while residual gases are released. The collapse of this primary foam can also be recorded, though this is often difficult in testing opaque glasses.

As an alternative, the pellet method uses compressed feed tablets placed on a solid alumina surface during heating until the feed is fully melted. The primary foam collapse can thus be correctly documented. Whereas the crucible images of cylindrical crucibles allow the determination of the feed volume and feed density as functions of temperature, only the profile area can be evaluated in the case of pellets using simple techniques with Photoshop software. Both techniques were used in this study.

3.6 Flux Migration Testing

Flux migration is suspect as a cause of cold-cap freezing. Inorganic salts in the feed begin to melt at a temperature of 300°C or even lower (the eutectic temperature can be as low as 150°C). Molten salt viscosity is low, comparable to that of water; therefore, molten salts can be highly mobile. Fortunately, molten salts adhere to solid grains by capillary forces. The salts can migrate only when the volume fraction of molten salts exceeds a certain level (Hrma et al. 2007).

The salt-migration tendency can be measured by a method recently developed for LAW feeds (Hrma et al. 2007). The feed is placed into a porous silica crucible and ramp heated to a temperature at which the salts are in molten states but below the temperature at which the feed is fully molten. Feeds are then removed from crucibles that are further heated to complete the salt decomposition reactions. The mass of salts in the crucible and the depth of their penetration are then determined and used for obtaining a quantitative measure for the salt-migration tendency. This technique was used to determine if flux migration is present in Al-Na-limited feed.

3.7 Temperature Field Evolution Monitoring

A method of monitoring the temperature field evolution in high-level waste (HLW) feeds was first used at the Savannah River National Laboratory (Stone and Josephs 2001, Bickford 2004). The feed was placed into a stainless-steel beaker and heated from the bottom while the walls were insulated. The time-temperature evolution was followed with a battery of thermocouples.

A modified version of this method has been used at Pacific Northwest National Laboratory (PNNL) for LAW feeds (Hrma et al. 2007). The feed was placed in a large ceramic crucible that was gradually heated in a furnace. Thermocouples were placed at different positions inside the feed to determine both horizontal and vertical gradients.

The outcome of this method is a map of the temperature field within the feed as it evolves during the conversion process. Materials from different positions within the crucible relate the feed-processing stages to the temperature field.

The method allows the thermal conductivity of the feed to be determined as a function of temperature or the degree of conversion (suitably defined) and thus provides insight into the heat transfer within the cold cap. This, in turn, can allow us to better design diagnostic experiments. Information on the reaction heats and heat capacity of the feed as a function of temperature can also be extracted from the data. This technique was used and is described in detail in the next section.

3.8 Experimental Approach

In this study, all tests performed were scoping in nature following the guidance of the test plan and with nonradioactive HLW feeds. The Nuclear Quality Assurance Requirements Description (NQARD) guidelines for scientific investigation (NQARD-1101), the calibration of laboratory measuring and testing equipment (NQARD-1201), and provisions for identifying samples (NQARD-801) were followed. Precautions were taken over and above those mentioned in the PNNL Integrated Operations System (IOPS) training. Data and observations were recorded on data sheets. Calculations used for scoping tests were performed in Microsoft Excel™, treated as hand-calculations, and independently reviewed. Only laboratory crucible tests were performed in this study; no scale-up tests were accomplished at this stage of investigation.

4.0 Procedures

4.1 VSL Feeds

Two feeds were obtained from VSL, the BL feed and the feed for Al-Na-limited HLW glass, previously used in Duratek melters (Matlack et al. 2007b, 2007c). Because the rates of melting of these feeds in a continuous melter were well documented (see Figure 1.1), and these are substantially different, it was deemed important for this study to test these feeds with respect to their responses to heating, and this preceded the feed variation study.

The feeds arrived in six containers, each containing 2000 mL of slurry. Samples of slurry feeds from VSL were prepared for testing by drying under a heat lamp for 2 to 3 days (Figure 4.1), and, if needed, on a hot plate while constantly stirring with a stainless steel putty knife, and finally in an oven at 105°C overnight. Dry feeds were crushed with a mallet until they passed through a 2-mm sieve (Figure 4.2).

Figure 4.1. Drying VSL Slurry Feeds Under Heat Lamp

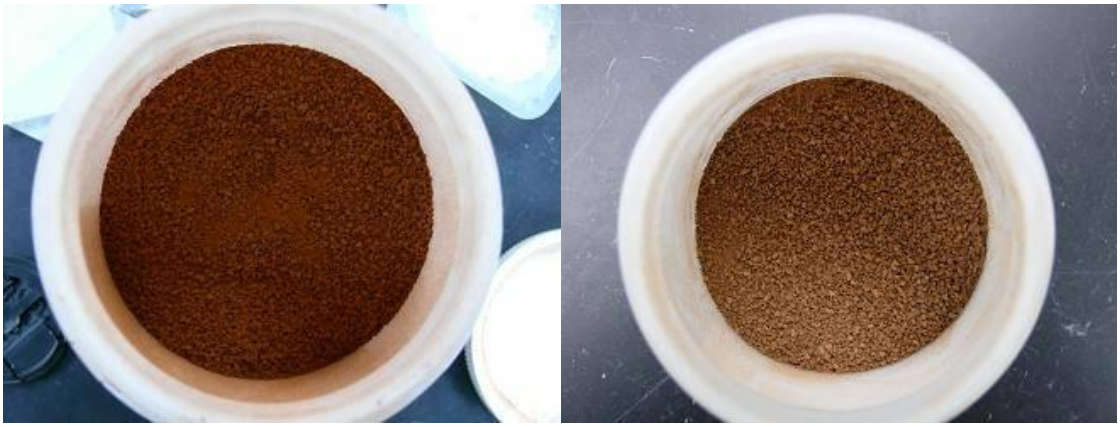

Figure 4.2. Dried Feed Granules: BL (left) and Al-Na-limited (right)

4.2 A-Series Feeds

In addition to the feeds obtained from VSL, we have prepared a series of feeds based on the VSL Al-limited HLW glass. This glass was chosen rather than the Al-Na-limited glass because it allows a greater range for varying the Na content. In all experiments, we had intended to keep the same waste loading as in the VSL glass, but decided to vary feed parameters that may influence the rate of conversion. The spectrum of such parameters can be quite large as the following list indicates.

- Some feed materials are more reactive than others. For example, zircon is more reactive than zirconia, and crushed silica is more reactive than soil aluminosilicates, but less reactive than alkali and alkali earth silicates. The rate of dissolution of refractory particles of the feed in the glass-forming melt is diffusion-controlled; it can be enhanced by the growth and motion of bubbles.
- The size of feed particles, such as fine silica or glass-maker's silica, affects the rate of melting in an intricate way. Fine silica is more reactive than silica sand. However, fine silica and fine alumina increase melt viscosity at early stages where gases are evolved in copious amounts and thus may generate stable primary foam.
- The extent of primary foam may play a double role: on the one hand, it enhances the dissolution of refractory particles by extending and subsequently breaking the bubble-separating films, and on the other hand, the sponge-like configuration may hinder the heat transfer.
- The composition and mineral form of feed additives affect the reaction path.
- The rate of conversion may be affected by the formation of intermediate crystalline phases.
- The presence of persistent molten ionic salts (sulfate) adds to the complexity of the conversion process. The chemical form of the salt (sodium sulfate, calcium sulfate, or iron sulfide) can be influenced by feed additives and reductants.
- The fraction of Li_2O, Na_2O, and B_2O_3 in feed additives affects the viscosity of the low-temperature melt when the more refractory particles are still solid. Lower viscosity and higher alkalinity help remove bubbles and dissolve sulfates and solids.
- Organics are added to feeds as reductants. They provide an internal heat source through exothermic reactions. If used at right proportions, they reduce foaming. Organics first react with oxidizing salts, such as nitrates and nitrites. The excess organics pyrolize (Bickford et al. 1990), turning to fine carbon that reacts with high-valance oxides (Mn_2O_3 and Fe_2O_3).

Based on the need to keep the scope within manageable limits, we settled on the following three series of experiments:

- A-Series, in which glass-forming and modifying additives were varied, starting from the A0-composition, seen in Table 4.1, and developed at VSL (however, the feed formulation was different from that of VSL)
- C- and S-Series, where cellulose or sucrose was added to A0 feed acidified with HNO_3
- A0X series, where silica-grain size was varied from small (~5 μm) to large (~500 μm).

4.2.1 Feed Composition

Table 4.1 presents the VSL formulation of the Al-limited waste glass. The waste and additive compositions are expressed in mass fractions of those constituents that are expected to remain in the final glass (changes caused by oxidation-reduction reactions and component volatilizations are neglected). The original waste composition was modified by removing radioactive components and renormalizing.

Table 4.1. VSL Formulation for Al-limited Waste Glass (Matlack et al. 2007b)

	w_i	a_i	g_i
Al_2O_3	0.5327		0.2397
B_2O_3	0.0042	0.2727	0.1519
CaO	0.0239	0.0909	0.0608
Fe_2O_3	0.1311		0.0590
Li_2O	0.0038	0.0618	0.0357
MgO	0.0026		0.0012
Na_2O	0.0796	0.1091	0.0958
SiO_2	0.1088	0.4655	0.3050
TiO_2	0.0002		0.0001
ZnO	0.0018		0.0008
ZrO_2	0.0088		0.0039
SO_3	0.0044		0.0020
Bi_2O_3	0.0254		0.0114
Cr_2O_3	0.0116		0.0052
K_2O	0.0031		0.0014
BaO	0.0012		0.0005
CdO	0.0005		0.0002
NiO	0.0089		0.0040
PbO	0.0091		0.0041
P_2O_5	0.0234		0.0105
F	0.0148		0.0067
	1.0000	1.0000	1.0000

To ease simulant preparation in the present study, the Al-limited waste composition was further simplified by deleting three minor components, TiO_2, BaO, and CdO, as shown in Table 4.2. This simplified composition was used for formulating all Al-limited test glasses (except the feeds with cellulose additions that had a higher content of Fe_2O_3). The waste loading was kept at a constant level of W=0.45; the content of silica was maintained at the SiO_2 mass fraction in glass of 0.3050 and 0.4655 in additives (see Table 4.1 and Table 4.3).

Table 4.2. Simplified Composition (in mass fraction) of Al-limited Waste

	w_i
Al_2O_3	0.5337
B_2O_3	0.0042
Bi_2O_3	0.0255
CaO	0.0240
Cr_2O_3	0.0116
F	0.0149
Fe_2O_3	0.1313
K_2O	0.0031
Li_2O	0.0038
MgO	0.0026
Na_2O	0.0797
NiO	0.0089
P_2O_5	0.0234
PbO	0.0091
SiO_2	0.1090
SO_3	0.0044
ZnO	0.0018
ZrO_2	0.0088

The additives shown in Table 4.1 contain five glass components; namely, B_2O_3, CaO, Li_2O, Na_2O, and SiO_2. This list was extended for A-Series feeds to contain also MgO. Table 4.3 summarizes the compositions of the additive portions of the six A-Series glasses. Glass compositions that result from mixing 55 mass% of these additives with 45 mass% of the waste composition listed in Table 4.2 is presented in Table 4.4.

Table 4.3. Composition (in mass fraction) of Additives for A-Series Glasses

	A0	A1	A2	A3	A4	A5
B_2O_3	0.2727	0.3000	0.2727	0.2000	0.2145	0.2727
CaO	0.0909	0.0636	0.0909	0.1636	0.0909	0.0455
Li_2O	0.0618	0.0618	0.1200	0.0618	0.1200	0.0847
MgO						0.0455
Na_2O	0.1091	0.1091	0.0509	0.1091	0.1091	0.0862
SiO_2	0.4655	0.4655	0.4655	0.4655	0.4655	0.4655

The components that varied in A-Series glasses are indicated by bold letters in Table 4.4; the red color indicates an increase, and the blue color a decrease in the component mass fraction in comparison to the base glass A0. Table 4.5 shows these changes in terms of proportions of the major oxides.

Table 4.4. A-Series Glass Compositions

	A0	A1	A2	A3	A4	A5
B_2O_3	0.1519	**0.1669**	0.1519	**0.1119**	**0.1199**	0.1519
CaO	0.0608	**0.0458**	0.0608	**0.1008**	0.0608	**0.0358**
Li_2O	0.0357	0.0357	**0.0677**	0.0357	**0.0677**	**0.0483**
MgO	0.0012	0.0012	0.0012	0.0012	0.0012	**0.0262**
Na_2O	0.0959	0.0959	**0.0639**	0.0959	0.0959	**0.0833**
Al_2O_3	0.2402	0.2402	0.2402	0.2402	0.2402	0.2402
Bi_2O_3	0.0115	0.0115	0.0115	0.0115	0.0115	0.0115
Cr_2O_3	0.0052	0.0052	0.0052	0.0052	0.0052	0.0052
F	0.0067	0.0067	0.0067	0.0067	0.0067	0.0067
Fe_2O_3	0.0591	0.0591	0.0591	0.0591	0.0591	0.0591
K_2O	0.0014	0.0014	0.0014	0.0014	0.0014	0.0014
NiO	0.0040	0.0040	0.0040	0.0040	0.0040	0.0040
P_2O_5	0.0105	0.0105	0.0105	0.0105	0.0105	0.0105
PbO	0.0041	0.0041	0.0041	0.0041	0.0041	0.0041
SiO_2	0.3051	0.3051	0.3051	0.3051	0.3051	0.3051
SO_3	0.0020	0.0020	0.0020	0.0020	0.0020	0.0020
ZnO	0.0008	0.0008	0.0008	0.0008	0.0008	0.0008
ZrO_2	0.0040	0.0040	0.0040	0.0040	0.0040	0.0040

Table 4.5. Component Ratios and Alkali Content (R_2O = Li_2O + Na_2O + K_2O, in Mass Fraction) of A-Series Glasses

	A0	A1	A2	A3	A4	A5
B_2O_3/Al_2O_3	0.63	0.69	0.63	0.47	0.50	0.63
Li_2O/Na_2O	0.37	0.37	1.06	0.37	0.71	0.58
B_2O_3/CaO	2.50	3.65	2.50	1.11	1.97	4.24
MgO/CaO	0.02	0.03	0.02	0.01	0.02	0.73
Li_2O/B_2O_3	0.24	0.21	0.45	0.32	0.56	0.32
R_2O	0.13	0.13	0.13	0.13	0.16	0.13

Glasses were formulated solely for testing the impact of the additive composition on the feed behavior during melting. The possible impact on the key glass properties has not been considered. Though it is not expected that these glasses would violate the acceptability requirements, it is possible, for example, that adding Na_2O can promote nepheline formation during the canister centerline cooling. Once the impact of additives on the feed behavior becomes known, it should not be a problem to formulate glasses with preferable melting behavior that also meets various required criteria.

However, one glass property, viscosity, is closely related to the rate of melting (see Section 1.3). Viscosities of A-Series glasses and VSL glasses are compared in Figure 4.3 and Table 4.6. All viscosities were calculated using *A* and *B* coefficients listed in Appendix A, Table 3.

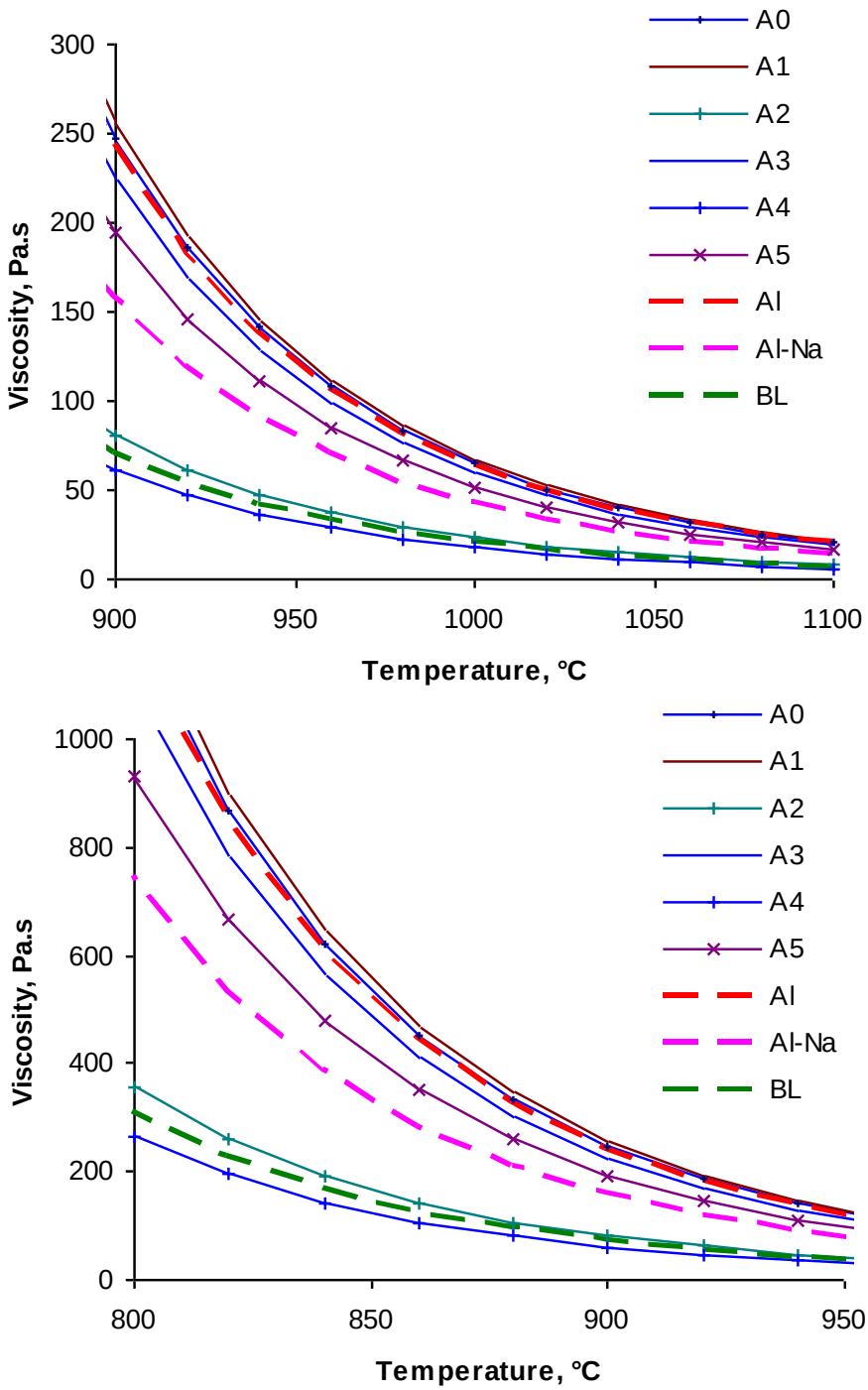

Figure 4.3. Calculated Viscosities of A-Series and VSL Glasses versus Temperature

Table 4.6. Estimated Temperatures (in °C) of A-Series and VSL Glasses at Various Viscosities

η, Pa·s	log(η/Pa·s)	A0	A1	A2	A3	A4	A5	BL	Al	Al-Na
10	1.0	1171	1174	1076	1163	1054	1150	1066	1170	1133
32	1.5	1061	1063	973	1053	952	1041	963	1059	1026
100	2.0	966	968	884	959	865	948	876	965	933
316	2.5	884	886	808	877	789	867	799	883	853

- As indicated in Table 4.4 and Table 4.5, B_2O_3 was increased in Glass A1 at the expense of CaO. This change resulted in a minor increase in the melt viscosity.
- In Glass A2, Li_2O was increased at the expense of Na_2O. This resulted in a substantial decrease in the melt viscosity.
- In Glass A3, CaO was increased at the expense of B_2O_3, resulting in a minor decrease of the melt viscosity.
- In Glass A4, Li_2O was increased at the expense of B_2O_3. This resulted in a large decrease in the melt viscosity.
- Finally, Glass A5 CaO was partially replaced with MgO. To keep the melt viscosity close to that of A0, the Li_2O-to-Na_2O ratio was somewhat increased.

Clearly, the Li_2O/Na_2O ratio has a profound effect on glass viscosity, especially at low temperatures. The B_2O_3/CaO ratio does not substantially affect melt viscosity; however, considering that B_2O_3 is a glass former and CaO a glass modifier, we can expect that these two oxides may affect the melting reactions through the reactivity of low-temperature melts.

If the waste simulant does not correspond to the actual tank waste, the behavior, including the rate of melting, of a feed with such simulant is likely to be different than the behavior of a melter feed with real radioactive waste. Therefore, as mentioned above, when preparing the Al-limited waste simulant, our intention was to make it as close as practically possible (within the scope of the present study) to what we understand constitutes the tank waste. VSL used simulants made from oxides and hydroxides, occasionally of carbonates, and with inorganic anions added in the form of sodium salts (Matlack et al. 2007b, 2007c). Since these oxides can take various forms, such as AlO(OH), $Na_6Ca_2Al_6Si_6O_{24}(CO_3)_2$ (cancrinite), etc., the selection of chemicals for simulant preparation can affect the rate of melting in a major way. This is especially the case of the Al-limited waste that contains 24 mass% of Al_2O_3, 6 mass% of Fe_2O_3, and 30.5 mass% of SiO_2 (in terms of glass oxides, see Table 4.1).

Table 4.7 lists feed recipes for 500 g of glass. Feeds were formulated with waste components similar to those existing in Hanford tanks. Although reactive additives were used, nitrates were avoided to keep in feed only NO_x originating from the waste.

Table 4.7. Feed Composition to Make 500 g Glass

	A0	A1	A2	A3	A4	A5
$Al(OH)_3$	183.74	183.74	183.74	183.74	183.74	183.74
$Bi(OH)_3$	6.40	6.40	6.40	6.40	6.40	6.40
CaO	30.39	22.89	30.39	50.39	30.39	17.89
$Fe(H_2PO_2)_3$	6.21	6.21	6.21	6.21	6.21	6.21
$Fe(OH)_3$	36.91	36.91	36.91	36.91	36.91	36.91
H_3BO_3	134.91	148.23	134.91	99.39	106.49	134.91
KNO_3	1.52	1.52	1.52	1.52	1.52	1.52
Li_2CO_3	44.15	44.15	83.72	44.15	83.72	59.71
$Mg(OH)_2$	0.85	0.85	0.85	0.85	0.85	18.93
$Na_2C_2O_4 \cdot 3H_2O$	0.88	0.88	0.88	0.88	0.88	0.88
Na_2CrO_4	5.57	5.57	5.57	5.57	5.57	5.57
Na_2SO_4	1.78	1.78	1.78	1.78	1.78	1.78
NaF	7.39	7.39	7.39	7.39	7.39	7.39
$NaNO_2$	1.69	1.69	1.69	1.69	1.69	1.69
$NaNO_3$	2.46	2.46	2.46	2.46	2.46	2.46
NaOH	48.53	48.53	27.90	48.53	48.53	40.43
$NiCO_3$	3.18	3.18	3.18	3.18	3.18	3.18
$Pb(NO_3)_2$	3.04	3.04	3.04	3.04	3.04	3.04
SiO_2	152.53	152.53	152.53	152.53	152.53	152.53
$Zn(NO_3)_2 \cdot 4H_2O$	1.33	1.33	1.33	1.33	1.33	1.33
$Zr(OH)_4 \cdot xH_2O$	2.74	2.74	2.74	2.74	2.74	2.74
Total Feed	676.20	682.02	695.14	660.67	687.35	689.25

4.2.2 Feed Preparation

This procedure is to outline the process for preparing HLW simulants for the melt rate testing for high alumina feeds. Feeds for 250 g of glass were made by adding reagent grade chemicals to 750 mL of deionized water (DIW) heated at a temperature of 60 to 80°C and stirred in a beaker with an impeller. Soluble salts of $NaNO_3$, $NaNO_2$, $Na_2C_2O_4$, Na_2SO_4 and $Zn(NO_3)_2 \cdot 4H_2O$ were added first, followed by $Zr(OH)_4 \cdot xH_2O$, Na_2CrO_4, KNO_3 and $Pb(NO_3)_2$, then by NaOH, then by CaO, $Bi(OH)_3$, $Mg(OH)_2$, $NiCO_3$, NaF and $Fe(H_2PO_2)_3$, and finally by the remaining chemicals H_3BO_3, SiO_2, Li_2CO_3, gibbsite, and $Fe_2O_3 \cdot xH_2O$ in that order.

Iron oxyhydrate that was prepared from $Fe(NO_3)_3 \cdot 9H_2O$. The nitrate was dissolved in DIW, mixed with NaOH, decanted, and repeatedly (10 to 15 times) washed with DIW until the pH of the supernate was constant (~10). The content of Fe_2O_3 in the slurry was determined by drying at 105°C followed by heating at 1000°C for 1 h. An impeller on a motor was used to mix the Fe slurry before weighing the amount needed for each feed.

Feed slurries were dried in stainless steel containers under an infrared light source (see Figure 4.1) until most water was evaporated and then on a hot plate with continuous stirring by hand with a stainless steel putty knife until the feed dried into hard, small clods. Drying was finished in an oven at 105°C overnight. Dry feeds were crushed with a mallet until they passed through a 2-mm sieve (see Figure 4.2).

4.2.3 Feeds with Nitric Acid and Cellulose or Sucrose

For testing the impact of the internal heat source, C- and S- Series feeds were made from A0 feed to which HNO_3 was added in the amount to reach pH 1 (from the initial pH 11) and then mixed with cellulose ($C_6H_{10}O_5$) or sucrose ($C_{12}H_{22}O_{11}$) to reach various C/N atomic ratios. Four C feeds were prepared as listed in Table 4.8. As mentioned above, C1, C2, and C3 feeds were prepared with excess iron (by 30%). This was caused by an error in calculation that passed undetected until the feeds were prepared. An additional feed, C1-2, was made with the correct iron content. Feeds C1 and C1-2 were acidified to pH 1, but no carbon source was added to them. Feeds with cellulose and correct iron content were not prepared. Instead, feeds were made with sucrose addition, listed in Table 4.9.

Table 4.8. Nitric Acid and Cellulose Additions to A0 Slurry Feed in the Amount to Make 250 g Glass

	HNO_3 (g)	Cellulose (g)	C/N
C1[(a)(b)]	316	0	-
C1-2	180	0	-
C2[(b)]	158	51.42	0.75
C3[(b)]	158	102.48	1.50

(a) The amount of HNO_3 to feed for 500-g glass (no cellulose added).
(b) Feeds C1, C2, and C3 contained 30% more Fe_2O_3 than A0 feed.

Table 4.9. Nitric Acid and Sucrose Additions to A0 Slurry Feed in the Amount to Make 250 g of Glass

	HNO_3 (g)	Sucrose (g)	C/N
S2	180	61.75	0.75
S3	180	123.50	1.50
S4	180	82.34	1.00
S5	180	74.10	0.90

4.2.4 Silica Grain Size Variation

The original A0 feed contained ~75-μm grains; A0S feed was A0 feed with fine silica (≤ 5 μm), and glass-maker's silica sand (350 to 850 μm) was used in A0L feed.

4.3 Testing Procedures

4.3.1 DTA-TGA

Feed samples for TGA-DTA were ground with a mortar and pestle; the analysis was applied to each feed.

4.3.2 Feed-Expansion Testing

To measure the volume changes of feeds in response to heating, 1.50 g of feed was pressed at 1000 psi to form a pellet 1.27 cm diameter and 0.6 cm thick. A pellet from each feed was placed on a solid alumina plate into a furnace. The furnace temperature was programmed to increase at 5°C/min to 1000°C and was then held for 30 minutes. Pictures were taken periodically through an opening in the furnace to monitor the expansion and collapse of the pellets. Volume changes were also measured with 21.8 g of loose dry feed samples placed in a cylindrical silica-glass crucible (11 cm height, 4.6 cm diameter). The furnace

temperature was programmed to increase 5°C/min to 1000°C; this temperature was then held for 30 minutes. Photographs were taken at regular intervals through an open window that allowed viewing the crucible. The images were evaluated to obtain the sample height and also, when possible, the sample volume.

4.3.3 Flux-Migration Testing

Flux-migration testing was performed for VSL Al-Na-limited feed only. An empty clay-type crucible was heat-treated in a silica crucible at 500°C for 1 hour and then cooled for 2 hours. Feed was then added to the clay crucible and heated from room temperature to 500°C at 5°C/min. After cooling for 2 hours, feed was removed. The empty crucible was heated from 650°C to 1000°C at 7°C/min and cooled for 2 hours. The crucible was weighed, and the fraction of molten ionic salt that migrated from the feed to the crucible walls was calculated.

4.3.4 Visual Observation, XRD, and SEM-EDS Analysis

To observe the response of HLW feed simulants to heating, 10-g samples of dry feed were placed into small ceramic crucibles (30-mm bottom diameter), heated at 5°C/min to desired temperature (500 to 1000°C by 100°C steps), and then air-quenched. Samples were sectioned, examined by optical microscopy, thin-sectioned for SEM-EDS examination, powdered, and then scanned by XRD.

4.3.5 Temperature Field Evolution and Heat Conductivity

To measure the temperature field evolution, feed was placed in a silica crucible 200 mm tall and 135 mm outer diameter. Fourteen type-K (chromel-alumel) thermocouples (TCs) were arranged inside the feed in three horizontal arrays 1 cm apart vertically along radial lines from the centerline to the crucible wall (Figure 4.4). The TCs were placed into the crucible first, then the bottom layer of TCs 123 mm from the crucible top, and finally the feed was added to the depth of 95 mm from the top of the crucible—the mass of the feed ranged from 271 to 490 g. An additional TC was placed near the outer wall of the crucible to measure the external temperature. The TCs were connected to a Fluke HYDRA data system that recorded the temperatures every minute for the duration of the test. The furnace temperature was programmed to increase at 5°C/min from room temperature to 1000°C and then held at 1000°C until a nearly uniform temperature was established throughout the sample. After the completion of a run, the TCs were removed, and the crucible was sectioned at the outer TC position to measure the crucible wall thickness.

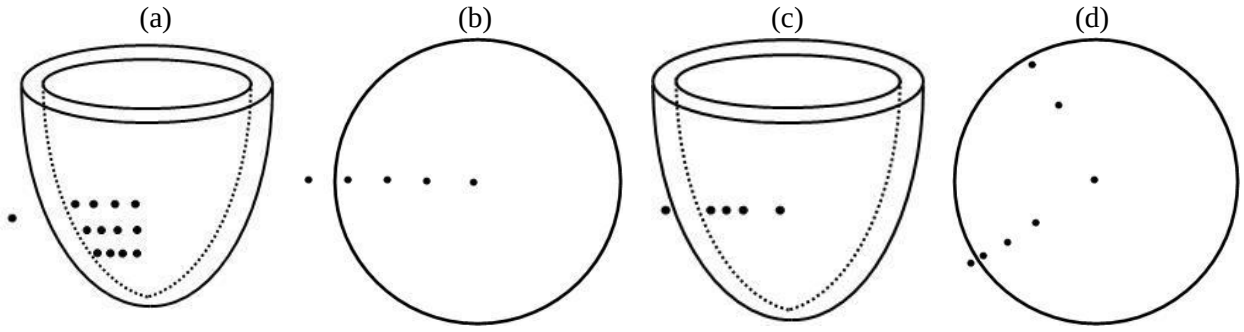

Figure 4.4. Initial TC Placement, Side-view (a) and Top-view (b); Revised TC Placement, Side-view (c), and Top-view (d)

After several runs, it was evident that the middle layer of TCs gave sufficient data; the other layers merely confirmed that the vertical temperature gradient was nearly zero within the small vertical area of 20 mm between the upper and lower layer of TCs. Using only one layer of TCs allowed a reduction in the complexity involved in setting up 14 TCs in a small area. In the one-layer arrangement (Figure 4.4c and d), six TCs were arranged in a wedge pattern, and the external TC was tied to the crucible via a platinum wire that was threaded through a small hole cut above the level of the feed and also tied to the TC placed against the inner wall of the crucible. The outside TC was covered with a thin layer (~0.5 mm) of refractory cement to accurately measure the temperature at the outer surface of the crucible. Thermocouples were calibrated using molten salts. See Appendix C for details.

Runs were conducted on the following feeds:

- Two feeds obtained from VSL
- A-Series feeds based on Al-limited waste
- S-Series feeds prepared by acidifying A0 feed with HNO_3 and mixing with various additions of sucrose with C/N of 0.75, 0.9, 1.0, and 1.5
- C-Series feed; only one C-Series feed was tested with C/N = 1.5.

To calculate the heat conductivity of feeds, it was necessary to know the heat conductivity of the crucible material (λ_c), the thickness of the crucible wall (h), the temperature difference across the crucible wall (ΔT_c), and the temperature gradient ($\partial T/\partial x$) at the crucible-feed interface where x is the horizontal distance. By Fourier's law, the heat flux (q) through the interface is

$$q = \lambda_f \frac{\Delta T_c}{h} = -\lambda_c \frac{\partial T}{\partial x} \tag{4.1}$$

Hence,

$$\lambda_f = -\lambda_c \frac{\Delta T_c}{h} \frac{1}{\partial T/\partial x} \tag{4.2}$$

Equation (4.2) was used to calculate the heat conductivity of feeds within the temperature interval where a quasi-steady state was established. See Figure 4.5 for an illustration of the temperature profile.

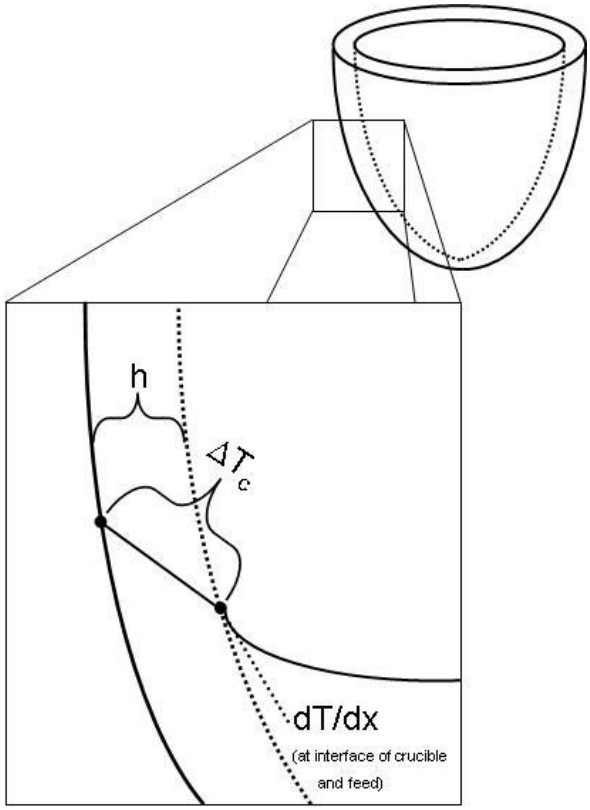

Figure 4.5. Graphical Representation of Temperature Profile

5.0 Results

5.1 VSL Feeds

5.1.1 Salt Migration Test

The mass fractions of water-soluble salts in VSL feed are listed in Table 5.1. Thus, dry Al-Na-limited feed contains 24.1 mass% of water-soluble salts other than borates. These salts turn into a single molten ionic salt phase at an elevated temperature. Assuming that H_3BO_3 became dissolved in this molten ionic salt phase, the mass fraction would increase to 49.6 mass%.

Table 5.1. Ionic Salt Mass Fractions in the BL and Al-Na-Limited VSL Feeds

	Baseline	Al-Na
Ionic Salt	0.0911	0.2414
Ionic Salt +Borate	0.4534	0.4962

The mass fraction of feed that migrated into the crucible at 500°C was 0.011±0.005; after heating at 1000°C, it decreased to 0.003±0.001. This small fraction was within experimental error, and no migrated salt was visible when the crucibles were cross-sectioned for examination (see Figure 5.1). This low mobility of molten salt within the feed can be attributed to the large specific surface area of the feed solids; a large volume of molten salt is immobilized by wetting feed solid particles, and virtually no molten salt can freely move. We can conclude that molten salt migration is unlikely to occur in the melter feed, and thus HLW cold caps are unlikely to freeze (harden) in the melter. Therefore, the test was not repeated for any other HLW feed used in this study.

Figure 5.1. Cross-Sectioned Silica Crucible After Salt-Migration Tests; VSL BL Feed (left) and Al-Na-Limited Feed (right)

5.1.2 Crucible Melts

Figure 5.2 and Figure 5.3 display photographs of feeds (VSL BL and Al-Na-limited) exposed to ramp heating at 5°C/min. The BL feed became compact at 600°C; the sample could be sectioned without

crumbling; the Al-Na-limited feed sample could be sectioned only when heated to 700°C. Both feeds produced bubbly melts. Smaller bubbles first coalesced to larger bubbles that escaped from the melt; the remaining small bubbles were no longer seen in the BL sample at 1000°C but still prevailed at this temperature in the Al-Na-limited glass sample. This slower removal of bubbles can only be caused by the high viscosity of the Al-Na-limited glass melt. The viscosity of this melt was twice as high at 900°C as that of the BL glass (see Figure 4.3). Hence, the nearly twice as high rate of melting of the BL glass as compared to Al-Na-limited glass could be at least partly attributed to its higher viscosity.

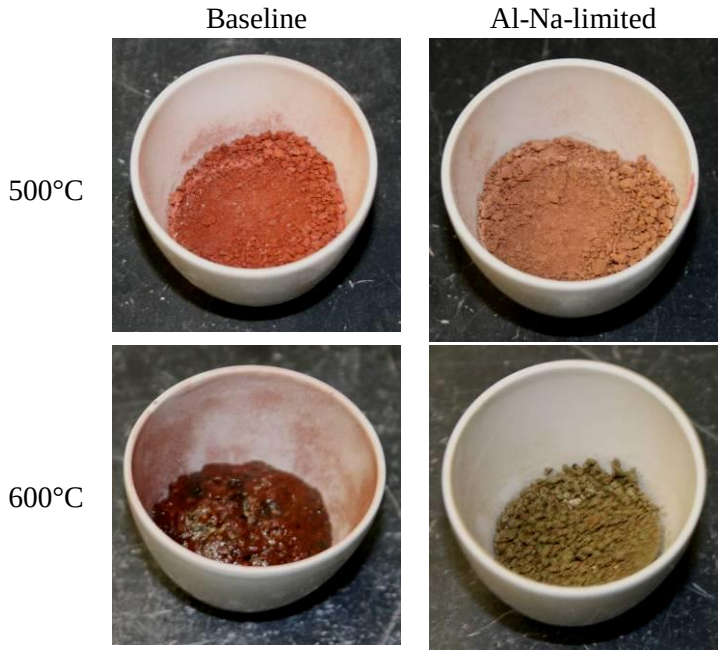

Figure 5.2. Feed Samples (VSL BL and Al-Na-limited) Heated at 5°C/min to 500 and 600°C

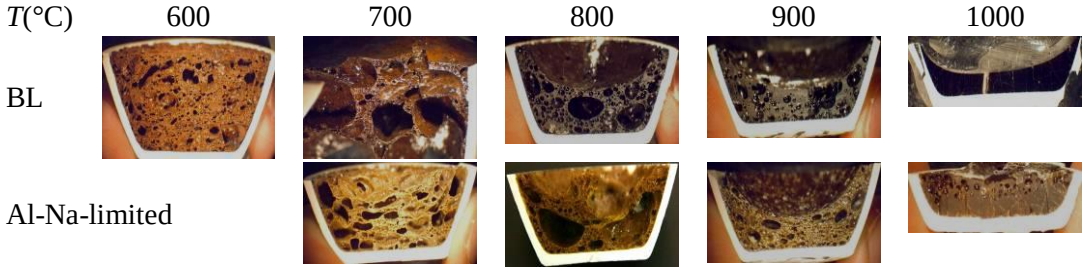

Figure 5.3. Cross-sections of Feed Samples (VSL BL and Al-Na-limited) Heated at 5°C/min to Temperatures from 600 to 1000°C

5.1.3 XRD

The XRD results are listed in Table 5.2 through Table 5.5. The first two tables show data based on the CaF_2 in the sample; the last two show crystal mass fractions with respect to the room-temperature mass of the feed (based on the TGA data). As Figure 5.4 indicates, the difference does not present a major correction to the data. Whatever data set is used, it appears that very little silica reacts with feed fluxes at

a temperature below 400°C; a small silica residue exists at 900°C whereas all silica is dissolved by 1000°C in both feeds (Figure 5.5). Even though the initial silica fraction was smaller in the Al-Na-limited feed; the kinetics of dissolution is probably more affected by the silica grain size than by the feed composition.

Table 5.2. Crystalline Phases in VSL BL Feed (mass fractions in sample)

T, °C	25	500	600	700	800	900	1000
Silica	0.436	0.327	0.270	0.137	0.072	0.070	
Corundum	0.021	0.018	0.010				
Hematite	0.058	0.100	0.050	0.018			
Spinel			0.116	0.108	0.054	0.044	0.034
Lithium borate		0.021					
Total	0.515	0.466	0.446	0.263	0.126	0.114	0.034

Table 5.3. Crystalline Phases in Al-Na-limited Feed (mass fractions in sample)

T, °C	25	500	600	700	800	900	1000
Silica	0.265	0.205	0.135	0.077	0.067	0.013	0.004
Corundum	0.168	0.198	0.109	0.048	0.008		
Magnetite						0.004	0.002
Nepheline			0.036	0.030			
Chromium oxide	0.010						
Lithium carbonate	0.040						
Magnesium phosphate		0.008					
Sodalite and Nosean		0.029	0.088	0.111	0.097		
Sodium borate	0.080	0.064					
Total	0.563	0.504	0.368	0.266	0.172	0.017	0.006

Table 5.4 and Table 5.5 are renormalized as a mass fraction of the original feed (based on TGA data below):

Table 5.4. Crystalline Phases in VSL BL Feed (mass fraction in original feed)

T, °C	25	500	600	700	800	900	1000
TGA factor	1.000	0.902	0.866	0.860	0.856	0.854	0.854
Silica	0.436	0.362	0.312	0.159	0.084	0.082	
Corundum	0.021	0.020	0.012				
Hematite	0.058	0.111	0.058	0.021			
Spinel			0.134	0.126	0.063	0.052	0.040
Lithium borate		0.023					
Total	0.515	0.516	0.515	0.306	0.147	0.133	0.040

Table 5.5. Crystalline Phases in Al-Na-Limited Feed (mass fraction in original feed)

T, °C	25	500	600	700	800	900	1000
TGA Factor	1.000	0.901	0.889	0.888	0.887	0.887	0.887
Silica	0.265	0.228	0.152	0.087	0.076	0.015	0.005
Corundum	0.168	0.22	0.123	0.054	0.009		
Magnetite						0.005	0.002
Nepheline			0.041	0.034			
Chromium oxide	0.01						
Lithium carbonate	0.04						
Magnesium phosphate		0.009					
Sodalite and Nosean		0.032	0.099	0.125	0.109		
Sodium borate	0.08	0.071					
Total	0.563	0.560	0.414	0.299	0.194	0.019	0.007

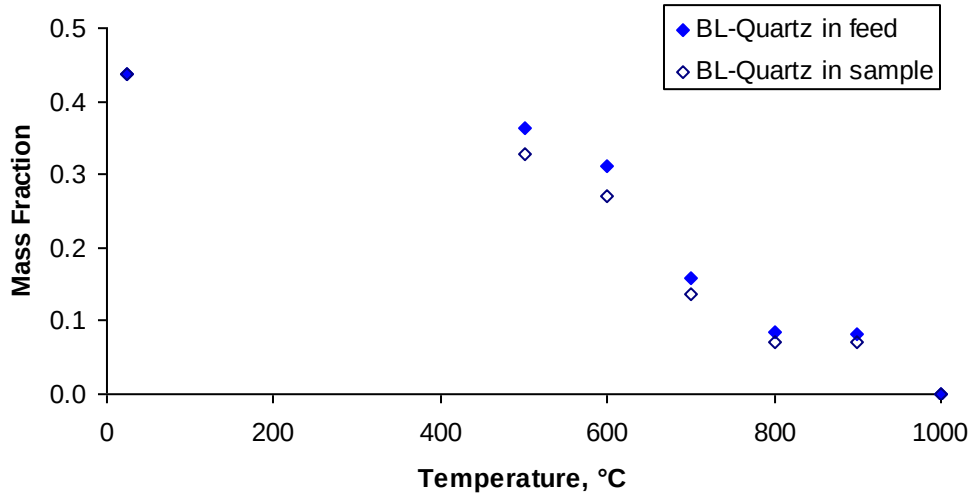

Figure 5.4. Fraction of Silica (Quartz) in VSL BL Feed Versus Temperature

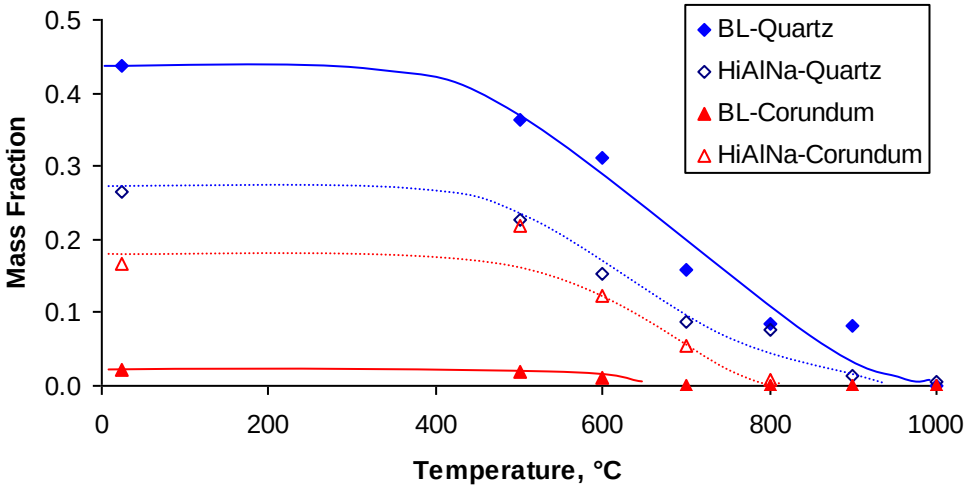

Figure 5.5. Fraction of Silica (Quartz) and Alumina (Corundum) with Respect to Room-Temperature BL and Al-Na-limited (HiAlNa) Feeds (the lines are drawn to guide the eyes)

Figure 5.6 displays the fractions of several intermediate crystalline phases in both VSL feeds as a function of temperature. Hematite is not a true intermediate phase, but can be considered as such provided that the room-temperature Fe_2O_3 was in the form of a colloidal oxyhydrate. Spinel was extremely difficult to identify because it can contain various elements, including Fe, Cr, Mg, Mn, Zn, and Li, that influence the XRD pattern. Spinel formed from hematite starting at 500°C and peaked just above 600°C. After hematite dissolved below 800°C, spinel was gradually dissolving, but remained in glass even at 1000°C, the temperature at which the heat treatment was terminated. Whereas iron-containing intermediate phases were dominant in the BL feed, aluminosilicates phases formed in the Al-Na-limited feed. Both nepheline and ionic salts-containing aluminosilicates appeared at temperatures above 400°C and were gone at 900°C.

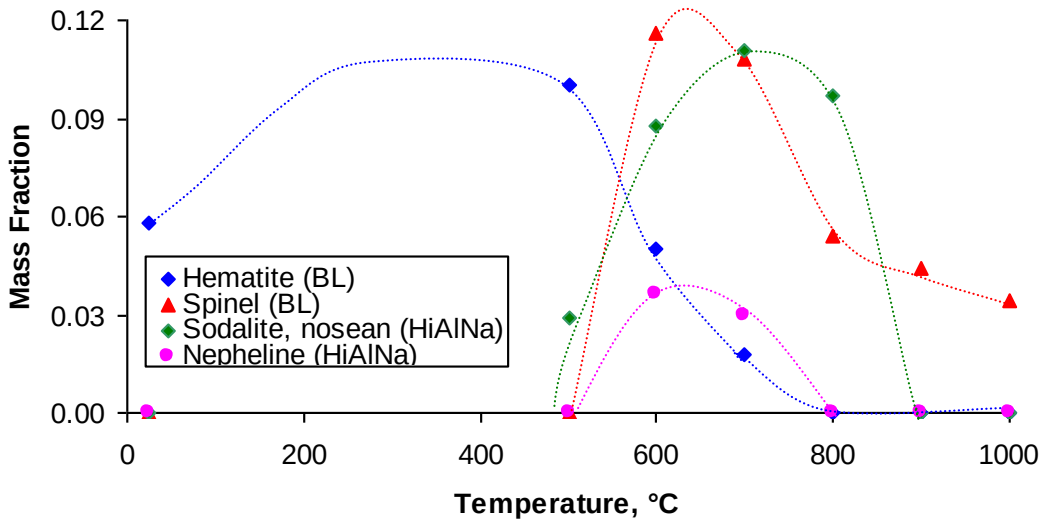

Figure 5.6. Fraction of Intermediate Crystalline Phases in Samples of BL and Al-Na-Limited (HiAlNa) Feeds (the lines are drawn to guide the eyes)

5.1.4 SEM-EDS

SEM images of feeds heat-treated to various temperatures are shown in Figure 5.7 through Figure 5.11 for the BL and in Figure 5.12 through Figure 5.15 for the Al-Na-limited feed. EDS data are listed in Table 5.6 through Table 5.10 for the BL and in Table 5.11 through Table 5.14 for the Al-Na-limited samples.

For the BL feed heat-treated to 600°C, the white particles in the top middle image in Figure 5.7 are crystals of hematite or possibly aegirine ($NaFeSi_2O_6$), based on the No. 1 composition in Table 5.6. The gray connected mass No. 2 in Table 5.6 is the glass phase. The box 1 in Figure 5.7, top right image, is a dissolving crystal of silica—see No. 3 in Table 5.6. A large spherolite in the bottom left and middle image in Figure 5.7, box 2 (No. 4 in Table 5.6) represents spinel, probably hausmannite, Mn_3O_4, or hetaerolite, $ZnMnO_4$. The white cluster of tiny crystals in Figure 5.7 (bottom right and left images) appears to have a composition (see No.5) close to almandine ($Fe_3Al_2Si_3O_{12}$), though the presence of this garnet is rather unlikely; hematite would be a better guess.

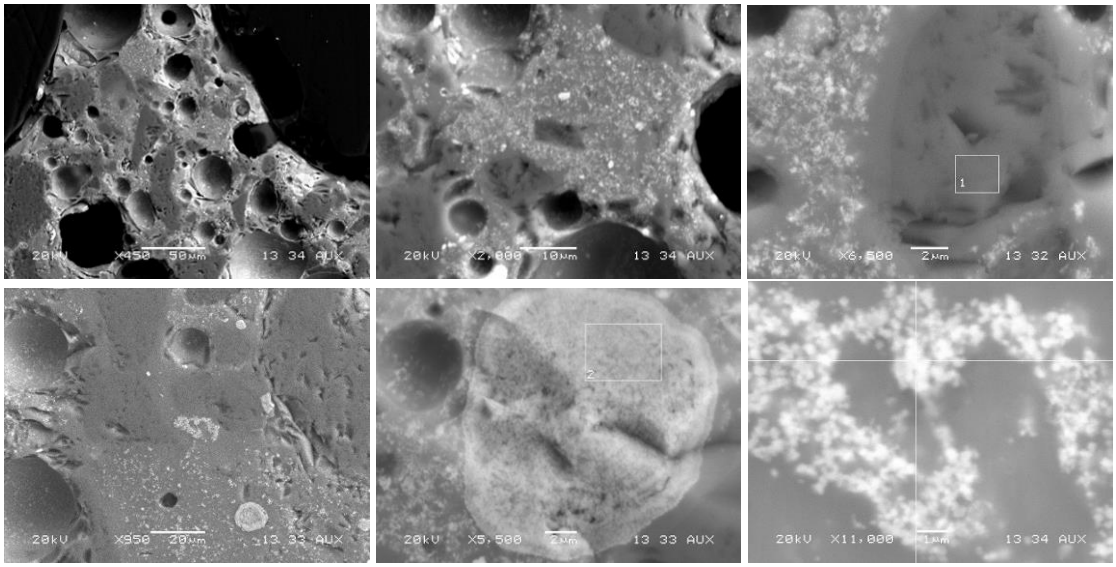

Figure 5.7. SEM Images of BL Feed Heat-Treated at 5°C/min to 600°C

Table 5.6. Atomic Fractions from EDS Analysis of Cations of Phases Shown in Figure 5.7[(a)]

	1	2	3	4	5	B
Al	0.02	0.04		0.02	0.15	0.067
Fe	0.16	0.16			0.35	0.102
Mg	0.05	0.03		0.10	0.06	0.019
Mn	0.06			0.63	0.01	0.037
Na	0.29	0.28				0.248
Ni	0.01					0.001
Si	0.35	0.44	1.00	0.19	0.40	0.509
Zn	0.06	0.03		0.06	0.03	0.017

Column B shows nominal BL glass composition in cations normalized to elements listed in the table.

Figure 5.8 presents images of BL feed heated to 700°C. The gray object (No. 12 in Table 5.7, see the box in the middle image, Figure 5.8) is a dissolving silica particle. The white round objects in the middle image, Figure 5.8 (No. 13 in Table 5.7) is spinel hausmannite (Mn_3O_4). The gray porous round object in Figure 5.8 (No. 14 in Table 5.7) is corundum, and the black irregular hexagon in the right image of the same figure (see the box) could be franklinite $(Fe,Mn,Zn)(Fe,Mn)_2O_4$ if one believes that the composition is listed as No. 15 in Table 5.7 (but the dark color casts doubt on it; this item should be rechecked in future studies).

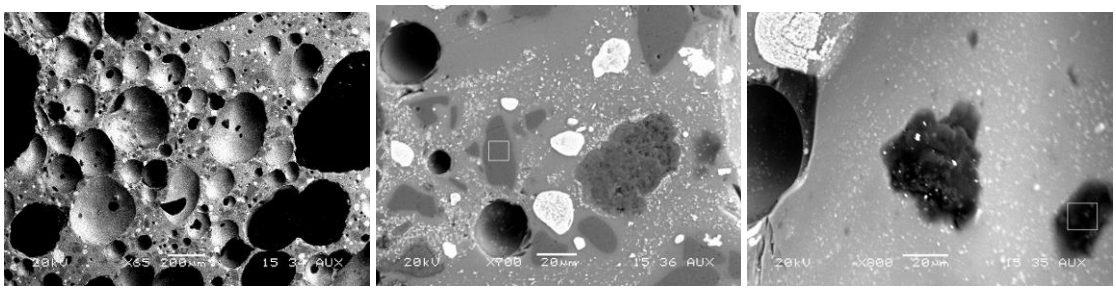

Figure 5.8. SEM Images of BL Feed Heat-Treated at 5°C/min to 700°C

Table 5.7. Atomic Fractions from EDS Analysis of Cations of Phases Shown in Figure 5.8[(a)]

	12	13	14	15	B
Al		0.03	0.98	0.03	0.067
Fe				0.56	0.103
Mg		0.06		0.03	0.019
Mn		0.69		0.06	0.037
Na			0.02		0.249
Si	1.00	0.17		0.24	0.509
Zn		0.05		0.09	0.017

Column B shows nominal BL glass composition in cations normalized to elements listed in the table.

Figure 5.9 shows SEM images of the BL feed heat-treated to 800°C. The white round object (Figure 5.9, middle; No. 21 in Table 5.8) is spinel, most likely a hausmanite-franklinite solid solution. In Figure 5.9, right, the white elliptical object (No. 22 in Table 5.8) is spinel franklinite, the dark-gray rounded object with a fractured interior (No. 23 in Table 5.8) is silica, and the small white round object in the bottom right corner (No. 24 in Table 5.8) is spinel magnetite-jacobsite-trevorite ($MnFe_2O_4$-$NiFe_2O_4$).

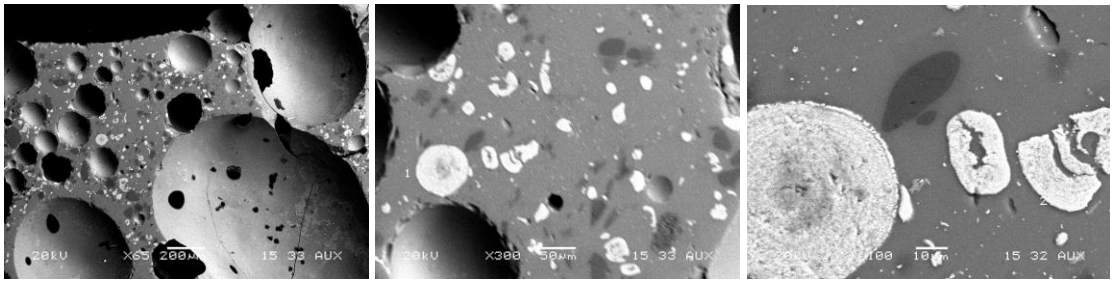

Figure 5.9. SEM Images of BL Feed Heat-Treated at 5°C/min to 800°C

Table 5.8. Atomic Fractions from EDS Analysis of Cations of Phases Shown in Figure 5.9[(a)]

	21	22	23	24	B
Al	0.04	0.03		0.04	0.067
Fe	0.07	0.20		0.37	0.103
Mg	0.06	0.04		0.04	0.019
Mn	0.54	0.41		0.11	0.037
Ni				0.04	0.249
Si	0.24	0.24	1.00	0.34	0.509
Zn	0.05	0.07		0.05	0.017

Column B shows nominal BL glass composition in cations normalized to elements listed in the table.

At 900°C (Figure 5.10), the BL feed turned mostly to glass—see the light-gray connected area (No. 31 in Table 5.9 presents the composition corresponding to box 1 in the left image of Figure 5.10). The accumulation of submicron white crystals is shown in the middle image. Their composition matches spinel jacobsite (No. 32 in Table 5.9). Silica particles still persist—see the dark-gray rounded object on the right (No. 33 in Table 5.9).

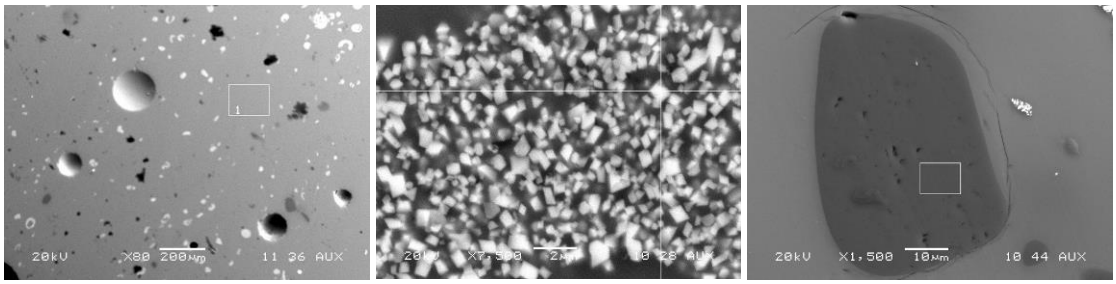

Figure 5.10. SEM Images of BL Feed Heat-Treated at 5°C/min to 900°C

Table 5.9. Atomic Fractions from EDS Analysis of Cations of Phases Shown in Figure 5.10[(a)]

	31	32	33	B
Al	0.07	0.04	0.01	0.067
Fe	0.08	0.25		0.102
Mg	0.02	0.04		0.019
Mn	0.03	0.16		0.037
Na	0.22	0.17		0.248
Ni		0.02		0.001
Si	0.56	0.28	0.99	0.509
Zn	0.02	0.05		0.017

Column B shows nominal BL glass composition in cations normalized to elements listed in the table.

Finally, at 1000°C, the BL feed sample consists almost entirely of glass—the gray connected area (No. 36 in Table 5.10). The white melting crystals (Figure 5.11, middle and right, No 37 in Table 5.10) are those of spinel $(Ni,FeMg,Mn)(Fe,Cr)_2O_4$.

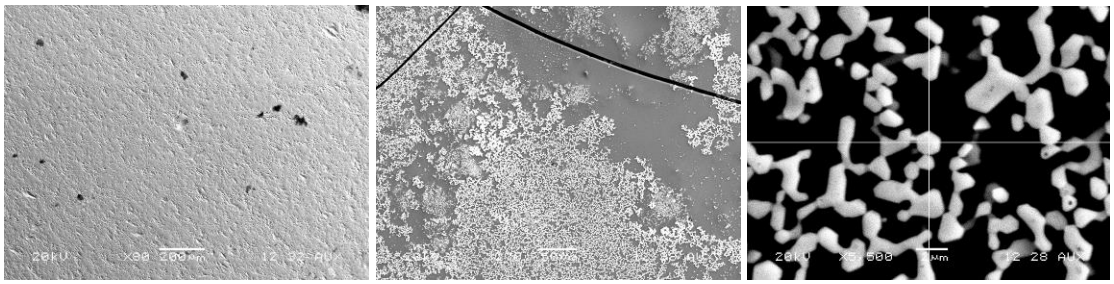

Figure 5.11. SEM Images of BL Feed Heat-Treated at 5°C/min to 1000°C

Table 5.10. Atomic Fractions from EDS Analysis of Cations of Phases Shown in Figure 5.11[(a)]

	36	37	B
Al	0.08	0.11	0.067
Cr		0.02	0.001
Fe	0.08	0.22	0.102
Mg	0.03	0.04	0.019
Mn	0.03	0.08	0.037
Na	0.22	0.19	0.248
Ni		0.03	0.001
Si	0.55	0.28	0.508
Zn	0.02	0.04	0.017

Column B shows nominal BL glass composition in cations normalized to elements listed in the table.

Thin sections could be made from the Al-Na-limited feed only of a sample heated to the minimum temperature of 700°C. The early glass composition (except B and Li) is listed as No. 6 in Table 5.11 (the box in the connected gray area in the top right image in Figure 5.12). The dark small irregular objects in the same image could be inclusions of phosphate glass (see No. 7 in Table 5.11). The small white grains between bubbles in top middle image, magnified at the bottom left of Figure 5.12, are particles of corundum (No. 8. in Table 5.11). The white object and tiny gray objects inside the bubble are magnified in the bottom middle image and correspond to either eskolaite (Cr_2O_3) or chromate (Na_2CrO_4)—see No. 9 and nepheline (No. 10), respectively. The tiny black objects inside the bubble shown in the bottom right image are crystals of nepheline (see No 11 in Table 5.11).

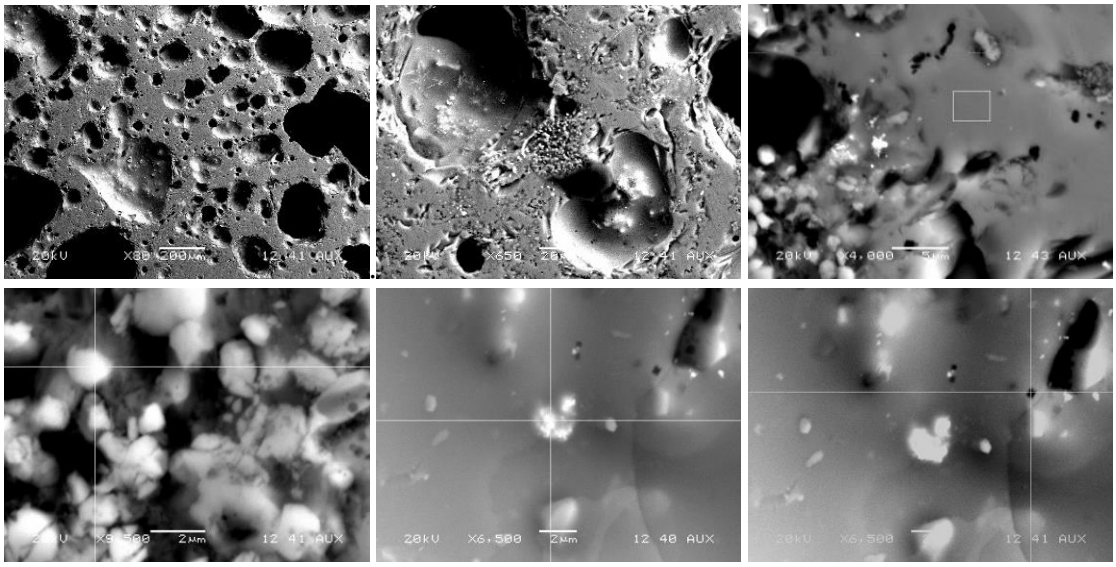

Figure 5.12. SEM Images of Al-Na-Limited Feed Heat-Treated at 5°C/min to 700°C

Table 5.11. Atomic Fractions from EDS Analysis of Cations of Phases Shown in Figure 5.12[(a)]

	6	7	8	9	10	11	H
Al	0.24	0.20	0.82	0.18	0.27	0.36	0.280
Bi	0.01	0.01		0.01	0.01		0.003
Ca	0.01	0.01	0.02	0.01	0.02	0.02	0.009
Cr		0.01		0.34		0.03	0.006
Fe	0.04	0.04		0.04	0.05	0.02	0.024
Na	0.20	0.13	0.15	0.16	0.19	0.17	0.274
P	0.03	0.17	0.01	0.01	0.02	0.02	0.019
Si	0.47	0.43	0.01	0.25	0.43	0.39	0.385

Column H shows nominal Al-Na-limited glass composition in cations normalized to elements listed in the table.

In a polished sample of Al-Na-limited feed heat-treated to 800°C at 5°C/min, the ghost-like gray irregular object in the middle image (Figure 5.13) is nepheline (columns 16-18 in Table 5.12). The white needles (Figure 5.13, right) are crystals of calcium phosphate (No. 19, Table 5.12). The two white spherolites on the right, top left corner (Figure 5.13) are eskolaite (No. 20, Table 5.12).

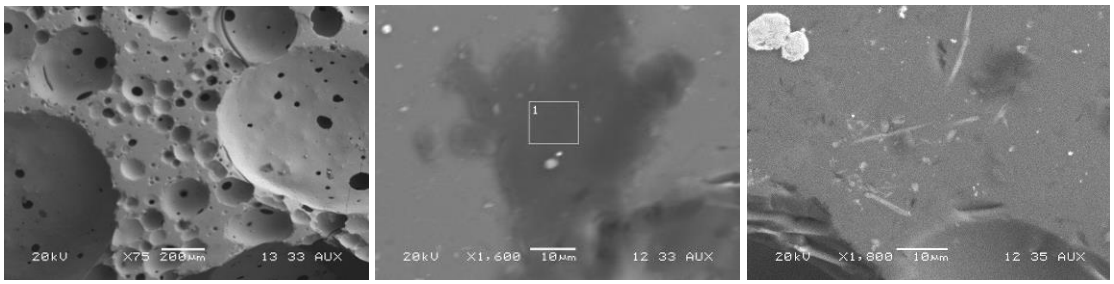

Figure 5.13. SEM Images of Al-Na-Limited Feed Heat-Treated at 5°C/min to 800°C

Table 5.12. Atomic Fractions from EDS Analysis of Cations of Phases Shown in Figure 5.13[(a)]

	16	17	18	19	20	H
Al	0.33	0.26	0.31	0.14	0.02	0.279
Bi	0.01	0.01	0.01			0.003
Ca	0.01	0.01	0.01	0.34		0.009
Cr	0.01		0.01		0.95	0.006
Fe	0.02	0.02	0.03	0.01		0.023
Mg	0.01	0.01	0.01			0.004
Na	0.23	0.41	0.24	0.12		0.273
P	0.03	0.02	0.02	0.24		0.019
Si	0.36	0.27	0.37	0.15	0.03	0.383

Column H shows nominal Al-Na-limited glass composition in cations normalized to elements listed in the table.

At 900°C, most of the Al-Na-limited sample was a connected amorphous phase as seen in Figure 5.14 left (see No. 25 and 29 in Table 5.13). Rounded silica particles are barely visible in the left image (see No. 30 in Table 5.13). Spinel forms a cluster of small white crystals in the middle image in Figure 5.14 (see No. 26 in Table 5.13). The white and gray irregular objects in the right image (Figure 5.14) are nepheline (Table 5.13, No. 27 and 28).

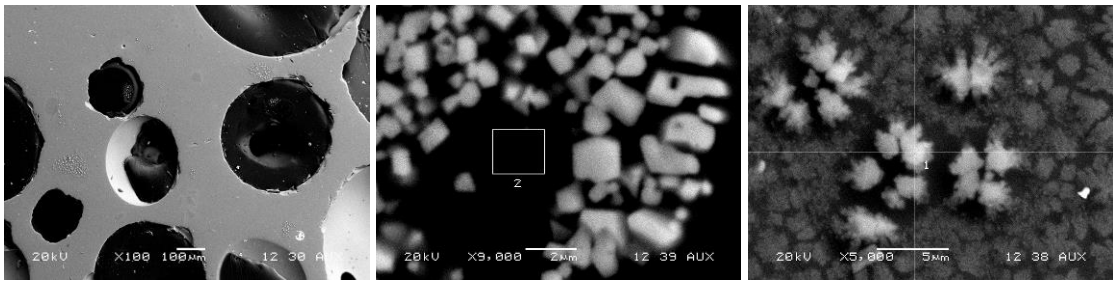

Figure 5.14. SEM Images of Al-Na-Limited Feed Heat-Treated at 5°C/min to 900°C

Table 5.13. Atomic Fractions from EDS Analysis of Cations of Phases Shown in Figure 5.14[(a)]

	25	26	27	28	29	30	H
Al	0.31	0.21	0.20	0.27	0.29	0.01	0.278
Bi					0.01		0.003
Ca	0.01	0.01	0.01	0.01			0.009
Cr	0.01	0.02		0.01			0.006
Fe	0.03	0.34		0.03			0.023
Mg		0.02		0.00	0.01		0.004
Na	0.23	0.15	0.49	0.21	0.18		0.273
Ni		0.06	0.02				0.001
P	0.02	0.01	0.01	0.03	0.03		0.019
Si	0.38	0.15	0.27	0.44	0.49	0.99	0.383
Zn		0.03					0.001

Column H shows nominal Al-Na-limited glass composition in cations normalized to elements listed in the table.

The glass phase in Al-Na-limited feed heated to 1000°C (Figure 5.15, No. 34 in Table 5.14) contains many bubbles with tiny crystals on their surfaces (see the middle and right image in Figure 5.15). According to EDS analysis (No. 35 in Table 5.14), these are crystals of spinel chromite ($FeCr_2O_4$).

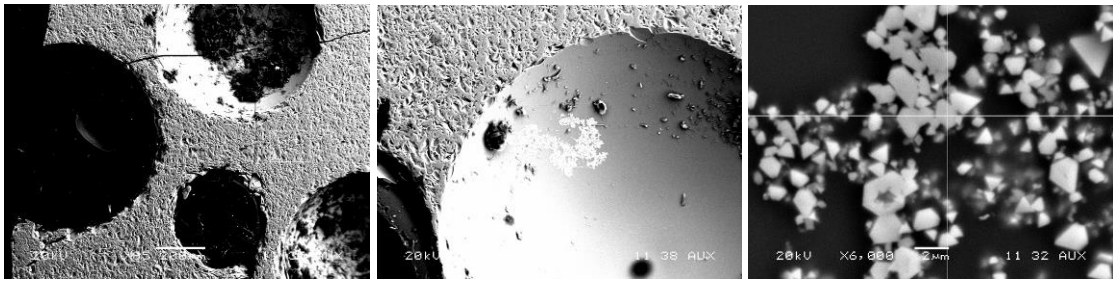

Figure 5.15. SEM Images of Al-Na-Limited Feed Heat-Treated at 5°C/min to 1000°C

Table 5.14. Atomic Fractions from EDS Analysis of Cations of Phases Shown in Figure 5.15[(a)]

	34	35	H
Al	0.28	0.14	0.283
Ca	0.01	0.01	0.010
Cr	0.01	0.30	0.009
Fe	0.02	0.17	0.037
Mg	0.00	0.02	0.003
Na	0.23	0.13	0.169
Ni		0.03	0.001
P	0.02	0.01	0.027
Si	0.42	0.12	0.459
Zn		0.07	0.002

Column H shows nominal Al-Na-limited glass composition in cations normalized to elements listed in the table.

Table 5.15 and Table 5.16 summarize the results of EDS and XRD analyses, showing that the XRD and EDS data mostly agree, even though some crystals detected by XRD were not found by SEM, or some crystals seen with SEM were present in an insufficient concentration for XRD.

Table 5.15. Crystalline Phases Detected with EDS (Y) and XRD (y) Analyses in the BL Feed Heated to Various Temperatures at 5°C/min

T, °C	600	700	800	900	1000
silica	Yy	Yy	Yy	Yy	
corundum	y	Y			
olivine	Y				
spinel	Y	Yy	Yy	Yy	Yy
hematite	Yy	y			

Table 5.16. Crystalline Phases Detected with EDS (Y) and XRD (y) Analyses in the Al-Na-Limited Feed Heated to Various Temperatures at 5°C/min

T, °C	700	800	900	1000
silica	y	y	Yy	y
corundum	Yy	y		
escolaite	Y	Y		
nepheline	Yy	Y	Y	
calcium phosphate		Y		
spinel			Yy	Yy

5.1.5 DTA-TGA

Figure 5.16 and Figure 5.17 show the mass losses and thermal effects of BL and Al-Na-limited heated feeds as monitored by DTA-TGA. In both feeds, the major mass loss begins at ~150°C and continues to 600°C; above 600°C, it proceeds with a rather slow rate.

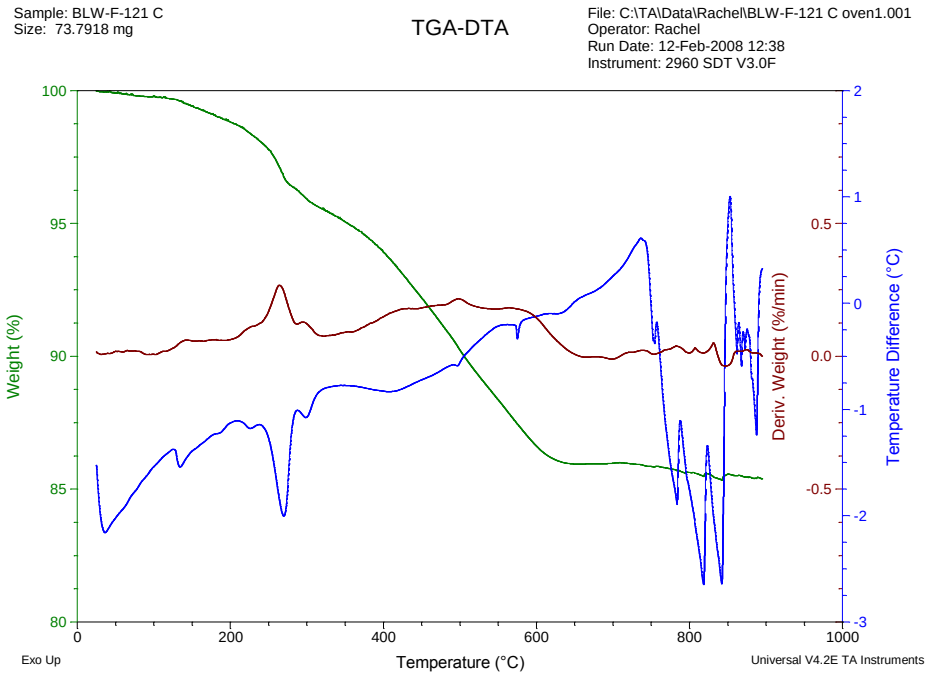

Figure 5.16. DTA-TGA for VSL BL Feed

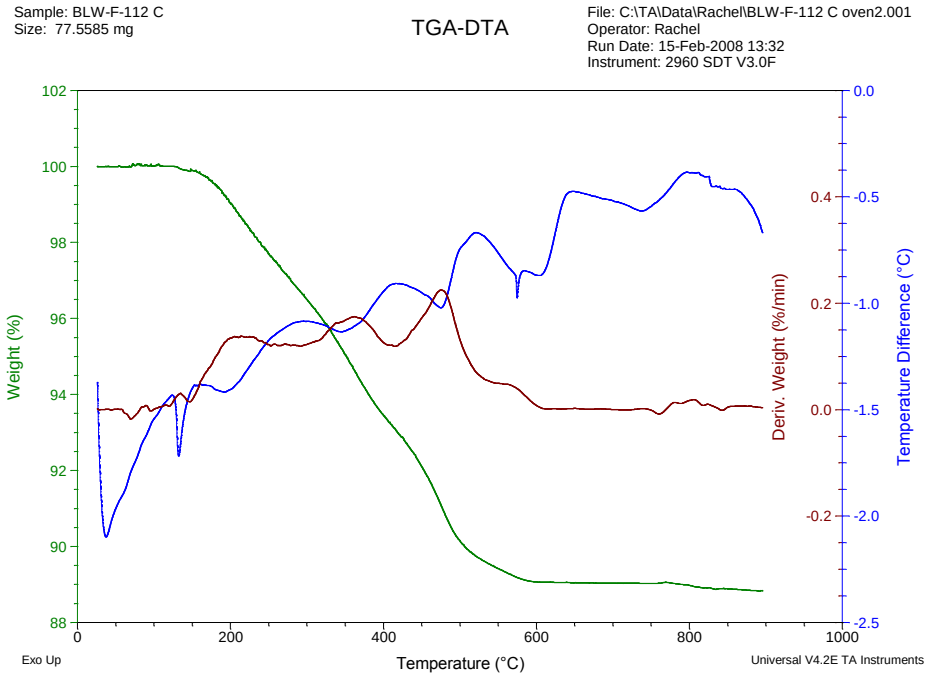

Figure 5.17. DTA-TGA for Al-Na-Limited Feed

5.1.6 Feed Expansion

Both pellets and loose batches were used for detailed characterization of the feed volume changes (i.e., expansion and contraction) during heating at 5°C/min. Selected sequences of photographic images and the measured values of the profile area, *A*, of feeds are shown in Appendix D. The normalized (or relative) area, defined as A/A_0, where A_0 is the area of the pellet profile at room temperature, is plotted in Figure 5.18 as a function of temperature for both VSL BL and Al-Na-limited (Al-Na); A0 feed data are also shown for comparison. Figure 5.19 depicts the change of the normalized average feed height (i.e., H/H_0, where H_0 is the initial average feed height) in silica-glass crucibles with temperature. Figure 5.20 displays the specific volume of the feeds in silica glass crucible tests (see Appendix D).

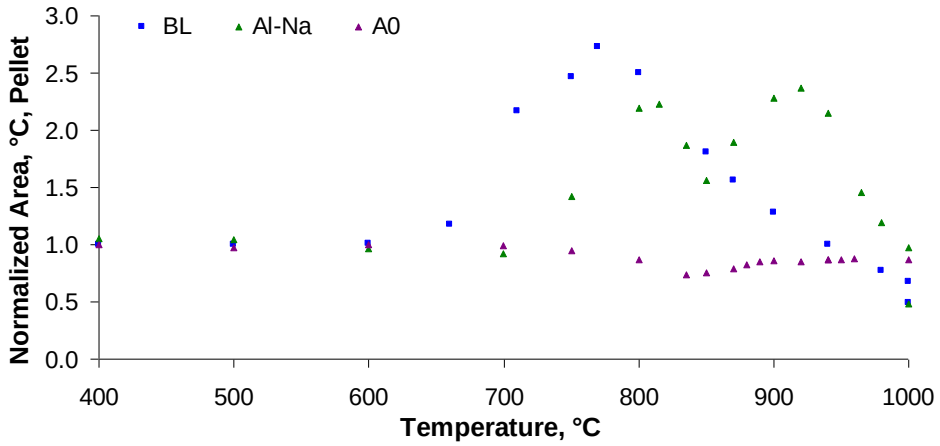

Figure 5.18. Normalized Pellet Profile Area Versus Temperature for VSL BL and Al-Na-Limited Feeds; A0 Feed Data are Included for Comparison

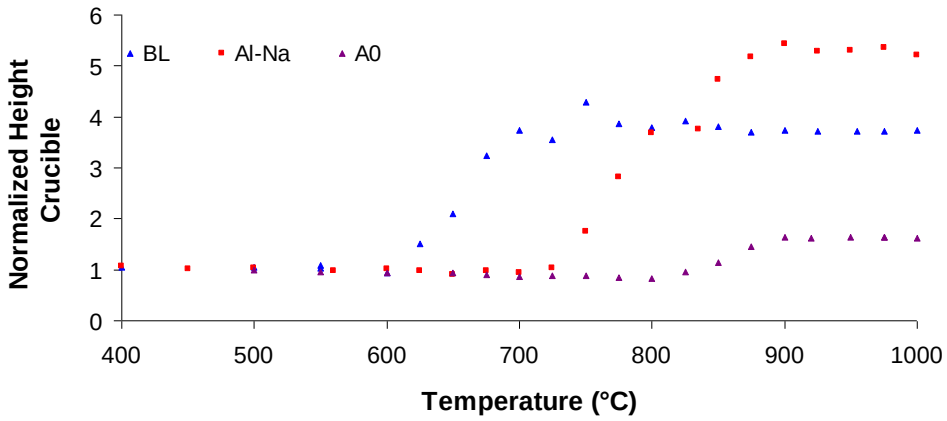

Figure 5.19. Normalized Feed Height Versus Temperature for VSL BL and Al-Na-Limited Feeds Placed in Silica-glass Crucible; A0 Feed Data are Included for Comparison

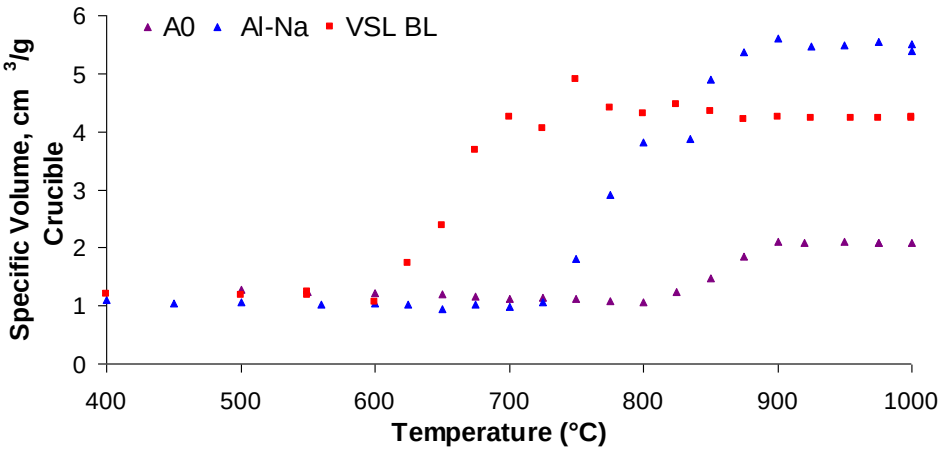

Figure 5.20. Specific Volume Versus Temperature for VSL BL and Al-Na-Limited Feeds Placed in Silica-Glass Crucible; A0 Feed Data Are Included for Comparison

Note that A0 feed expanded much less than VSL feeds. This can be attributed to the differences in formulating simulants and selecting the physical and chemical forms of glass-forming and glass-modifying additives.

As Figure 5.18 through Figure 5.20 show, feeds rapidly expanded at temperatures within the range of 600 to 900°C. Feed volumes reached maximum and then began to collapse to the volume of a bubble-free melt. The volume of the Al-Na-limited pellet exhibited two maximums in Figure 5.18, an event never observed in subsequent testing; it was probably caused by the collapse of a large bubble. Primary foam collapse could not be observed in silica-glass crucibles because the walls became opaque when contacted by glass. However, both maximum and minimum relative areas could be obtained from both pellet and crucible test data.

The expansion interval was further evaluated to obtain the maximum expansion rate. As Figure 5.21 and Figure 5.22 illustrate, a third-order polynomial trend line was fitted to data points around the inflection point (the point of the maximum expansion rate). The maximum rate and the corresponding relative area and temperature were determined from the polynomial coefficients. The results are listed in Table 5.17.

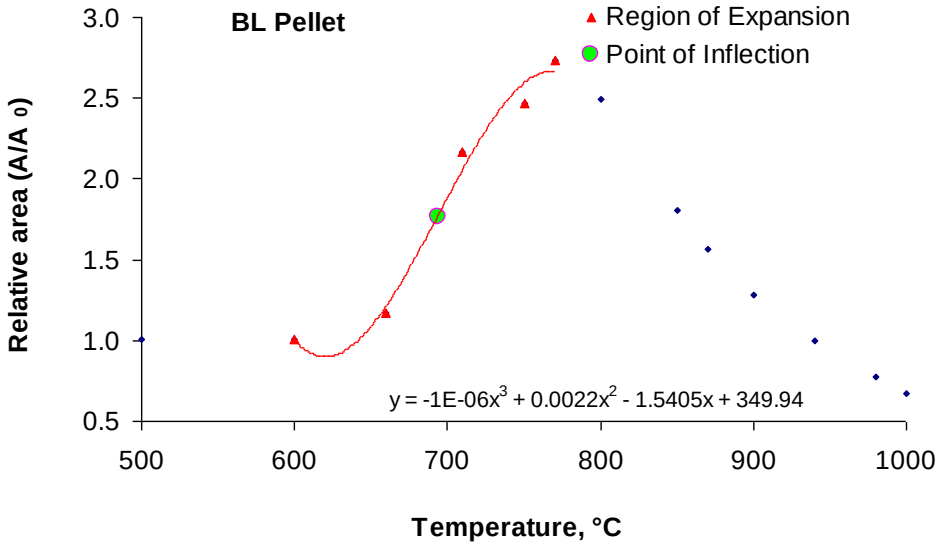

Figure 5.21. Third-order Polynomial Fit to Expansion Segment of Pellet Profile Area Versus Temperature for VSL BL Feed to Determine Maximum Expansion Rate

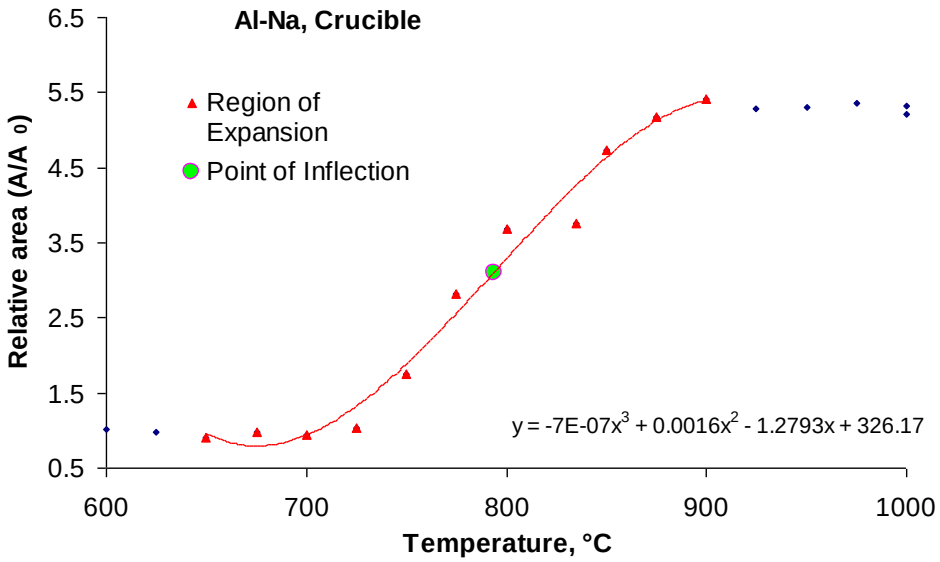

Figure 5.22. Third-order Polynomial Fit to Expansion Segment of Profile Area Versus Temperature for Al-Na-Limited Feed Placed in Silica-glass Crucible to Determine Maximum Expansion Rate

Table 5.17. Expansion Segment Parameters for VSL BL and Al-Na-limited Feeds

		Pellet		Crucible	
		BL	Al-Na	BL	Al-Na
A/A_0	Min	1.01	0.92	0.93	0.98
	Inflection	1.76	1.67	1.57	3.09
	Max	2.73	2.37	4.29	5.42
T, °C	Min	600	700	600	700
	Inflection	694	766	625	794
	Max	770	920	750	900
$d(A/A_0)/dT$, 10^{-3} K^{-1}	Inflection	17.8	13.1	29.0	29.2

These results show that the minimum volume of feed at the start of expansion was close to the initial (room temperature) volume. The major difference between the fast-melting BL feed and the slow-melting Al-Na-limited feed was that the latter expanded up to a higher temperature, ~900°C, as compared to ~750°C for the former. Thus, the VSL-BL feed became a bubble-free glass at a temperature lower by more than 100°C than the Al-Na-limited feed.

The extent of expansion was similar for both feeds, considering the high degree of uncertainty associated with the maximum expansion value; persistence or a collapse of a large bubble, obviously a random event, can considerably affect the volume of feed at the maximum expansion (the unusual double maximum of Al-Na-limited feed seen in Figure 5.18 is an extreme example of it).

The density of loose feed was ~1 g/cm^3. This value changed little from room temperature up to the beginning of expansion (~600°C). During the expansion, the feed turned to primary foam whose density decreased to a value as low as ~0.2 g/cm^3 (the specific volume of ~5 to 6 cm^3/g), containing less than

8 vol% of condensed phase. Both feed and foam have densities much lower than the bubble-free melt (~2.7 g/cm^3) and thus float on the melt in the melter and resist mixing with it until the bubbles collapse. This is true also for A0 feed that expanded much less.

5.1.7 Temperature Field Evolution Measurement

To observe the melt history and feed-to-glass conversion without the interference of thermocouples, several heat treatments were performed with several feeds heated to 1000°C at 5°C/min. The crucibles were then sectioned as seen in Figure 5.23. Large bubbles are trapped under the cold-top portion of Al-Na-limited feed. BL glass with ascending bubbles is molten at the bottom of the crucible while the remaining feed is bridged above a large cavity, a result of the internal collapse of primary foam.

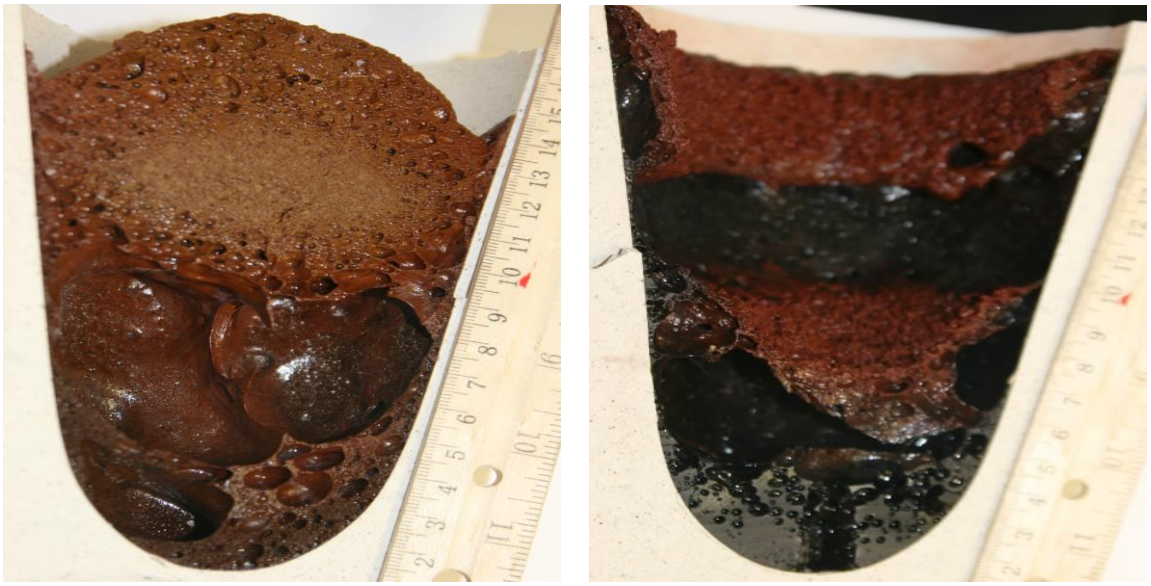

Al-Na-limited VSL-Baseline

Figure 5.23. Sections of VSL Feeds Heat-Treated to 1000°C at 5°C/min

Figure 5.24 through Figure 5.27 show the temperature field evolution during the heat treatment of BL and Al-Na-limited feeds. The first two graphs display *T* as a function of time with the distance from the wall as a parameter, whereas in Figure 5.26 and Figure 5.27, *T* is a function of the distance at various times of the experiment. The temperature distribution is close to parabolic as the trend lines indicate. The second-order polynomials shown in the figures were used to calculate the temperature gradient at the interface.

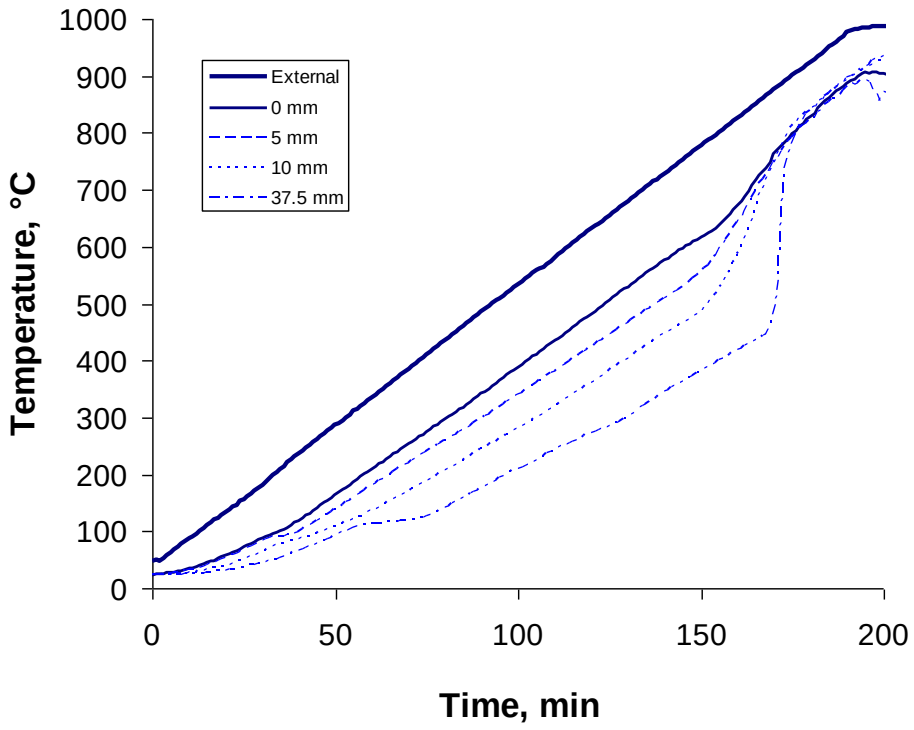

Figure 5.24. Temperature Versus Time and Distance from Crucible Wall (legend) for VSL BL Feed

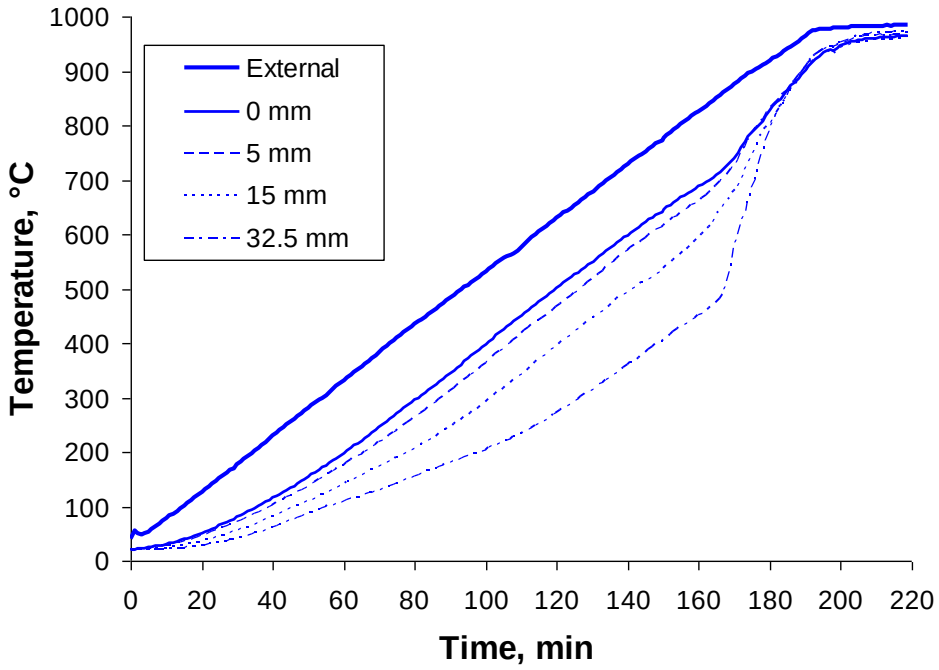

Figure 5.25. Temperature Versus Time and Distance from Crucible Wall (legend) for Al-Na-Limited Feed

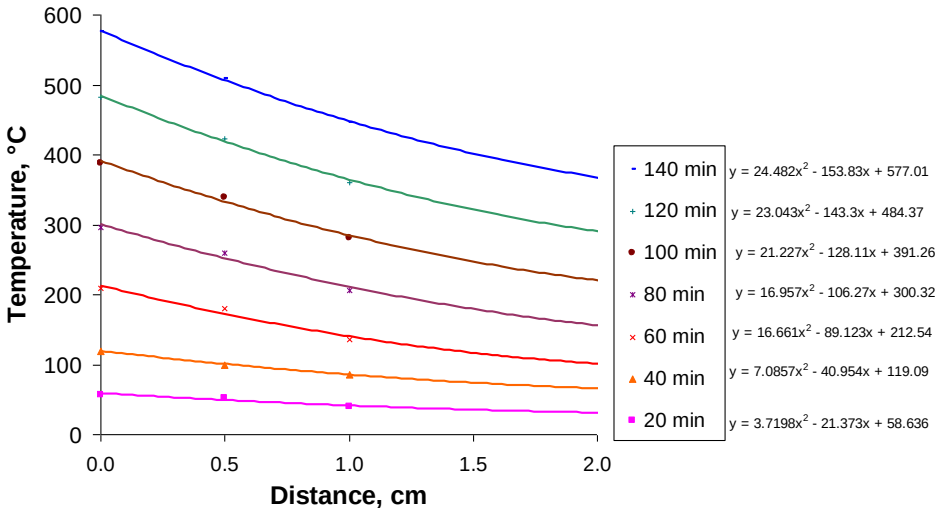

Figure 5.26. Temperature Versus Distance from Crucible Wall and Time (legend) for VSL BL Feed

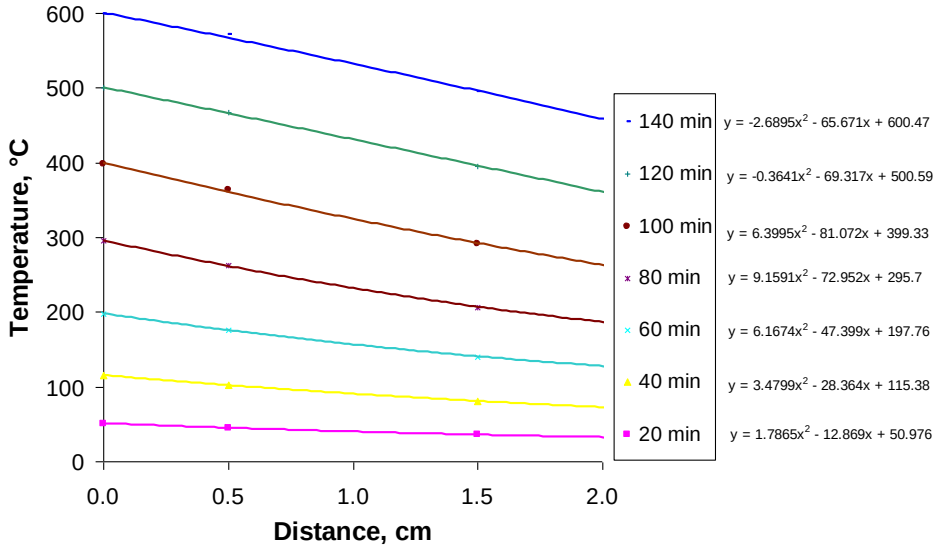

Figure 5.27. Temperature Versus Distance from Crucible Wall and Time (legend) for Al-Na-Limited Feed

Figure 5.28 shows the heat flux through the crucible wall into the feed as a function of the interface temperature. The heat flux was calculated by Equation (4.1), using the heat conductivity value for the crucible wall as λ_c = 1.3 W/m^2/K. Based on the temperature gradients in the feed at the interface, the heat conductivity of the feed was calculated by Equation (4.2). The result is displayed in Figure 5.29.

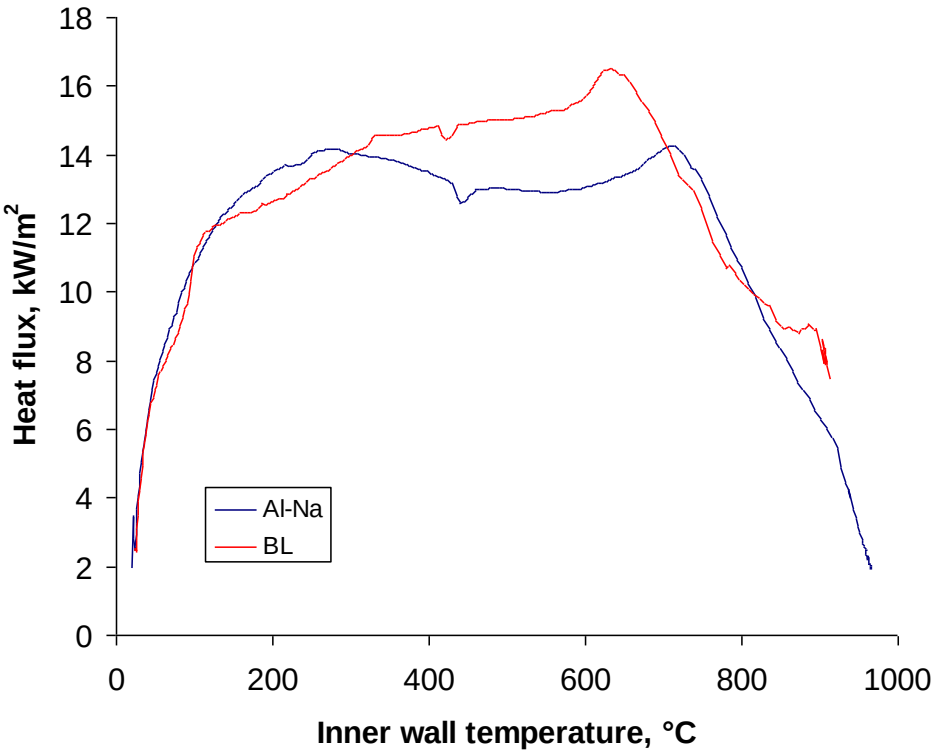

Figure 5.28. Heat Flux Through Crucible-Feed (VSL BL and Al-Na-limited) Interface Versus Interface Temperature

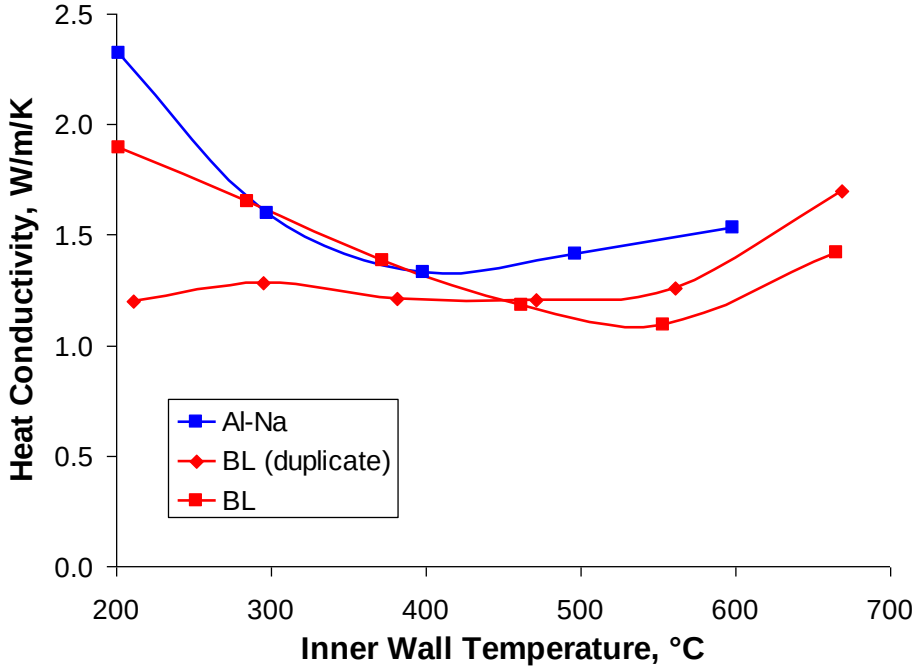

Figure 5.29. Heat Conductivity of Feeds (VSL BL and Al-Na-limited) Versus Temperature

Reasonable values of λ_f lie between 300 and 600°C. Based on Figure 5.28, it appears that a quasi-steady state was reliably established above 300°C. Below 200°C at the interface (up to 60 min of heating), as seen in Figure 5.24 and Figure 5.25, the whole crucible content is heated almost uniformly, with little temperature gradient, probably because the heat is conducted throughout the feed by the hot steam from chemically bonded water. Between 200 and 300°C, the temperature field is influenced by melting of the inorganic salts that consumes heat and flattens the temperature profile. Above 600°C, the glass-forming melt forms and retains large bubbles seen in Table 5.23 and creates an internal cavity. As a result, the temperature indicated by the thermocouples became equal throughout the crucible radius, from wall to axis (see Figure 5.24 and Figure 5.25), and the heat flux sharply decreased. The apparent heat conductivity of the feed is therefore rather high outside the temperature interval from 300 to 600°C and has no physical meaning.

Within the temperature interval from 300 to 600°C, $\lambda_f = 1.28 \pm 0.17$ W/m^2/K for the VSL BL and $\lambda_f = 1.99 \pm 0.82$ W/m^2/K for Al-Na-limited feed. Thus, though the heat conductivity of Al-Na-limited feed is somewhat higher, there is no significant difference between the feeds; moreover, λ_f is virtually independent of temperature within the temperature interval of 300 to 600°C.

5.2 A-Series Feeds

5.2.1 Feed Composition Variation (A0 through A5 Compositions)

The DTA-TGA curves in Figure 5.30 show that the large mass loss from A0 feed was caused by iron hydroxide dehydration and the loss of gasses from molten ionic salts. This result is typical for all feeds studied in this project.

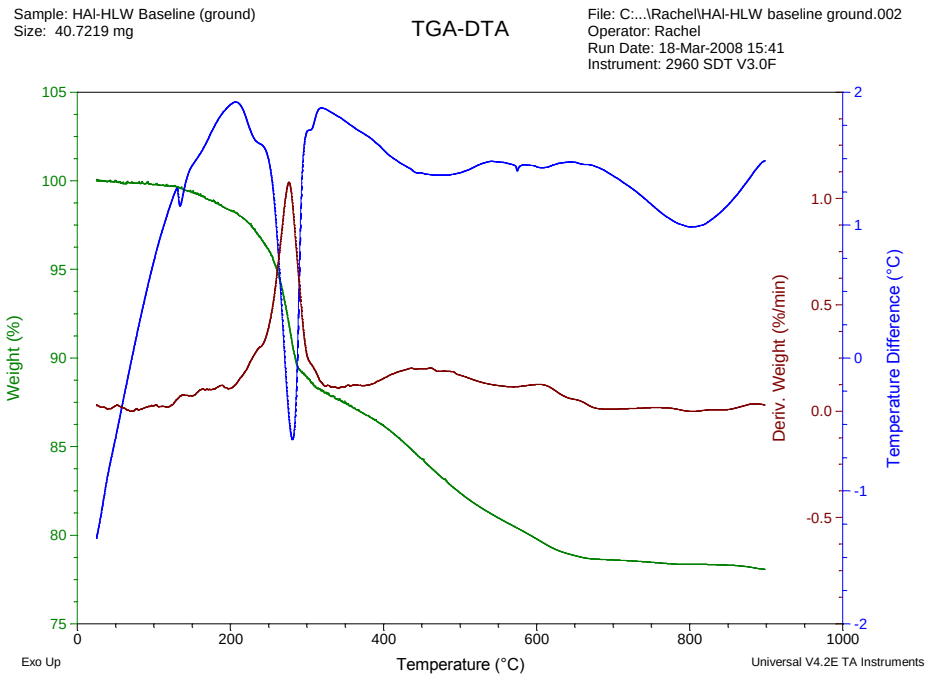

Figure 5.30. DTA-TGA of A0 Feed

The photographs of A2 and A3 feeds heated to 1000°C at 5°C/min in large crucibles and then sectioned are displayed in Figure 5.31. Unlike the VSL feeds (Figure 5.23), large bubbles are not combined into a single cavity as in Al-Na-limited feed, and melt is not accumulated at the bottom as in BL-glass feed. The feed for the low-viscosity glass A2 (similar to BL glass, see Figure 4.3) formed large uniformly distributed bubbles, and the feed for the high-viscosity glass A3 (see Figure 4.3 and Table 4.6) formed small uniformly distributed bubbles.

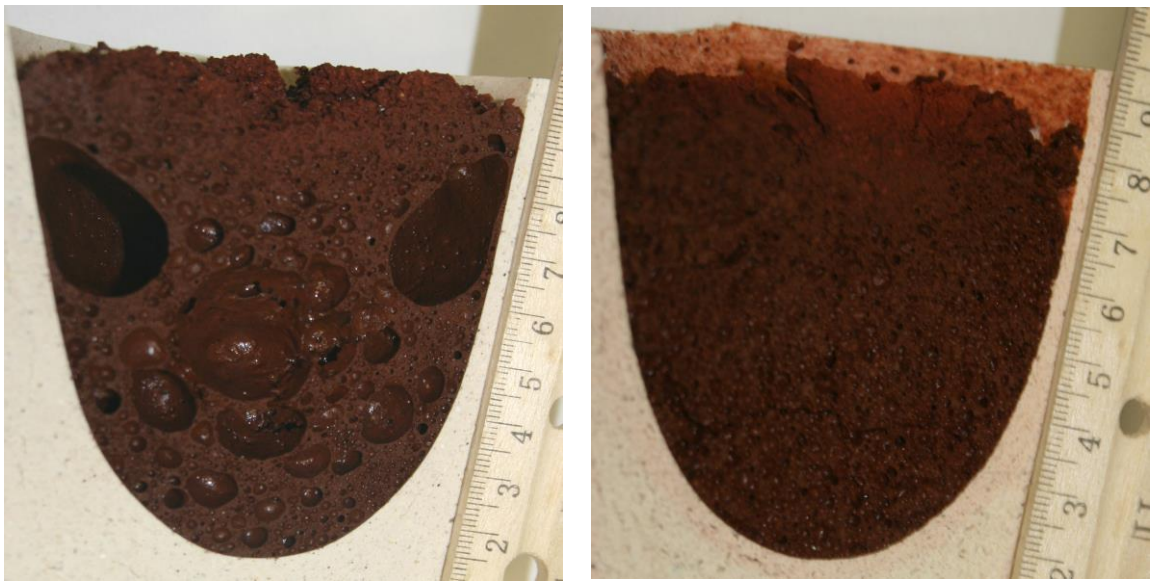

A2 A3

Figure 5.31. Sections of A2 and A3 Feeds Heat-Treated to 1000°C at 5°C/min

Figure 5.32 displays the fraction of solid silica measured by XRD with RIQAS software in three A-series feeds: the BL A0, and feeds yielding the glass with the highest (A1) and the lowest (A4) viscosities. There is virtually no difference between the rates of silica dissolution in these feeds. The solid silica is virtually gone when the temperature exceeds 900°C.

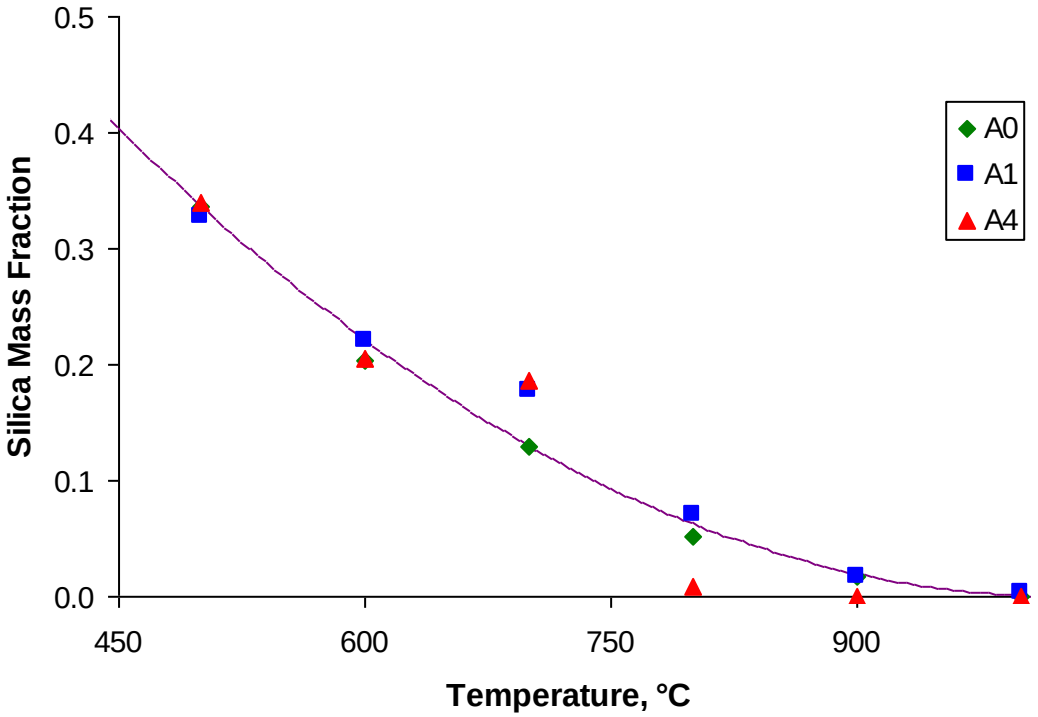

Figure 5.32. Solid Silica Mass Fraction Measured by XRD with RIQAS Software of Three A-Series Feeds Versus Temperature (the trendline, $s_U = 1.2055\times10^{-6}(1028.5 - T)^2$, where s_U is the undissolved silica fraction, was fitted using the least-square regression)

The feed expansion data were processed for A-series feeds in the same manner as described above for VSL feeds. Selected photographic images of the feeds heated at 5°C/min and the data obtained from these images with Photoshop software are summarized in Appendix D. Table 5.18 and Table 5.19, as well as Figure 5.33 and Figure 5.34, show that A feeds reached the minimum volume around 800°C (within the range from 750 to 850°C). The expansion was most rapid around 850°C in pellets (within the range from 830 to 880°C) and around 900°C in crucibles (within the range from 860 to 950°C). The maximum expansion was reached around 910°C in pellets (within the range from 870 to 960°C) and around 980°C (within the range from 950 to 1030°C) in crucibles. The average difference between temperatures of maximum and minimum volume was 110°C for pellets and 180°C for crucibles. Primary foam reached maximum expansion when $\log(\eta/\text{Pa}\cdot\text{s}) = 2.13\pm0.18$ (pellets) and 1.72 ± 0.35 (crucibles).

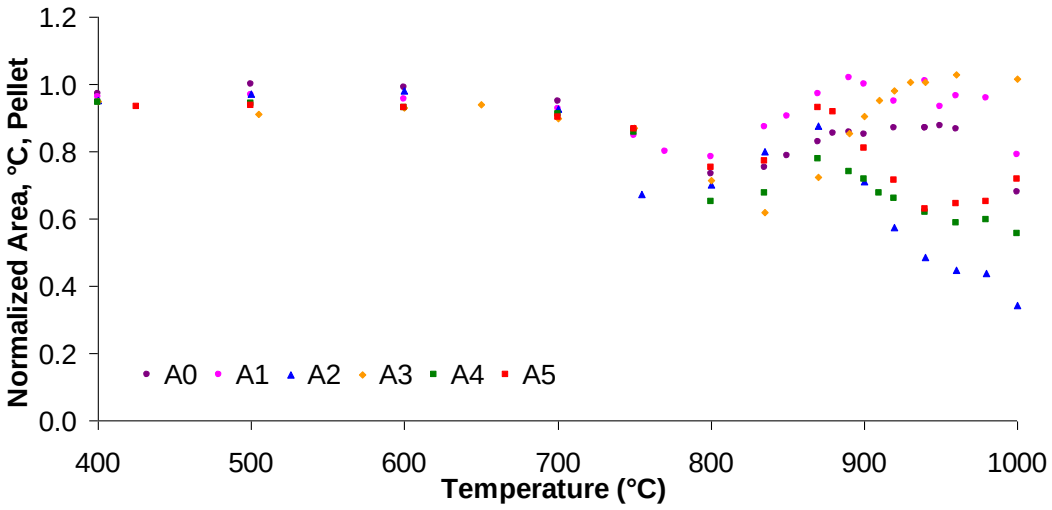

Figure 5.33. Normalized Pellet Area Versus Temperature for A-Series Feeds

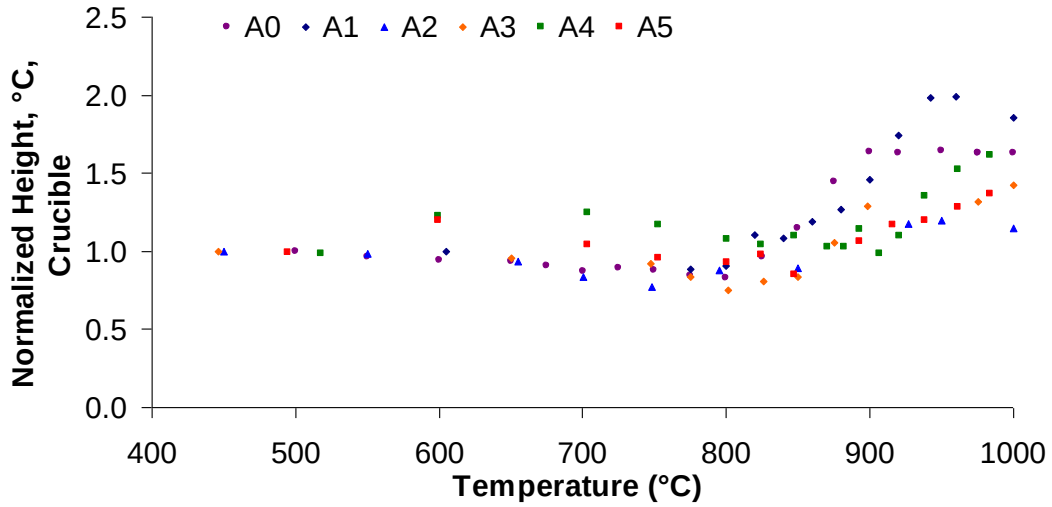

Figure 5.34. Normalized Sample Height Versus Temperature for A-Series Feeds in Crucible Tests

Table 5.18. Pellet Expansion-Segment Parameters for A-Series Feeds

		A0	A1	A2	A3	A4	A5
A/A_0	Min	0.68	0.79	0.67	0.62	0.65	0.75
	Inflection	0.79	0.90	0.77	0.83	0.69	0.82
	Max	0.88	1.02	0.88	1.03	0.78	0.93
T	Min	800	800	755	835	800	800
	Inflection	852	845	826	884	844	845
	Max	950	940	870	960	870	870
$d(A/A_0)/dT$	Inflection	2.5	3.4	3.0	6.1	3.1	5.2
$\log(\eta/Pa{\cdot}s)$ at T_{max}		2.09	2.16	2.09	1.99	1.97	2.48

Table 5.19. Expansion-Segment Parameters for A-Series Feeds in Crucible

		A0	A1	A2	A3	A4	A5
H/H_0	Min	0.83	0.90	0.78	0.84	1.04	0.85
	Inflection	1.31	1.67	0.98	1.14	1.30	1.16
	Max	1.64	1.99	1.19	1.42	1.72	1.42
T	Min	800	800	748	775	824	847
	Inflection	862	917	858	885	945	901
	Max	950	960	950	1000	1029	1007
$d(H/H_0)/dT$	Inflection	10.1	9.2	2.8	6.1	9.3	6.7
$\log(\eta/Pa{\cdot}s)$ at T_{max}		2.09	2.05	1.62	1.77	1.11	1.68

The relative expansion extent was lower in pellets (average minimum 0.69 and average maximum 0.92) than in crucibles (average minimum 0.87 and average maximum 1.56). Interestingly, although the feed was compressed in pellets, its maximum volume was generally lower than the initial volume, whereas the feeds expanded on average by 50% compared to the initial volumes of loose samples in crucibles. Generally, at the temperature at which the feed reached maximum volume, the melt viscosity was ~10^2 Pa·s (Table 5.18 and Table 5.19); the high-alkali glass A4 is an exception.

An attempt to use linear regression to correlate the temperature of maximum expansion with glass composition showed no results: R^2_{adj} had negative values. However, interesting results were obtained for pellets with feed composition, namely with the contents of boric acid and lithium carbonate. As observed in Table 5.20, both boric acid and carbonates (Li_2CO_3 was the only carbonate in the feed) decrease the temperature at which expansion begins (T_{min}) and at which it is most rapid (T_{inf}). The low values of R^2_{adj} indicates that the contents of H_3BO_3 and Li_2CO_3 in the feed are not the only parameters the affect the temperature at which primary foam begins to collapse (T_{max}). Obviously, the primary foam collapse is a result of two competitive factors: the rate of gas generation (H_2O from H_3BO_3 and CO_2 from Li_2CO_3) and the decreasing viscosity of melt. Nevertheless, a high value of T_{Li2CO3} implies that CO_2 is still vigorously evolving at T_{max}, and thus primary foam is collapsing through gas generation and not by melt drainage.

Table 5.20. The Coefficients and Statistical Parameters in the Linear Relationship (T_{min}, T_{inf}, T_{max}) = T_0 + $T_{H3BO3}x_{H3BO3}$ + $T_{Li2CO3}x_{Li2CO3}$ where x_{H3BO3} and x_{Li2CO3} Are Amounts in g per g Glass of H_3BO_3 and from Li_2CO_3 in Feeds Listed in Table 4.7 (all temperatures are in °C)

Coefficients	T_{H3BO3}	T_{Li2CO3}	T_0	R^2	R^2_{adj}	StError
T_{min}	-456	-511	975	0.993	0.812	11.0
T_{inf}	-382	-386	992	0.942	0.978	2.8
T_{max}	-254	-1052	1100	0.826	0.709	23.9

Figure 5.35 displays the heat conductivity of A-series feeds. Unfortunately, these data were obtained with the initial experimental setup at which the thermocouples at the external and internal surfaces of crucible walls were not properly fixed in position. Hence, the temperature difference across the crucible wall was of uncertain value and was probably larger than the true value, which in turn resulted in unrealistically high values of heat conductivities of several feeds.

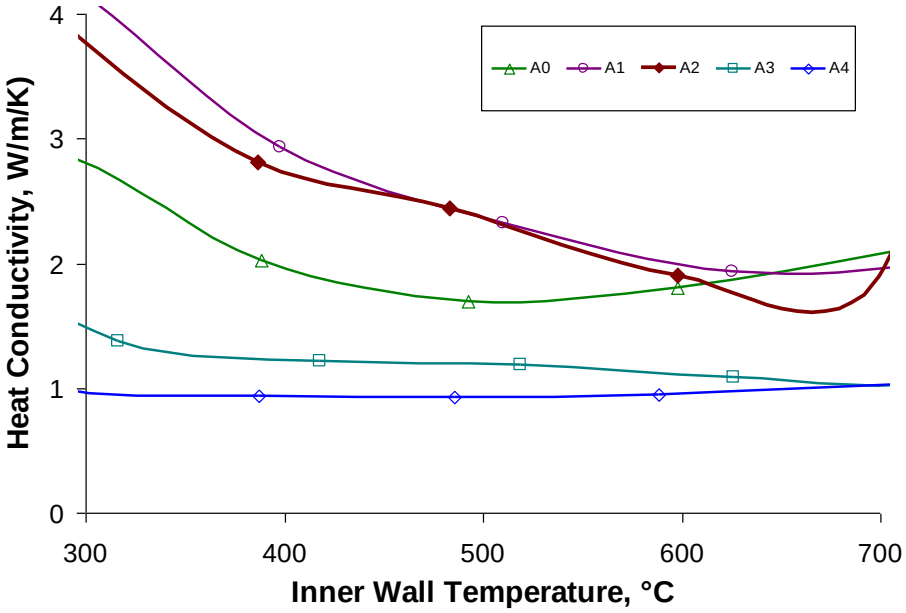

Figure 5.35. Heat Conductivity Results for A-Series Feeds Obtained with the Initial Experimental Setup

5.2.2 Effect of Silica-Grain Size (A0X-series)

The feed expansion data for A0X-series of A0 feed with variously sized silica grains were processed for all feeds in the same manner as described above for VSL feeds. The images and data obtained are shown in Appendix D and graphically presented in Figure 5.36 through Figure 5.38.

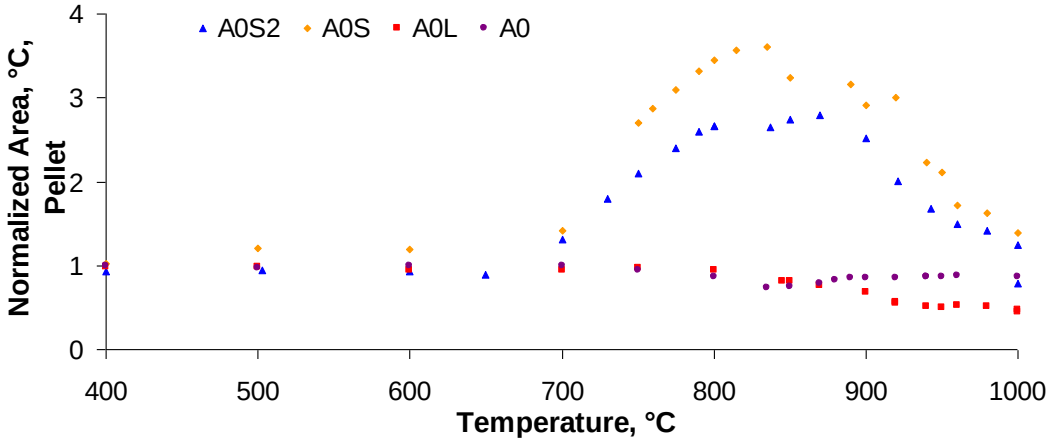

Figure 5.36. Normalized Pellet Area Versus Temperature for A0X-Series Feeds

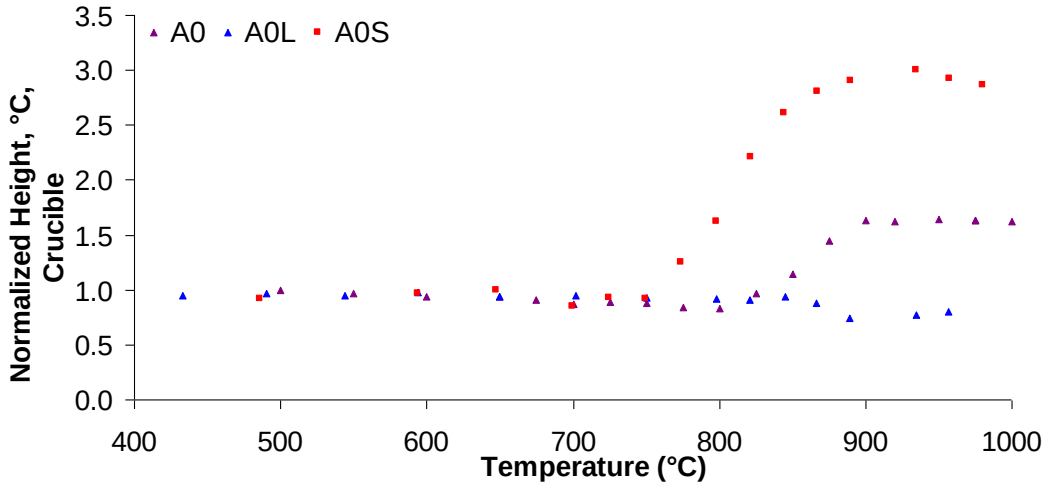

Figure 5.37. Normalized Sample Height Versus Temperature for A0X-Series Feeds in Crucible Tests

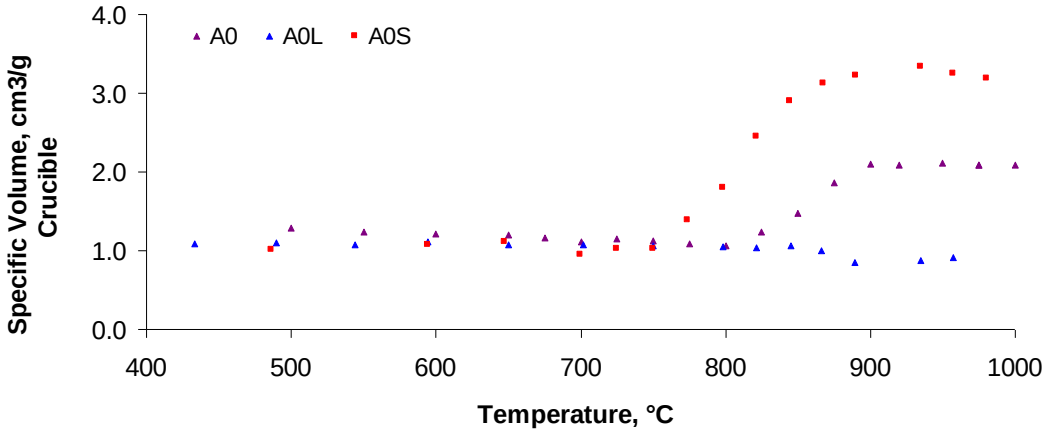

Figure 5.38. Specific Volume Versus Temperature for A0X-Series Feeds in Crucible Tests

The temperature interval of expansion increased as silica grain size increased, see Table 5.21, Table 5.22, and Figure 5.39, starting with the minimum expansion temperature of ~700°C for feed with 5-μm silica grains reaching nearly 900°C for feed with 500-μm silica grains. The maximum expansion was reached at a temperature ~200°C higher than the minimum. As the silica grain size increased, all three temperatures, minimum, inflection, and maximum, grew exponentially as $T = T_\infty - B\exp(-s/s_0)$ where s is the average silica grain size and T_∞, B, and s_0 are coefficients; B = 226°C and s_0 = 124 μm are common for all three temperatures (T_{min}, T_{inf}, and T_{max}) whereas $T_{\infty,min}$ = 907°C, $T_{\infty,inf}$ = 982°C, and $T_{\infty,max}$ = 1089°C. Since T_{min} > 900°C as s > 430 μm, we can conclude that primary foam no longer occurs when the average silica grain size exceeds ~400 μm. This conclusion is based on insufficient data, and thus cannot be taken for granted. More experiments with various grain sizes will be performed in FY'09. Note that the size 400 μm is too large for slurry feed that requires keeping a stable and uniform suspension in the slurry-feed tank.

Table 5.21. Pellet Expansion-Segment Parameters for A0X-Series Feeds

		A0S	A0S2	A0
A/A_0	Min	1.42	0.89	0.68
	Inflection	2.12	1.82	0.79
	Max	3.24	2.79	0.88
T	Min	700	650	800
	Inflection	731	732	852
	Max	850	870	950
$d(A/A_0)/dT$	Inflection	23.3	14.8	2.5
Size	µm	5	5	75

Table 5.22. Expansion-Segment Parameters for A0X-Series Feeds in Crucibles

		A0S	A0	A0L
H/H_0	Min	0.85	0.83	0.75
	Inflection	2.11	1.31	0.84
	Max	3.00	1.64	0.92
T	Min	700	800	890
	Inflection	813	862	999
	Max	935	950	1076
$d(H/H_0)/dT$	Inflection	18.6	10.1	1.5
Size	µm	5	75	500

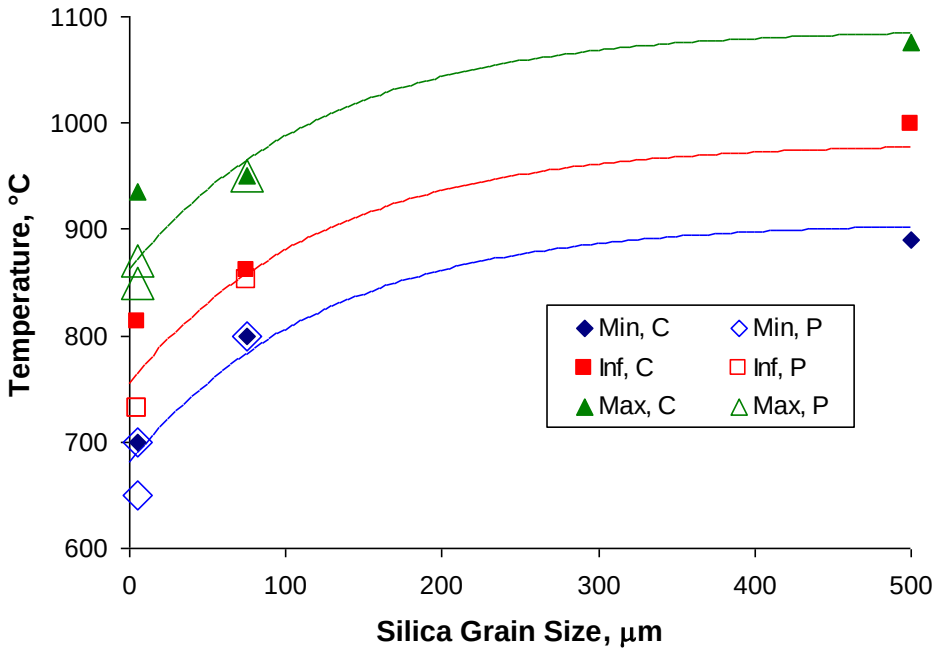

Figure 5.39. Feed Expansion Interval Temperatures (minimum, inflection, and maximum) Versus Silica Grain Size for Feeds Processed in Crucibles (C) and in Pellets (P)

The expansion extent, expressed as A/A_0 for pellets and H/H_0 for feed in crucibles (see Table 5.21 and Table 5.22), decreased exponentially with silica grain size as seen in Figure 5.40 where the lines represent exponential equations of the form $Y = Y_\infty + (Y_0 - Y_\infty)\exp(-s/s_0)$ where Y stands for A/A_0 or H/H_0. The values of coefficients s_0 = 72 μm and Y_∞ = 0.22 are common for all three values of Y (Y_{max}, Y_{inf}, and Y_{min}) while the remaining values are Y_{0max} = 3.17, Y_{0inf} = 2.11, and Y_{0min} = 1.06. The coefficient values are approximately the same for feeds in pellets and in crucibles. As Figure 5.36 through Figure 5.38 show, feed with 500-μm silica grains barely expanded at all. Such a non-expanding feed does not form primary foam, but cannot prevent secondary foam that necessarily occurs as long as Fe_2O_3 is being reduced to FeO. The dispersed dissolving solid particles that survive 900°C are taken with the current into the high-temperature melt zone where the residual silica is likely to fully dissolve (however, large heavy crystals of spinel have a tendency to settle).

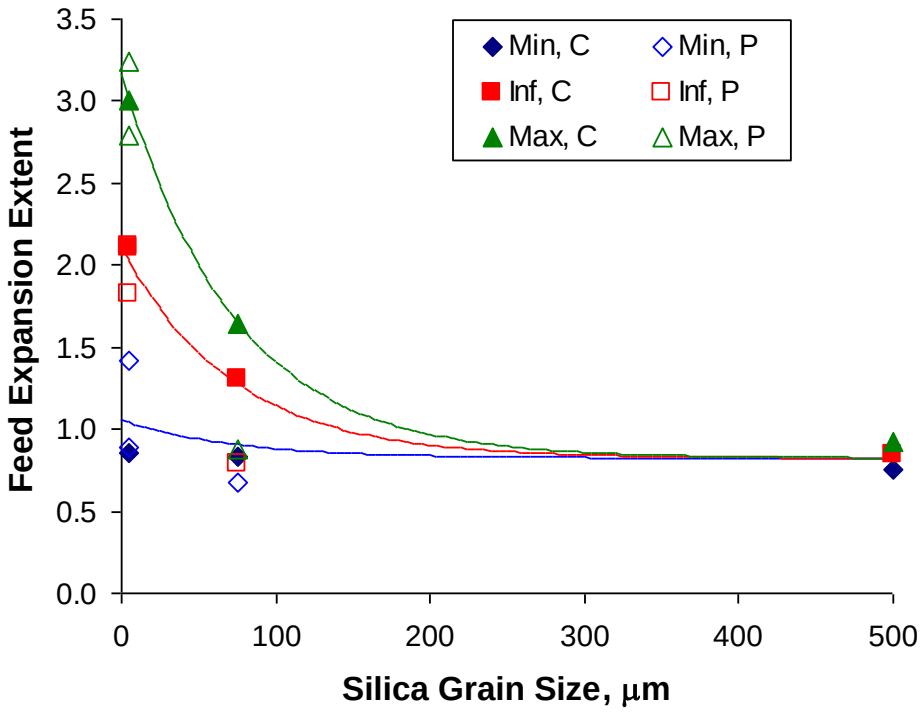

Figure 5.40. Feed Expansion Extent (A/A_0 or H/H_0) Versus Silica Grain Size

The maximum rates of expansion followed an exponential trend that can be expressed by the equation $R = R_0\exp(-s/s_0)$, where R stands for $d(A/A_0)/dT\big|_{inflexion}$ or $d(H/H_0)/dT\big|_{inflexion}$, s_0 = 116 μm, and R_0 = 19.7. Both crucible and pellet data were included in the regression analysis (Figure 5.41).

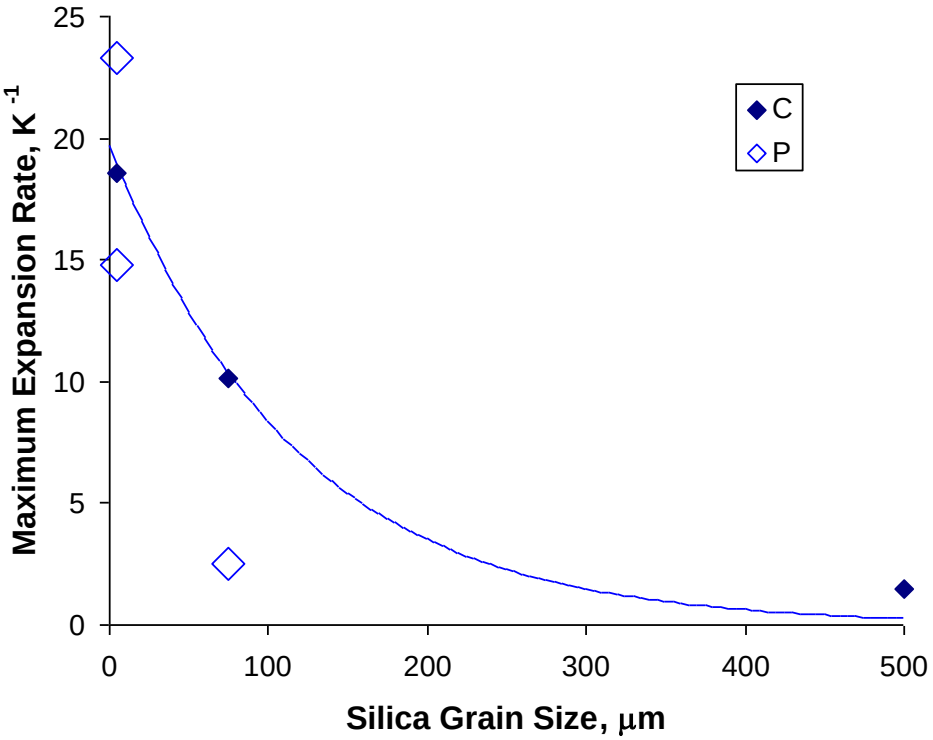

Figure 5.41. Maximum Expansion Rate Versus Silica Grain Size for Feeds Processed in Crucibles (C) and in Pellets (P)

5.2.3 Effect of Exothermal Reaction (C and S-series Testing)

The A0-based feeds of S- and C-series (see Table 4.8, Table 4.9, Table 5.23, and Table 5.24) contained carbohydrates (sucrose and cellulose). Figure 5.42 shows the mass fraction of solid silica, determined with XRD, as it decreased with increasing temperature in A0 feed and two feeds with C/N = 0.75, one with sucrose (S2) and the other with cellulose (C2) addition. The silica fraction is related to feed mass (not to glass mass), as in Figure 5.32. As TGA data indicate (Figure 5.30), the feed mass decreases up to the temperature of 950°C.

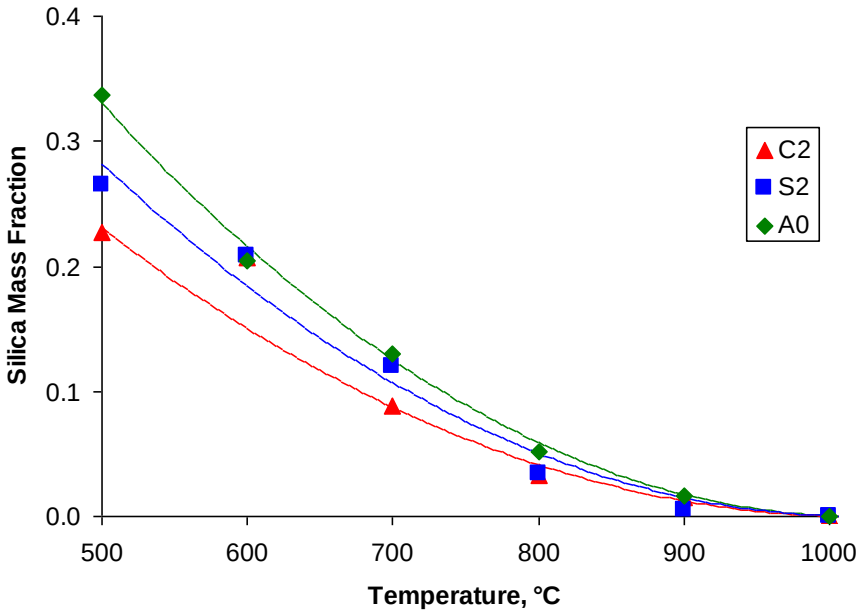

Figure 5.42. Solid (undissolved) Silica Mass Fraction (by XRD) Versus Temperature for A0 Feed and Feeds with C/N = 0.75

The lines in Figure 5.42 represent second-order trendlines of the form

$$s_U = s_{U0}(T_0 - T)^2 \tag{5.1}$$

where s_U is the undissolved silica mass fraction, T_0 = 1020°C (the same for all three curves) is the temperature at which solid silica disappears from the melt, and the coefficient s_{U0} = 1.217×10^{-6} μm/K^{2}for A0, 0.850×10^{-6} μm/K^2 for C2, and 1.040×10^{-6} μm/K^2 for S2.

The feed-expansion data were processed for all S- and C-series feeds in the same manner as described for VSL feeds. The photographic images and data tables can be seen in Appendix D. As Figure 5.43 and Figure 5.44 and Table 5.23 and Figure 5.27 demonstrate, S-feeds reached the minimum volume around 800°C for pellets and at a temperature ~50°C higher for crucibles. The expansion was most rapid around 870°C in pellets (within the range from 850 to 890°C) and around 890°C in crucibles (within a broad range from 810 to 950°C). Maximum expansion was reached around 930°C in pellets (within the range from 900 to 950°C) and around 970°C (within the range from 850 to 1030°C) in crucibles. The average difference between temperatures of maximum and minimum volume was 110°C for pellets and 120°C for crucibles.

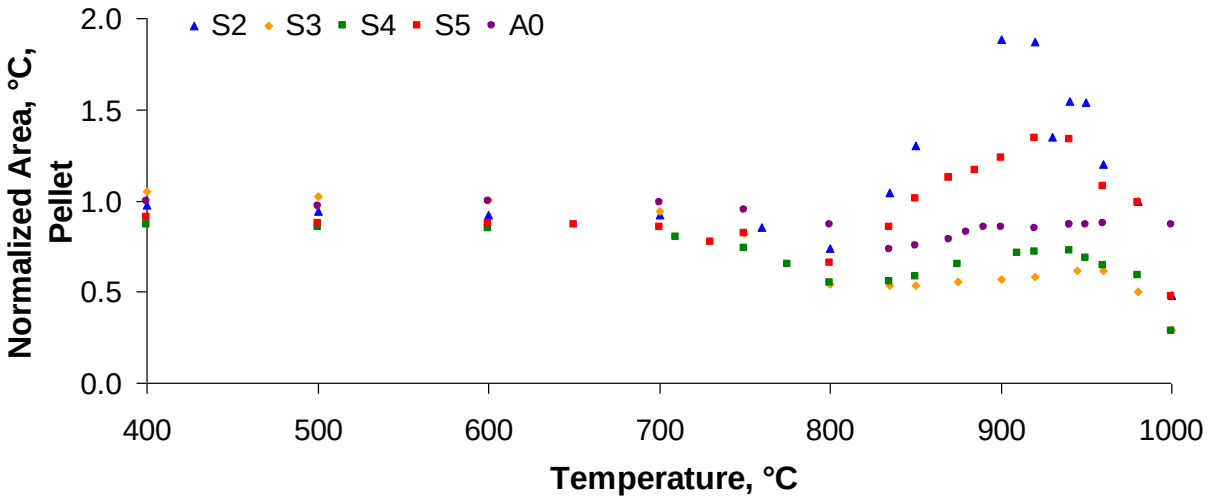

Figure 5.43. Normalized Pellet Area Versus Temperature for S-Series Feeds

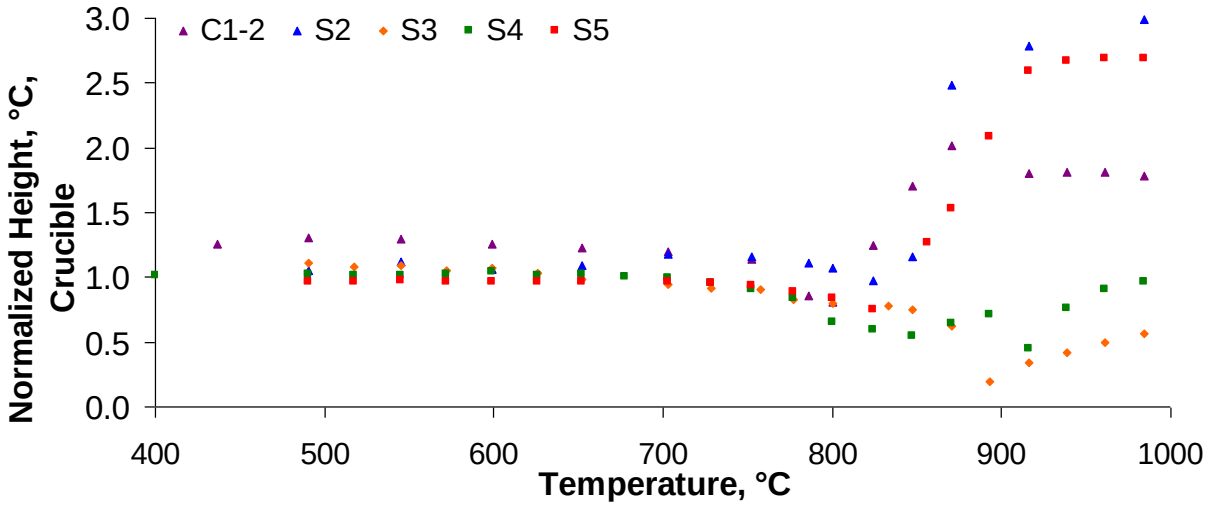

Figure 5.44. Normalized Sample Height Versus Temperature for S-Series Feeds in Crucible Tests

Table 5.23. Pellet Expansion-Segment Parameters for S-Series Feeds

		S2	S5	S4	S3
A/A_0	Min	0.74	0.65	0.55	0.53
	Inflection	1.36	1.01	0.64	0.56
	Max	1.88	1.34	0.73	0.62
T	Min	800	800	800	850
	Inflection	852	856	871	890
	Max	900	920	940	945
$d(A/A_0)/dT$	Inflection	15.7	7.1	2.4	0.4
C/N		0.75	0.90	1.00	1.50

Table 5.24. Expansion-Segment Parameters for S- and C-Series Feeds in Crucibles

		C1-2	S2	S5	S4	S3	C1	C2	C3
H/H_0	Min	0.81	0.98	0.75	0.45	0.20	0.93	1.01	0.75
	Inflection	1.51	2.08	1.75	0.83	0.51	1.83	1.46	1.03
	Max	2.02	3.04	2.69	0.99	0.57	2.63	1.75	0.99
T	Min	801	824	824	916	893	849	847	801
	Inflection	816	882	877	945	956	904	904	810
	Max	870	1007	1029	1007	1029	1029	939	847
$d(H/H_0)/dT$	Inflection	15.6	25.7	23.0	3.0	2.9	21.6	14.6	4.3
C/N		0.00	0.75	0.90	1.00	1.50	0.00	0.75	0.90

The higher temperatures at which feed expansion occurred in crucibles as compared to pellets could be caused by the different mode of heat transfer from the furnace to the feed. Pellets received direct radiation heat from the heating elements as did the thermocouple. The heating of feed in pellets was close to uniform because of the small volume of pellets and their large surface-to-volume ratio. On the other hand, some of the heat radiation could be reflected back from the silica-glass crucibles while the larger mass of crucible feeds and their smaller surface-to-volume ratio lead to temperature difference between the furnace thermocouple and the feed during the heat treatment at 5°C/min.

Figure 5.45 shows that the temperatures for the expansion interval nearly linearly increased with the C/N ratio with identical slopes (the common slope of the lines in Figure 5.45 is 59°C, and the intercepts are 751, 806, and 865°C). However, no such relationship could be established for crucible data. It seems that feeds in crucibles are more subjected to random events, such as growth and collapse of large bubbles, than feeds in pellets.

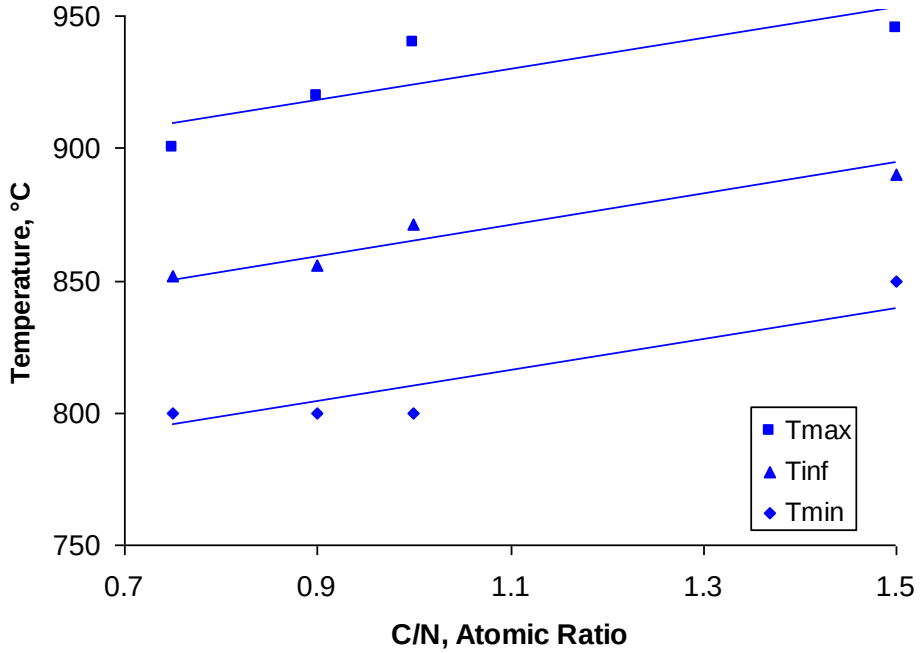

Figure 5.45. Maximum, Inflection, and Minimum Temperatures of Rapid Expansion Interval Versus C/N Ratio for Pellets with Sucrose

As seen in Figure 5.46, the expansion extent of the S-series feeds was lower in pellets than in crucibles. For both pellets and crucibles, the expansion of feeds with sucrose was high at C/N < 1; for C/N = 0.75, A/A_0 reached 1.9 for pellets, and H/H_0 climbed as high as 3.0 for crucibles. With increasing C/N > 1, expansion slightly decreased.

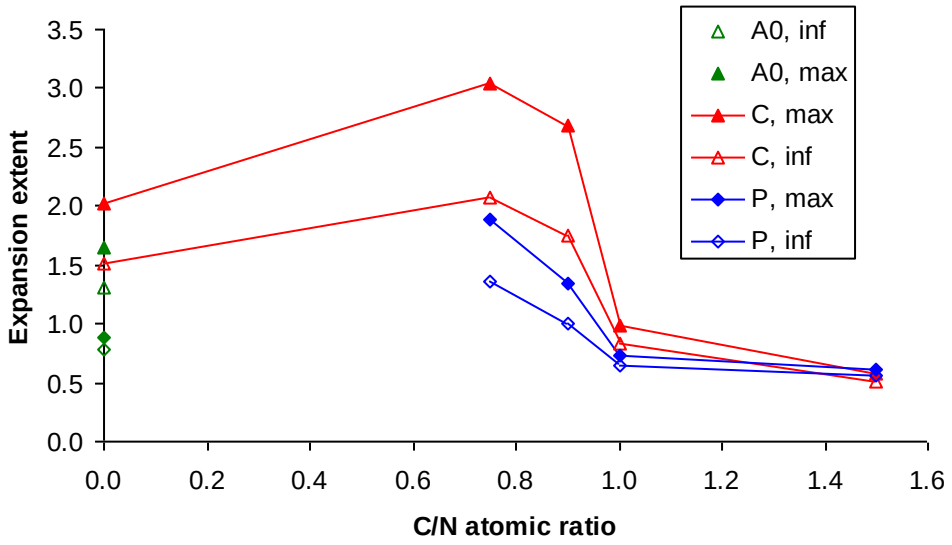

Figure 5.46. Inflection and Maximum Expansion Extent for Acidified A0 Feeds with Sucrose Addition (green data points stand for original A0, both pellets [diamonds] and crucibles [triangles])

Figure 5.47 displays data obtained for feeds with cellulose, C2 and C3 (C1 is an acidified feed without any carbohydrate addition). These experiments do not suffice for establishing relationships between the expansion behavior and the C/N ratio, but the experiments showed that feeds with cellulose behave somewhat differently than feeds with sucrose. The feeds with cellulose reacted rather violently at a temperature of 200°C, precluding the pellet expansion test to be performed.

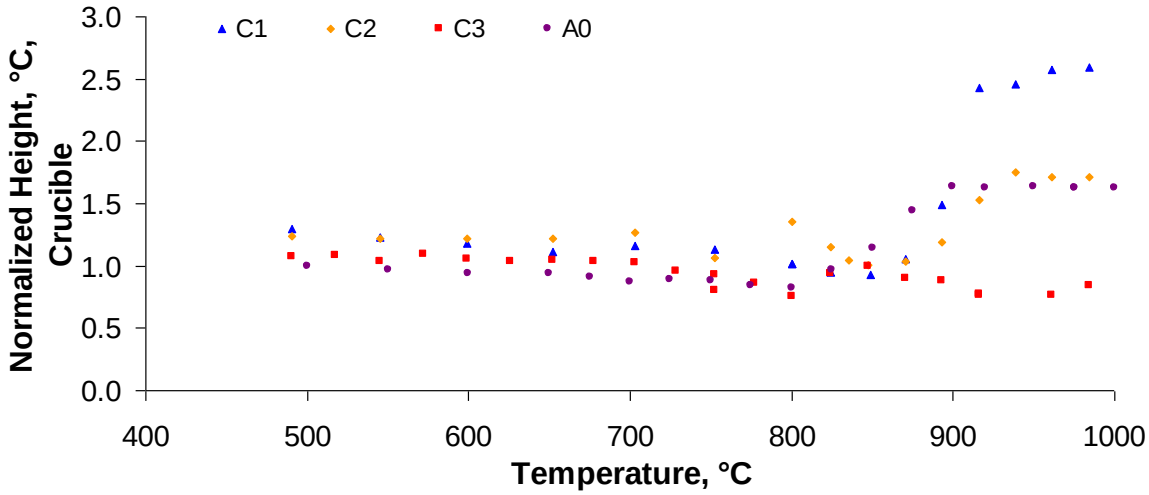

Figure 5.47. Normalized Sample Height Versus Temperature for C-Series Feeds in Crucible Tests

Figure 5.48 and Figure 5.49 show the temperature field evolution in S3 and C3 feeds in large crucibles, both with C/N = 1.5. The temperature-versus-time curves bring evidence for an exothermic reaction between nitrate and carbohydrate that started at a temperature as low as 100°C and heated the feed locally to a temperature as high as 350°C in case of sucrose addition and 700°C in case of cellulose.

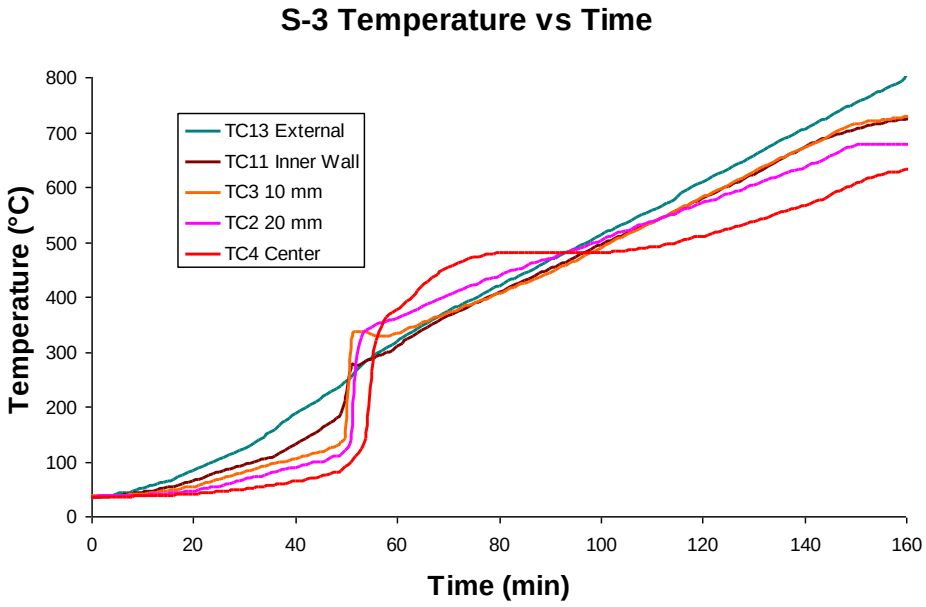

Figure 5.48. Temperature Field Evolution in S3 Feed

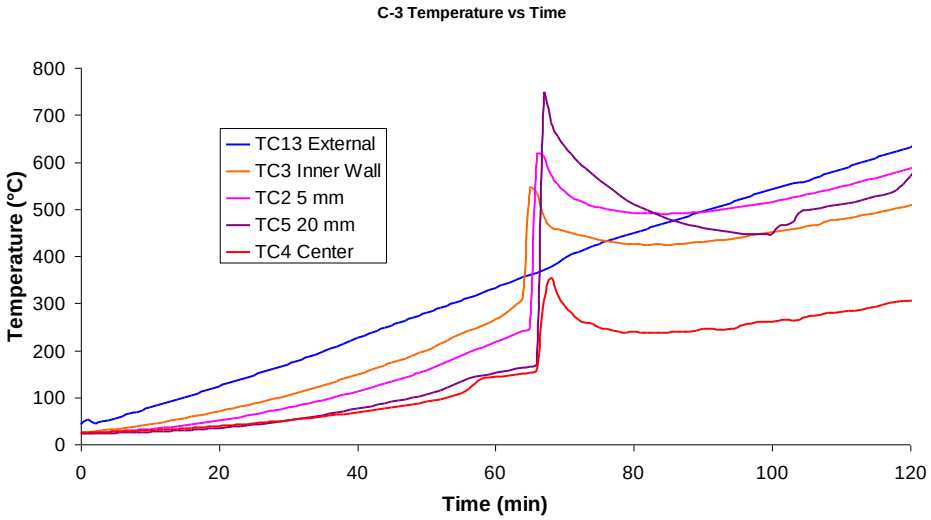

Figure 5.49. Temperature Field Evolution in C3 Feed

The likely reaction between the nitric acid and sucrose is

$$12HNO_3 + C_{12}H_{22}O_{11} = 12CO_2 + 17H_2O + 6NO + 3N_2 \quad \Delta H = -3277 \text{ kJ/mol}$$

The heat generated per gram of sucrose is 9.6 kJ.

The reason why the temperature increase caused by the exothermal reaction was higher when cellulose was used is not well understood (see also discussion in Section 6.4). The heat of the reaction between sodium nitrate and cellulose, between 6 and 12 kJ/kg cellulose according to the reaction path, is comparable to the reaction heat of sucrose. It is possible that sucrose partially reacted with HNO_3 while the feed was being dried or that some of the sucrose did not react with nitrate and instead pyrolized to form elemental carbon. Also, cellulose, being less dispersed than sucrose (cellulose does not dissolve in water), increased the temperature locally beyond the temperature of feed solids. As the temperature eventually equilibrated, the overall temperature decreased from the peak level to a level comparable with that of the feeds with sucrose.

6.0 Discussion

6.1 Relationship Between Feed Behavior and Rate of Melting

While one can expect that exothermal reactions within the cold cap will increase the rate of melting, the question of how feed expansion is related to the rate of melting remains open. Is the high rate of melting associated with zero primary foam or does vigorous bubbling enhance heat transfer and assist melt homogenization?

In a large-scale melter, the rate of melting is determined by the rate at which the heat from the melt is delivered to the cold cap, i.e., by the heat flux through the interface between the cold cap and the melt. This interface is positioned at the temperature at which the primary foam collapses, i.e., at a temperature slightly higher than the temperature of maximum expansion (or a temperature at which melt viscosity drops below 10^2 Pa·s).

If the temperature of maximum expansion is high, the temperature difference between the melt (usually fixed at 1150°C) and the temperature at the interface (the driving force for the heat transfer in melter without bubbling) is lower. This temperature difference can vary from 250°C to 400°C depending on feed composition and makeup, but is of minor importance for melters equipped with bubblers.

Figure 1.2 shows that melt viscosity imposes an upper limit on the rate of melting. However, it is unclear whether viscosity affects the rate of melting predominantly by affecting the heat transfer on the melt side or via the stability of the primary foam. Apart from viscosity, the temperature of primary foam formation and its extent depend on the rate of glass-phase supply from chemical reactions. Primary foam collapses from within when enough gas is evolved to cause the melt films separating the bubbles to break.

Whereas the CO_x evolution from carbonates and melt viscosity affects the formation of primary foam, oxygen evolution from redox reactions produces secondary foam. Fining (or redox) bubbles form inside the melt, rise by buoyancy, and accumulate under the cold cap, creating a stable layer of secondary foam that resists convection and inhibits heat transfer. It is possible that large bubbles produced by bubbling sweep the small fining bubbles from the melt and remove them through the vent holes in the cold cap. However, if secondary foam is not forcibly removed, it collapses by drainage of melt from between the bubbles when the viscosity is low enough. By Stokes law, $\eta = (2/9)\Delta\rho g r^2 t/h$, where $\Delta\rho$ is the density difference between the melt and the bubble, g is the acceleration due to gravity, r is the bubble radius, t is the time, and h is the thickness. Using the values $\Delta\rho = 2.7\times10^3$ kg/m^3, $g = 10$ m/s^2, $r = 1\times10^{-3}$ m, $t = 100$ s, and $h = 0.01$ m, we obtain $\eta = 60$ Pa·s. As Figure 4.3 indicates, the temperature at which the viscosity of the order 10^2 Pa·s is reached varies between 700 and 950°C, depending on glass composition. However, melt viscosity is also strongly affected by the extent to which silica grains are dissolved, and thus by the silica-grain sizes. Since primary foam internally collapses at the viscosity of the order 10^2 Pa·s, the transition between primary and secondary foam is probably continuous. At viscosity $<10^2$ Pa·s, the melt viscosity is influenced by temperature and by the extent of silica-grain dissolution.

As mentioned above, the relationship between foam formation and the rate of melting is unknown at present. Nevertheless, a possible impact of primary foam on the rate of melting is discussed in the next two subsections based on assumptions that need to be verified by melter studies.

6.2 Effect of Primary Foam Thickness on Rate of Melting

In a one-dimensional, and thus grossly oversimplified situation, the heat flux needed for slurry-feed drying and feed reactions in the upper cold cap must pass through the layer of primary foam. Thus, we can write

$$q = \lambda_L \Delta_L T / h_L \tag{6.1}$$

where q = heat flux for conversion
λ_L = lower layer heat conductivity
$\Delta_L T$ = temperature difference across the lower layer
h_L = lower layer thickness.

Disregarding the heat consumed in the primary-foam layer, we have

$$q = NQ \tag{6.2}$$

where N is the rate of melting, and Q is the conversion heat.

Suppose that a feed melt rate is 43 kg of glass produced per m^2 per hour, i.e., $N = 1.2\times10^{-2}$ kg/m^2s, the heat for water evaporation is 2.4×10^6 J/kg glass, and the heat for feed conversion is 2.2×10^6 J/kg glass, i.e., $Q = 4.6\times10^6$ J/kg glass. Then, by Equation (6.2), the heat flux needed for feed processing is $q = 55$ kW/m^2.

Can this heat flux occur through primary foam? If the primary foam spans 700°C and 900°C, then $\Delta T = 200$ K. Unfortunately, we know neither the value of λ_L nor that of h_L. Based on Equation (6.1), $\lambda_L/h_L = 0.27$ kW/m^2K. Accordingly, to sustain the rate of melting at 43 kg/m^2h, λ_L must increase from 0.8 to 1.9 W/mK when h_L increases from 3 to 7 mm.

In reality, λ_L is not a function of h_L but has a value that depends on the void fraction in the foam and the rate of gas evolution within the foam. If we assume that $\lambda_L = 1$ W/mK, which is approximately the value of the heat conductivity of molten glass, then we can conclude, using the above values of parameters, that when h_L increases from 3 to 7 mm, N decreases from 52 to 26 kg/m^2h. The value of 43 kg/m^2h is obtained when $h_L = 3.7$ mm.

Provided that λ_L does not vary significantly from feed to feed, we can expect that the rate of melting is strongly influenced by the primary foam layer thickness.

6.3 Effect of Conversion Rate on Rate of Melting

The above calculation assumes that $\Delta T = 200$ K regardless of h_L. However, when $h_L = 0$, i.e., primary foam does not form, then also $\Delta T = 0$ because no lower layer exists. Then the rate of melting depends solely on the rate of conversion.

If we disregard the complexity of feed melting reactions as a first approximation, we can write

$$N = k\rho h_U \quad (6.3)$$

where k is the conversion rate coefficient, ρ is the feed density, and h_U is the upper (reacting) layer thickness.

For $N = 1.2\times10^{-2}$ kg/m^{2}s and $\rho = 1\times10^3$ kg/m^3, we get $N/\rho = 1.2\times10^{-5}$ m/s = 0.72 mm/min. This is roughly the velocity at which feed moves through the reacting layer (the velocity is somewhat higher because N is related to glass, and thus the mass flux of feed is higher before off-gas is released).

As in the case of the primary-foam layer, we do not know the values of k and h_U individually. Assuming that h_U does not change much from feed to feed (e.g., h_U = ~2 mm), we can conclude that N increases roughly linearly with feed reactivity (k) and thus the choice of feed additives is important.

6.4 Effect of Exothermic Reaction on Rate of Melting

Since, by Equation (6.2), $N = q/Q$, then, for a given value of q, a decrease in Q via an exothermic reaction within the reacting layer will increase the rate of melting.

The reaction of sucrose with a nitrate can produce, according to the reaction path, 6 to 12 MJ/kg. Provided that 0.3 kg of sucrose per kg of glass is added to the feed that contains a sufficient fraction of nitrates to provide oxygen for an exothermic reaction, the amount of heat produced by such a reaction will be 1.8 to 3.0 MJ/kg of glass. As a result, the conversion heat will decrease to level of 1.6 to 2.8 MJ/kg, and thus, for q = 55 kW/m^2, the rate of melting will increase 1.7 to 2.9 times, from 43 kg/m^2/h to a level of 71 to 126 kg/m^2/h.

Accordingly, the rate of melting can increase 2 to 3 times by adding sucrose if a sufficient fraction of nitrates exists in the waste or is provided in the form of nitrate additives. A possible negative impact on primary foam can be mitigated by using an optimum size of silica grains.

6.5 FY 2009 Work

In FY 2009, an examination of the feed conversion process continues in the following areas:

- The impact of silica grain size on feed expansion and the extent of conversion are being examined more systematically. Two types of silica are used: glass-maker's sand and crushed quartz of various size fractions. It is evident that silica grains strongly interact with gas bubbles. Large grains tend to cluster.
- The HNO_3 addition is being systematically reduced to determine the minimum effective amount. Also, feed additives are used in the form of nitrates to eliminate acidification. The impact of sucrose addition on conversion reactions and primary-foam formation is being elucidated.
- The effect of combined variations of silica grains and sucrose-nitrate addition is examined.

6.6 Mathematical Modeling

One of the goals of this work is to bring sufficient insight into feed melting to develop a mathematical model of the cold cap that can be implemented as a part of the overall melter model. The model development can begin with a one-dimensional cold cap combined with a two- or three-dimensional

melter model. It can start with an oversimplified version and fitting parameters (e.g., effective heat conductivity of the primary-foam layer). A realistic model of the upper layer, including chemical reactions, phase transitions, and water evaporation, can be fully developed based on results of thermal analyses.

6.7 Large-Scale Testing

Large-scale testing is already being performed by other projects. It is important that large-scale tests are run with waste simulation mimicking the tank waste. The main goals of large-scale testing should consist of adding glass-forming and glass-modifying agents in a suitable chemical and physical form to achieve a higher feed-melting rate and in adding chemicals (e.g., organics, such as carbohydrates) that provide a heat supply to feed at temperatures below 500°C. Optimizing silica-grain size is also important.

7.0 Conclusions

Understanding the relationship between the melter-feed makeup and the feed-to-glass conversion process will help accelerate the rate of glass processing that in continuous glass melters is jointly controlled by the rate of heat-transfer from molten glass to and through the cold cap and by the kinetics of various chemical reactions and phase transitions within the cold cap. Though it is impossible to determine the rate of melting in a large continuous melter with laboratory crucible experiments alone, laboratory studies allow relationships to be obtained between the feed responses to heat treatment and the feed-makeup parameters that ultimately control the rate of melting.

The main factors that control the feed response to heating, including conversion reactions and the extent of gas entrapment in the glass-forming melt, are the nature of inorganic salts (nitrates and carbonates) and the size of silica particles. In addition, a powerful source of internal heat within the cold cap can be provided through exothermic reactions of carbohydrates, such as sucrose or cellulose, with oxyanionic salts, especially nitrates and nitrites. These parameters have been examined in various laboratory tests such as flux migration testing, DTA-TGA, XRD, SEM-EDS, visual examination and optical microscopy of crucible melts, photographic recording of feed pellets and loose batches in quartz-glass crucibles, and temperature-field-evolution monitoring.

To simulate in the laboratory the conditions the feed experiences within the cold cap, the feeds were heated at a constant rate (5°C/min) rather than using isothermal heat treatments, and the waste was made with chemicals close to those existing in the tank waste. The main results can be summarized as follows:

- The feed migration test showed that the mobility of molten salt within HLW feeds is suppressed by the large specific surface area of the feed solids.
- The temperature-field-evolution measurement allowed the heat conductivity of feeds within the temperature interval from 300 to 600°C to be determined and showed that the exothermal reaction between nitrate and sucrose resulted in a temperature jump from ~100°C to ~300°C.
- Volume changes of feeds were determined quantitatively as functions of temperature using pellets and loose batches placed in silica-glass crucibles. Primary foam density was as low as ~0.2 g/cm^3. The feed expansion was controlled mainly by the content of boric acid and carbonate in the feed, and the collapse of primary foam was controlled by melt viscosity and the content of carbonates. Oxygen evolution from redox reactions produces secondary foam. The silica grain size affected the feed expansion temperature as well as the extent of expansion. This effect is attributed to the impact of the grain size on the rate of grain dissolution that in turn affects melt viscosity. Sucrose addition influenced feed expansion in a complex manner.
- Examination by XRD indicated that the early reaction (below 500°C) of silica with fluxes slowed down the dissolution of silica in the later stages. Hematite formed from amorphous iron oxyhydrate and completely dissolved below 800°C. Spinel formed from hematite starting at 500°C, peaked just above 600°C, and remained in the glass even at 1000°C. These results were confirmed with SEM-EDS.
- DTA-TGA tests showed that the major mass loss begins in feeds at ~150°C and continues to 600°C; above 600°C, it proceeds at a slow rate.

A simplified model of the cold cap consists of an upper layer of granular solids soaked with low-viscosity molten salts and a lower layer of a glass-forming melt with primary foam and dispersed solid residues, mainly silica. The thickness of the primary-foam layer depends on the magnitude of the internal gas-phase source and the viscosity of the glass-forming melt. The present study demonstrated that the gas-phase source within the glass-forming melt can be decreased, and perhaps entirely eliminated, if the feed anions are mainly or exclusively nitrates; that the stability of primary foam is affected by the source of silica; and that exothermic reactions between organics, such as sucrose, and an oxygen source from nitrates and nitrites occur at early stages of the feed conversion process, but influence this process up to and including the formation of primary foam.

8.0 References

Anderson LD, T Dennis, ML Elliott, and P Hrma. 1994. "Noble Metal Behavior During Melting of Simulated High-Level Nuclear Waste Feeds." *Ceram. Trans*. 39:213-220.

Bader E. 1979. "The Effect of Cullet on Melting Reactions in Borosilicate and Soda-Leme Silicate Glass Batches." *Silikattechnik* 30:112-115.

Bickford DF. 2004. "Laboratory measurements of glass melting rate." *Ceram. Trans.* 155:57-68.

Bickford DF, P Hrma, and BW Bowen II. 1990. "Control of Radioactive Waste Glass Melters: II, Residence Time and Melt Rate Limitations." *J. Am. Ceram. Soc*. 73:2903-2915.

Bunting JA and BH Bieler. 1969. "Batch-Free Time Versus Crucible Volume in Glass Melting." *American Ceram. Soc. Bull.* 48:781-785.

Cable M. 1984. "Principals of Glass Melting." In: *Glass Science and Technology*. DR Uhlmann and NJ Kreidl (Eds.), Academic Press, Orlando, Florida (pp. 1-44.

Cable M and MQ Siddiqui. 1983. "The replacement of Soda by Caustic Soda in Laboratory Glass Melting trials." *Glass Tech.* 24:193-198.

Chapman C. 2004. *Investigation of Glass Bubbling and Increased Production Rate*. REP-RPP-069, Duratek, Inc., Columbia, Maryland.

Elliott ML, CC Chapman, LL Eyler, and DD Yasuda. 1989. *Preliminary Studies of Vitrification Rate Enhancement*. Pacific Northwest Laboratory, Richland, Washington.

Hrma P. 1982. "Thermodynamics of Batch melting." *Glastechnische Berichte* 55:138-150.

Hrma P. 1988. "Complexities of Batch Melting." In: *Adv. in Fusion of Glass*, pp. 10.1-18, *Am. Ceram. Soc.*, Westerville, Ohio.

Hrma P. 1990a. "Batch Melting Reactions." In: A Paul, *Chemistry of Glass*. Prentice Hall, London (pp. 157-178).

Hrma P. 1990b. "Melting of Foaming Batches: Nuclear Waste Glass." *Glastech. Ber*. 63K:360-369.

Hrma P. 2008. "Arrhenius Model for High-Temperature Glass Viscosity with a Constant Pre-Exponential Factor." *J. Non-Cryst. Solids* (accepted).

Hrma P, CE Goles, and DD Yasuda. 1991. "Drainage of Primary Melt in a Glass Batch." *Ceram. Trans*. 23:361-367.

Hrma P, J Matyáš, and D-S Kim. 2002. "The Chemistry and Physics of Melter Cold Cap." In: *9th Biennial Int. Conf. On Nucl. And Hazardous Waste Management, Spectrum '02*, American Nuclear Society, CD-ROM.

Hrma P, LM Bagaasen, MJ Schweiger, MB Evans, BT Smith, BM Arrigoni, D-S Kim, CP Rodriguez, ST Yokuda, J Matyas, WC Buchmiller, AB Gallegos, A Fluegel. 2007. *Bulk Vitrification Performance Enhancement: Refractory Lining Protection Against Molten Salt Penetration*. PNNL-16773, Pacific Northwest National Laboratory, Richland, Washington.

Izak P, P Hrma, and MJ Schweiger. 2001. "Kinetics of Conversion of High-Level Waste to Glass." *ACS Symp. Series* 778:314-328.

Josephs JE and ME Stone. 2001. *Melt Rate Improvement for DWPF MB3: Sugar Addition Test*. WSRC-TR-2001-00158, Westinghouse Savannah River Company, Aiken, South Carolina.

Kim D-S and P Hrma. 1990. "Volume Changes During Batch to Glass Conversion." *Ceram. Bull*. 69[6]:1039-1043.

Kim D-S and P Hrma. 1991. "Foaming in Glass Melts Produced by Sodium Sulfate Decomposition under Isothermal Conditions." *J. Am. Ceram. Soc*. 74[3]:551-555.

Kim D-S and P Hrma. 1994. "Laboratory Studies for Estimation of Melting Rate in Nuclear Waste Glass Melters." *Ceram. Trans*. 45:409-419.

Kot WK and IL Pegg. 2007. Preparation and Testing of HLW Algorithm Glasses to Support Small Scale Melter Testing, VSL-07R1240-1, Vitreous State Laboratory, The Catholic University of America, Washington, DC.

Lambert DP, TH Lorier, DK Peeler, and ME Stone. 2001. *Melt Rate Improvement for DWPF MB3: Summary and Recommendations*. WSRC-TR-2001-00148, Westinghouse Savannah River Company, Aiken, South Carolina.

Lorier TH. 2001. *Melt Rate Improvement for DWPF MB3: Crucible Studies*. WSRC-TR-2001-001451, Westinghouse Savannah River Company, Aiken, South Carolina.

Lucktong C and P Hrma. 1988. "Oxygen Evolution during MnO-Mn_3O_4 Dissolution in a Borosilicate Melts." *J. Amer. Ceram. Soc*. 71[5]:323-328.

Lutze W, W Gong, FC Perez-Cardenas, KS Matlack, IL Pegg, and P Schill. 2007. Tenting and Modeling the Behavior of Platinoids During Vitrification of High-Level Radioactive Waste. Part 1. Glass Technology: European Journal of Glass Science and Technology A 48, 263-275.

Matlack KS, H Gan, W Gong, IL Pegg, CC Chapman, and I Joseph. 2007a. *High Level Waste Vitrification System Improvements*. VSL-07R1010-1, Vitreous State Laboratory of the Catholic University of America, Washington, D.C.

Matlack KS, W Kot, W Gong, and IL Pegg. 2007b. *Small Scale Melter Testing of HLW Algorithm Glasses: Matrix 1 Tests*. VSL-07R1220-1, Vitreous State Laboratory of the Catholic University of America, Washington D.C.

Matlack KS, WK Kot, IL Pegg, and I Joseph. 2007c. *High Level Waste Glass Development Testing (Test Plan)*. VSL-07T1360-1, Vitreous State Laboratory at the Catholic University of America, Washington D.C.

Matlack KS, W Kot, W Gong, and IL Pegg. 2008. Small Scale Melter Testing of HLW Algorithm Glasses: Matrix 2 Tests, VSL-08R1220-1, Vitreous State Laboratory, The Catholic University of America, Washington, DC 20064.

Nemec L. 1974. "Refining of Glass Melts." *Glass Technology* 15:153-156.

Russell III, HH and WR Ott. 1980. "The Effect of Pre-reaction on Some Zink Opal Glass Melting Trials." *Glass Tech.* 21:237-243.

Schill P. 1982. "Mathematical Model of Batch Melting in All-Electrical Furnaces." *Silikaty* 26:155-163 and 209-222.

Smith PA, JD Vienna, and P Hrma. 1995. "The Effect of Melting Reactions on Laboratory-Scale Waste Vitrification." *J. Mat. Res*. 10[8]:2137-2149.

Smith ME, DH Miller, and TH Lorier. 2004a. *The Impact of Frit 202 on Melt Rate for the SB3 Feed System*. WSRC-TR-2004-00453, Savannah River National Laboratory, Aiken, South Carolina.

Smith ME, DH Miller, and TH Lorier. 2004b. *Impact of Feed Preparation Acid Stoichiometry and Redox on Melt Rate for the SB3-Frit 418 Feed System*. WSRC-TR2004-00350, Savannah River National Laboratory, Aiken, South Carolina.

Smith ME, TM Jones, and DH Miller. 2007. *Sludge Batch 4 Baseline Melt Rate Furnace and Slurry-Fed Melt Rate Furnace Tests with Frits 418 and 510*. WSRC-TR-2007-00450, Savannah River National Laboratory, Aiken, South Carolina.

Stone ME and JE Josephs. 2001. *Melt Rate Improvement for DWPF MB3: Melt rate Furnace Testing*. WSRC-TR-2001-001468, Westinghouse Savannah River Company, Aiken, South Carolina.

Taylor TD and KC Rowan. 1983. "Melting Reactions of Soda-Lime Silica Glasses Containing Sodium Sulfate." *J. Am. Ceram. Soc*. 66:227-228.

Thomason CV and FW Wilburn. 1960. "The Application of Differential Thermal Analysis and Gravithermic Analysis to the Study of Reactions Between Glass Materials: Part 2." *Physics and Chemistry of Glasses* 1:52-69.

Vierneusel U, H Goerk, and KH Schuller. 1981. "Suppression of Segregation in Crucible Melts." *Glastechnische Berichte* 54:332-337.

Wilburn FW and CV Thomasson. 1958. "The Application of Differential Thermal Analysis and Thermogravimetric Analysis to Study of Reactions Between Glass Materials: Part 1." *J. Soc. Glass Tech.* 42:156-175T.